on
CONVOLUTIONAL PROCESSES
and
DISPERSIVE GROUNDWATER FLOW

PROEFSCHRIFT

ter verkrijging van de graad van doctor
aan de Technische Universiteit Delft,
op gezag van de Rector Magnificus Prof. Ir. K.F. Wakker
in het openbaar te verdedigen ten overstaan van een commissie
door het College van Dekanen aangewezen
op maandag 13 juni 1994 te 13.30 uur

door

CORNELIS MAAS
civiel-ingenieur

geboren te 's Gravenhage

Dit proefschrift is goedgekeurd door de promotoren:
Prof. dr. ir. A. Verruijt, Technische Universiteit Delft
Prof. dr. ir. O.D.L. Strack, University of Minnesota

Aan mijn vrouw Adrie
en onze kinderen
Marieke en Peer

Acknowledgements

TABLE OF CONTENTS

Contents

CHAPTER 1: PURPOSE

1.1 Introduction

In 1987 the author was commissioned to lead an investigation into the environmental effects of a proposed plant for the recovery of bank groundwater, in behalf of a water company in the western part of the Netherlands. The task included the hydrological design of a well field (Maas, [1988]). A suitable site was found along a branch of the river Rhine (Figure 1.1).
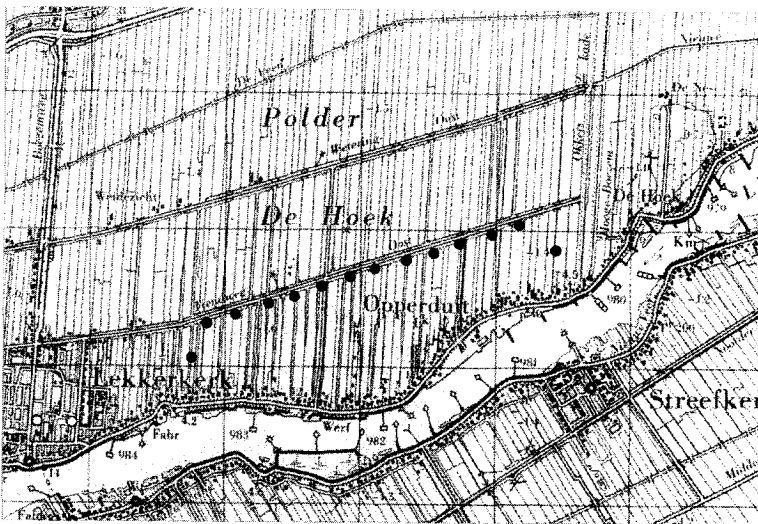
Figure 1.1   *Topographic map showing the layout of a well field for the recovery of bank groundwater.*

By its definition bank groundwater is infiltrated surface water. It has some qualitative aspects in common with natural groundwater and many with the river where it originates from. Quality fluctuations of the river water can be retraced in the recovered groundwater, in a dampened and retarded way. The amount of dampening and retardation can be influenced to a certain degree by a proper

arrangement of the well field. The prospects of bank groundwater recovery are relatively favorable along the lower course of the Rhine. The low-lying polders cause the river to infiltrate its water permanently. In contrast to the upper course it is possible to capture bank groundwater at quite a distance from the river bank, thus creating a large underground mixing reservoir to dampen quality fluctuations.

As some real and some potential sources of groundwater contamination were traced near the selected site, it was decided to confine the capture zone to the area between the wells and the river bank. It can be shown that such is possible by placing wells of equal strengths in a semi elliptical array (Figure 1.2), tuning the discharge to the original rate of river water infiltration.
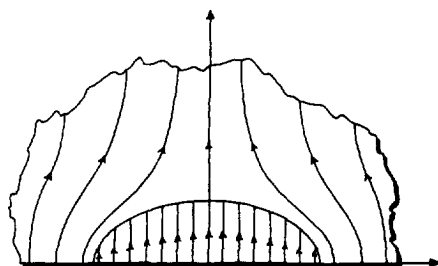
Figure 1.2 *Semi elliptical array of wells in uniform flow.*

The lengths of the ellipse's axes can be chosen arbitrarily, although the choice influences the total amount of groundwater that can be withdrawn. Thus one has some freedom to influence the mixing properties of the well field. Another degree of freedom lies in the spacing of the wells along the ellipse. The mixing properties of a well field can be characterized by its *impulse response*. This can be thought of as a function of time, describing the development of the concentration of some inert and conservative contaminant in the groundwater recovered, following an event of instantaneous pollution of the river. Equivalently, the impulse response function can be interpreted as the frequency distribution of the detention times of the water particles recovered. Typically, the impulse response function shows no negative values. As a rule, some particles reach the well field soon and some reach the well field never, while the bulk concentrates around some mean detention time, causing the impulse response function to show a peak there. The impulse response function of the projected well field was calculated approximately. To that end it was recognized that the infiltrating river water is to pass through a number of "subsystems", whose impulse response functions could be calculated by means of analytical (as opposed to numerical) methods. The first subsystem is the part of the aquifer between the river bottom and the river bank. As the river is relatively shallow, particles that infiltrate near the middle of the river need a longer time to reach the river bank than particles infiltrating near the shore. The second subsystem distinguished is the part of the aquifer between the bank and the wells. Wells closer to the river are, of course, reached sooner than wells at a greater distance. Additional spreading of

detention times is known to be caused by macroscopic dispersion, which occurs all the way between the river bottom and the wells. This mechanism was treated as a separate subsystem, which can be defended by the argument that dispersion is a very complicated process, which defies an exact quantification anyhow. The fourth and last subsystem is the immediate vicinity of the individual wells. Flow around the wells causes spreading of detention times, its effect being dependent on the well spacing and on the amount of water pumped. The four resulting impulse response functions are schematically pictured in Figure 1.3.
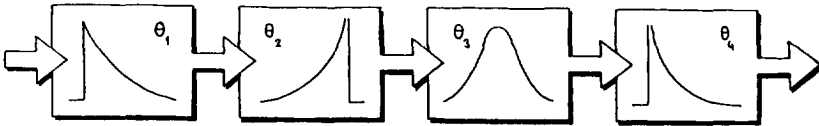
Figure 1.3 *Impulse response functions of the four subsystems.*

Each box shows the typical character of the impulse response function of the corresponding subsystem. The two functions amenable to adjustment are the second and the fourth ones. As their characters are quite antipodal, we expected to have good control of the impulse response function of the composite system. We aimed at designing the well field such that the dominating quality fluctuations of the river water would be dampened optimally. Using Duhamel's principle, it can be shown that the impulse response function of the composite system can be derived from those of the subsystems by convolution:

$$\Theta(t) = \iiiint \theta_1(\tau_2 - \tau_1) \cdot \theta_2(\tau_3 - \tau_2) \cdot \theta_3(\tau_4 - \tau_3) \cdot \theta_4(t - \tau_4) d\tau_4 d\tau_3 d\tau_2 d\tau_1 \quad (1.1)$$

(More on convolution will be said in the following chapter). The resulting function $\Theta(t)$ is depicted in Figure 1.4 for a particular choice of the design parameters. The river water was supposed to be contaminated by a radio-active substance. The function $\Theta(t)$ is shown for various rates of decay.

$\Theta(t)$ turns out to show a distinct maximum. Although it has an infinitely long tail, its shape is more or less symmetrical. The function reminds us of the Gaussian distribution. *The surprising part is that we were not able to alter this Gaussian-like character, no matter how we changed the free parameters.* We could change the height of the peak, and move its location, but the basic shape remained unaffected. It occurred to us that the convolutional process was to be held responsible for this result. Some experimental calculations revealed that if we added some more systems to the four pictured in Figure 1.3, the result looked even more like a Gaussian distribution, no matter how fancy the impulse response functions of the subsystems were chosen. Each system added, however, appeared to increase the variance of the resulting Gaussian-like shape, at the same time shifting its maximum to the right. By analogy to the Central Limit Theorem of statistics we suspected that only the means and variances of the
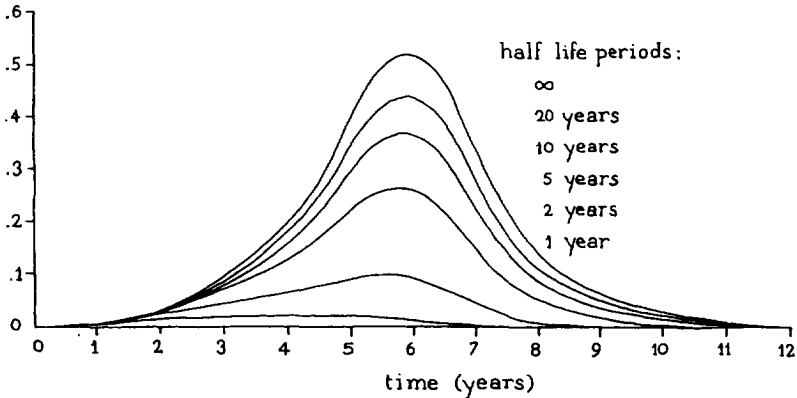
Figure 1.4   *Impulse response function of the well field.*

impulse response functions of the subsystems contributed to the final result, the other characteristics being somehow neutralized by each other. Thus, in order to calculate the impulse response of a composite system, it might not be necessary to know the impulse response of the constituent subsystems exactly and it would probably suffice to use only crude models for them, as long as they yield the mean and the variance.

The project budget at the time not being tailored to such investigations, the idea was shelved to be elaborated at a better occasion.

1.2 Aim of the LCMR-project

That occasion presented itself in 1990, when the author had the opportunity to take part in a research project at the University of Minnesota, sponsored by the Legislative Commission on Minnesota Resources (LCMR). The broader aim of this project is the "implementation of spatial and seasonal variability of chemical transport in Minnesota groundwater." The part of the project relevant to this report is to "investigate the effect of soil irregularities on the spreading of contaminants, develop a mathematical formulation, and implement this in the computer program MLAEM" (cited from the MFRC Work Program 1989). Program manager is Prof. O.D.L. Strack of the University of Minnesota, who developed the computer program referred to. MLAEM is a groundwater model based on Analytical Elements, as opposed to the usual numerical methods of computation, of which Finite Elements are probably most frequently used. (The basic principles of the analytical element method are given in Strack [1989].) As to contaminant transport the program is presently apt to calculate flow lines in piecewise homogeneous media. The spreading of contaminants by dispersion due to soil irregularities has not yet been taken into account.

Much work has been done on dispersion in the past two decades. Theoretical developments are now almost completely in the domain of stochastic geohydrology, which is becoming a discipline in its own right (Dagan [1989]). In spite of apparent progress the fundamentals are still subject to discussion (Sposito et al. [1986]). From the deterministic point of view, applied mathematicians have devoted much effort to the development of effective numerical schemes to solve the "classical" dispersion-convection equation, which by its nature is an unruly task. The problems encountered are in the field of numerical mathematics rather than physics. The analytical element method, being essentially non-numerical, does not benefit from progress in this field.

As dispersion in porous media is a vast field of research, bounds had to be set as to the aim of the LCMR-project. Implementation in MLAEM being the final goal it was decided to focus on analytical methods for one-dimensional dispersive transport in non-uniform flow. The neglect of transverse dispersion (in this stage) is defendable by the fact that recent field studies invariably reveal transverse dispersion to be small as compared to longitudinal dispersion. Only "ideal contaminants" are considered, i.e., it is supposed that the contaminating particles do not interfere with the groundwater flow process. The irregularities of the medium are assumed to be non-systematic. We will refer to them as heterogeneities.

1.3 Scope of the report

Transport through irregular (i.e. heterogeneous) porous media shows some similarities to the process sketched in Section 1.1. Following a stream line, one can think of the porous medium as a chain of subsystems, that have to be passed by the groundwater particles. On the basis of our former experience we expected that not all of the peculiarities of the subsystems would contribute to the final spreading of a contaminant. Consequently it might not be necessary to know the detailed structure of the subsystems. We conjectured that it would be possible to characterize the final spreading by two or three parameters. This idea has been elaborated in Chapter 2, in a very general setting. The theory is applied to one-dimensional contaminant transport in Chapter 3.

A simultaneous, but quite different track has been trod by Strack [1992], who proposed an entirely new differential equation to describe dispersive transport through porous media. His work is part of the project but it is not covered by this report. Only the results are quoted here and solutions to Strack's equation are given for the uniform flow case. The two approaches meet in Chapter 4, where they are confronted with a series of simulated column experiments.

CHAPTER 2: ON THE SHAPE OF

BREAKTHROUGH PROFILES

2.1 Aim of the chapter

In this chapter we will go more deeply into the conjecture formulated in the foregoing sections. Our hypothesis is that signals of finite duration, transmitted through a series of linear systems, eventually assume a simple shape that can be characterized appropriately by just a few parameters. Tentatively, we call this shape *skew Gaussian*, the meaning of which should be intuitively clear from the discussion in the preceding chapter. As the theory develops, a more accurate description will evolve. Although the setting of this chapter is more or less abstract, we will emphasize the applicational aspects and rely on an intuitive approach rather than going into mathematical details.

2.2 Simple example of a convolutional limit
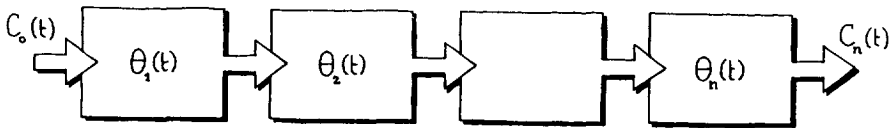
Figure 2.1   *A series of systems transferring a signal.*

Consider a series of systems that convert an input signal into an output signal (Figure 2.1). Here the word signal means an observable and measurable phenomenon, which changes its magnitude in the course of time, and which has the property that it propagates. Examples are waves of sound, plumes of contaminant and the likes. The medium, or part of it, through which the signal propagates we call a system. Usually a signal changes its shape while passing through a system, so that one might say the system transforms the signal. The

system is *linear* if the transformation L is linear in a mathematical sense:

$$L(\alpha c_{in}) = \alpha L(c_{in}) \tag{2.1}$$

for any scalar α and

$$L(c_{in}^1 + c_{in}^2) = L(c_{in}^1) + L(c_{in}^2) \tag{2.2}$$

where c_{in}^i is any input signal. For a single linear system, Figure 2.2, the relation between input signal and output signal can be expressed by a convolution integral

$$L\{c_{in}(t)\} = \int_{-\infty}^{+\infty} c_{in}(\tau)\theta(t - \tau)d\tau = c_{out}(t) \tag{2.3}$$

where $\theta(t)$ is a function that is completely determined by physical characteristics of the system. The mathematical meaning of $\theta(t)$ can best be understood by sending an impulse signal (Dirac's delta) through the system. It then follows from (2.3) that

$$c_{out}(t) = \int_{-\infty}^{+\infty} \delta(\tau)\theta(t - \tau)d\tau = \theta(t) \tag{2.4}$$

which means that in case of an impulsive input signal the output signal reveals the shape of $\theta(t)$. $\theta(t)$ is, therefore, called the *impulse response function* of the linear system.
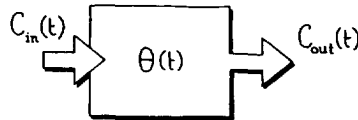
Figure 2.2   *A single linear system.*

    Figure 2.3 clarifies the computational meaning of the convolution integral (2.3). $c_{in}(t)$ and $\theta(t)$ are depicted as two arbitrary functions of time. $c_{in}(t)$ is drawn in the usual way, as a function of the integration variable τ, while $\theta(\tau)$ is shown as a mirror image. The origin of $\theta(\tau)$ is shifted over a distance t, and the overlapping parts of c_{in} and θ are indicated by shading. On the overlapping interval, c_{in} and θ are multiplied to yield the lower picture of Figure 2.3. The area $\mathcal{A}$ then equals the convolution product of c_{in} and θ, at time t.
    When a signal is transmitted through a series of linear systems, as in Figure 2.1, the relation between input signal and output signal can obviously be given by a repeated convolution integral:

$$c_{out}(t) = \int_{-\infty}^{+\infty} \int_{-\infty}^{+\infty} \cdots \int_{-\infty}^{+\infty} c_{in}(\tau_1) \cdot \theta_1(\tau_2 - \tau_1) \cdot$$
$$\cdot \theta_2(\tau_3 - \tau_2) \dots \theta_n(t - \tau_n)d\tau_1 d\tau_2 \dots d\tau_n \tag{2.5}$$
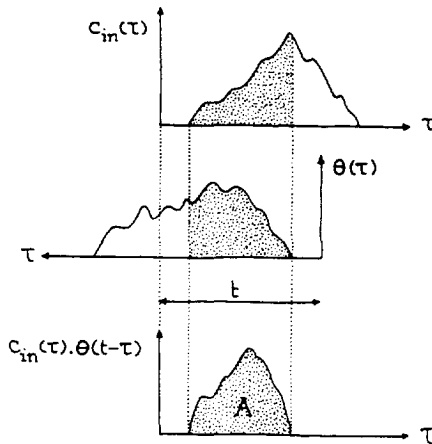
Figure 2.3   *Computational meaning of the convolution product.*

In order to gain some feeling for the way a repeated convolution product effects an input signal, consider a simple example, where the signal is an impulse (Dirac's delta) and the systems all have the same impulse response function, which is chosen to be the block function of unit area, shown in Figure 2.4. After the first system has been passed, the signal shows the shape of the impulse response function itself. The second system changes the signal into a triangle, whose area is still unity, and whose base is twice the base of the impulse response function. This result is easily grasped intuitively, if one realizes the computational meaning of the convolution product, depicted in Figure 2.3. After three systems, the signal has got three branches of second order polynomials, and it already shows resemblances to a Gauss-curve. One may notice that

    a) each convolution causes the mean of the signal to shift an equal amount to the right.

    b) each convolution causes the spreading of the signal to increase. Although it cannot be inferred accurately from the pictures in Figure 2.4, it is easily shown that the variance, too, increases with an equal amount after each convolution, such that after n convolutions the variance equals n times the variance of the original impulse response function.

    c) outside a certain t-interval, the signal is identically zero, so the "front" of the signal propagates at finite velocity.

Notions a) and b) remind us of the Central Limit Theorem of statistics, to which we will turn later (Section 2.3).

    In order to see that repeated convolution by a block-shaped function may indeed yield a Gauss-curve as the number of convolutions approaches infinity, consider the complex Fourier transform of (2.5). It is well-known that this integral transform changes a convolution of functions into the product of the transformed functions

$$\bar{c}_{\text{out}}(\omega) = \bar{c}_{\text{in}}(\omega) \cdot \bar{\theta}_1(\omega) \cdot \bar{\theta}_2(\omega) \dots \bar{\theta}_n(\omega) \tag{2.6}$$
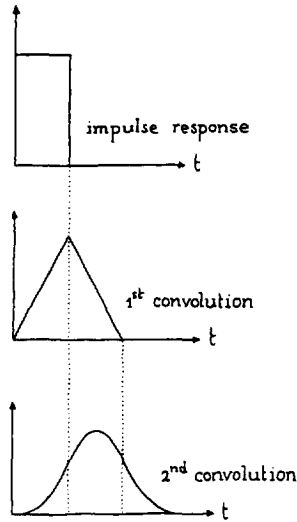
Figure 2.4 *Repeated convolution of an impulse signal by a series of systems having a block-shaped impulse response function of unit area.*

where

$$\bar{c}_{\text{out}}(\omega) = \int_{-\infty}^{+\infty} c_{\text{out}}(t)e^{i\omega t}dt \tag{2.7}$$

and likewise for the other functions in (2.6).

The block-shape function of Figure 2.4 is given by

$$\begin{cases} \theta(t) = \frac{1}{2a} & 0 \le t \le 2a \\ \theta(t) = 0 & t < 0 \text{ and } t > 2a \end{cases} \tag{2.8}$$

where $2a$ is the width of the block. Using (2.7) its Fourier transform is found to be

$$\bar{\theta}(\omega) = \frac{1}{2a}e^{i\omega a}\frac{\sin(\omega a)}{\omega a} \tag{2.9}$$

Moreover, $\bar{c}_{\text{in}}(\omega) = 1$ because $c_{\text{in}}(t)$ was supposed to be Dirac's delta. It now follows from (2.6) that

$$\bar{c}_{\text{out}}(\omega) = e^{in\omega a}\left(\frac{\sin(\omega a)}{\omega a}\right)^n \tag{2.10}$$

and we are to investigate the behavior of $\bar{c}_{\text{out}}(\omega)$ as $n \to \infty$. To that end, we expand the term $(\frac{\sin(\omega a)}{\omega a})^n$ in a Taylor series, which turns out to give

$$1 - \frac{1}{1!}\left(\frac{1}{6}na^2\omega^2\right) + \frac{1}{2!}\left(\frac{1}{6}na^2\omega^2\right)^2[1 + O(\frac{1}{n})] - \dots \tag{2.11}$$

This series approaches the Taylor series of $\exp(-\frac{1}{6}na^2\omega^2)$ if n approaches infinity, so

$$\left(\frac{\sin(\omega a)}{\omega a}\right)^n \sim e^{-\frac{1}{6}na^2\omega^2} \qquad (n \to \infty) \tag{2.12}$$

and it thus follows from (2.10) that

$$\bar{c}_{out}(\omega) \sim e^{in\omega a} \cdot e^{-\frac{1}{6}na^2\omega^2} \qquad (n \to \infty) \tag{2.13}$$

The output signal $\bar{c}_{out}(t)$ can now be recovered from this expression by Fourier inversion. The result is

$$c_{out}(t) \sim \frac{1}{\sqrt{2\pi\sigma^2}} \cdot e^{-\frac{(t-na)^2}{2\sigma^2}} \qquad (n \to \infty) \tag{2.14}$$

where

$$\sigma^2 = \frac{1}{3}na^2 \tag{2.15}$$

which is Gauss' function indeed. Its mean value is $t = na$ and its variance equals $\frac{1}{3}na^2$, which one might have spotted already from Figure 2.4.

2.3 Relation to the Central Limit Theorem

We already mentioned a resemblance to the Central Limit Theorem, which reads as follows:
Let x_i $(i = 1, 2, \ldots, n)$ be a sequence of independent identically distributed random variables, each having finite mean μ and finite variance σ^2. Let s_n be given by

$$s_n = \sum_{i=1}^{n} x_i \tag{2.16}$$

Then in the limit, as n approaches infinity, the distribution of s_n approaches a normal (i.e. Gaussian) distribution with mean $n\mu$ and variance $n\sigma^2$.

In fact, transferring a signal is mathematically equivalent to adding up n random variables. In order to appreciate this, consider two random variables x_1 and x_2 and introduce the transformation

$$\begin{aligned} w &= x_1 + x_2 \\ x_2 &= x_2 \end{aligned} \tag{2.17}$$

which, when solved inversely for x_1 and x_2, gives

$$\begin{aligned} x_1 &= w - x_2 \\ x_2 &= x_2 \end{aligned} \tag{2.18}$$

By means of the inverse transformation (2.18) the joint probability element

$$f(x_1, x_2)dx_1x_2 = f(x_1)f(x_2)dx_1dx_2 \tag{2.19}$$

($f(x_1)$ and $f(x_2)$ being the probability density functions of x_1 and x_2) transforms into the joint probability element $f(w, x_2)dx_2dw$:

$$f(w, x_2)dx_2dw = f_1(w - x_2)f_2(x)|J|dx_2dw \tag{2.20}$$

where $|J|$ is the Jacobian of the inverse transformation (2.18):

$$|J| = \begin{vmatrix} \dfrac{\partial x_1}{\partial w} & \dfrac{\partial x_1}{\partial x_2} \\ \dfrac{\partial x_2}{\partial w} & \dfrac{\partial x_2}{\partial x_2} \end{vmatrix} = \begin{vmatrix} 1 & -1 \\ 0 & 1 \end{vmatrix} = 1 \tag{2.21}$$

Integrating out the variable x_2 in (2.20) yields the probability density function of the sum $w = x_1 + x_2$, namely

$$f(w) = \int_{-\infty}^{+\infty} f_1(w - x_2)f_2(x_2)dx_2 \tag{2.22}$$

(The above was taken from [Springer, 1979], p 47). It is thus seen that adding up two random variables involves finding the convolution of their probability density functions, just like finding the impulse response of two linear systems involves finding the convolution of their respective impulse responses.

Likewise, determining the impulse response function of n linear systems is mathematically equivalent to determining the probability density function of the sum of n random variables. Therefore, the limit theorems of statistics apply to contaminant transport, provided that the impulse response functions satisfy certain conditions set to probability density functions. We will see that this is not quite the case, and we will have to extend the mentioned limit theorems slightly to serve our purpose.

There exists a more general version of the Central Limit Theorem, which states that under fairly general conditions, the Gaussian limit will also be approached if the random variables have differing probability density functions. The conditions referred to are due to Lindeberg (e.g. Von Mises, 1964, p 294). Being purely mathematical, Lindeberg's conditions are not easily put in words. For practical use one may say that the sum of any finite number of standard deviations of the individual density functions must be small as compared to the sum of all standard deviations. This is obviously the case for identically distributed random variables of finite mean and variance. According to Von Mises, it is also true if the individual density functions differ from zero only on a finite interval. We take the opportunity to point out that not any series of linear systems, discernible in the theory of groundwater flow, satisfies Lindeberg's conditions. A

counter example is the propagation of a disturbance of the groundwater poten-
tial through a semi-infinite porous medium. The medium can be thought of as
a series of linear systems and the disturbance of the potential can be considered
as a signal to be transmitted. Such a signal will never attain a Gaussian shape.
As a matter of fact, the impulse response function in question can be shown to
be of infinite variance.

In an earlier stage of this project, when we were not yet fully aware of an
analogy with random variables, we proved the convergence to the Gaussian limit
in a heuristic way. Although elegant and rigorous proofs of the Central Limit
Theorem can be found in several standard texts (i.e. Cramér, 1970), we add our
own ad hoc derivation as an appendix to this chapter, because it is slightly more
general in certain respects (admitting, for instance, impulse response functions
of non-unit areas), while, on the other hand, it is more tailored to suit our
physical application. The extension to impulse response functions of non-unit
areas is necessary, because contaminants in groundwater are frequently subject
to physical or chemical decay. An example was already given in Figure 1.4.
Conversely, matter (or other properties of a contaminant) may be produced
somehow during the transport process. Examples are degradation products and
reaction heat. We will discuss the consequences after we have introduced some
statistical terms.

2.4 Moments of impulse response functions

In view of things to come, we interrupt our discourse to introduce the notion
of *moments* of a function. Moments, like distributions, are widely used in the
area of statistics. According to Shohat and Tamarking (1943), these concepts
originated earlier in the field of mechanics. There, the word distribution refers to
loads distributed on structural parts. Important work on the theory of moments
was done towards the end of the nineteenth century by Stieltjes, who reportedly
used mechanical concepts of mass, stability, etc., on many occasions, in solving
analytical problems.

The rth moment M_r of an impulse response function $\theta(t)$ is defined by

$$M_r = \frac{\int_{-\infty}^{+\infty} t^r \theta(t) dt}{\int_{-\infty}^{+\infty} \theta(t) dt} \tag{2.23}$$

The denominator equals the area under the impulse response function. The
first moment M_1 corresponds to the "center of gravity" of $\theta(t)$, which can be
identified intuitively with the *mean* travel time of the transferred signal. We will
adopt the *symbol* μ for M_1, as is common in statistics. Higher order moments
are usually "centralized" with respect to μ, according to the formula

$$\overset{c}{M}_r = \frac{\int_{-\infty}^{+\infty} t^r \theta(t - \mu) dt}{\int_{-\infty}^{+\infty} \theta(t) dt} \tag{2.24}$$

Employing the binomial expansion, it follows easily that

$$M_r = \overset{c}{M}_r + \binom{r}{1}\overset{c}{M}_{r-1}\mu + \binom{r}{2}\overset{c}{M}_{r-2}\mu^2 + \cdots$$

$$\cdots + \binom{r}{r-2}\overset{c}{M}_2\mu^{r-2} + \binom{r}{r-1}\overset{c}{M}_1\mu^{r-1} + \mu^r \qquad (2.25)$$

(Notice that the second last term vanishes, as $\overset{c}{M}_1 = 0$). In particular,

$$M_2 = \overset{c}{M}_2 + \mu^2 \qquad (2.26)$$

$$M_3 = \overset{c}{M}_3 + 3\overset{c}{M}_2\mu + \mu^3 \qquad (2.27)$$

$$M_4 = \overset{c}{M}_4 + 4\overset{c}{M}_3\mu + 6\overset{c}{M}_2\mu^2 + \mu^4 \qquad (2.28)$$

The second centralized moment $\overset{c}{M}_2$ equals the *variance* of $\theta(t)$, to be indicated by the *symbol σ^2*. σ is the *standard deviation* of $\theta(t)$. Other characteristics of $\theta(t)$, are its *skewness*:

$$\overset{1}{\gamma} = \frac{\overset{c}{M}_3}{\sigma^3} \qquad (2.29)$$

and its *excess*:

$$\overset{2}{\gamma} = \frac{\overset{c}{M}_4}{\sigma^4} - 3 \qquad (2.30)$$

(Abramowitz and Stegun [1964], p 928).

2.5 Symmetrical and skew convolutional limits

Now that we are equipped with the necessary jargon, we can resume our discussion of convolutional limits. If we consider a series of linear systems whose individual impulse response functions satisfy the Lindeberg conditions, then we know now that

$$c_{\text{out}}(t) \sim \frac{1}{\sqrt{2\pi\sigma^2}}\exp\left\{-\frac{(t-\mu)^2}{2\sigma^2}\right\} \qquad (n \to \infty) \qquad (2.31)$$

where

$$\mu = \sum \mu_i \qquad (2.32)$$

and

$$\sigma^2 = \sum \sigma_i^2 \qquad (2.33)$$

Here, μ_i and σ_i^2 are the mean and the variance, respectively, of the ith system in the series. Now, suppose that the individual systems are non-conservative. Then

their impulse response functions have non-unit areas. They can be normalized, however, according to

$$\overset{n}{\theta}_i(t) = \frac{\theta_i(t)}{A_i} \tag{2.34}$$

where A_i is the area of $\theta_i(t)$ given by

$$A_i = \int_{-\infty}^{+\infty} \theta_i(t)dt \tag{2.35}$$

The normalized impulse response functions do satisfy the conditions set to probability density functions of random variables. As summing of random variables was seen to be mathematically equivalent to convolving impulse response functions, it follows that the limit theorems of statistics apply to contaminant transport, provided that the limits are multiplied by the product of the constants A_i. Thus, we arrive at the following extension of (2.31):

$$c_{\text{out}}(t) \sim \frac{A}{\sqrt{2\pi\sigma^2}} \exp\left\{-\frac{(t-\mu)^2}{2\sigma^2}\right\} \qquad (n \to \infty) \tag{2.36}$$

where

$$A = \prod_{i=1}^{n} A_i \tag{2.37}$$

It is important to notice that, in case of identical subsystems,

$$\mu = n\mu_i \tag{2.38}$$
$$\sigma^2 = n\sigma_i^2 \tag{2.39}$$
$$A = (A_i)^n = \exp\{n \ln A_i\} \tag{2.40}$$

for any i. Identical subsystems can be associated with identical sections of a straight stream tube in a homogeneous porous medium. We then get

$$\mu :: x \tag{2.41}$$
$$\sigma^2 :: x \tag{2.42}$$
$$\ln A :: x \tag{2.43}$$

where x is the distance traveled by a contaminant, measured from the spot of its instantaneous release. Notice that the non-conservative case exhibits exponential decay or growth.

For future reference we mention that the step response of a series of systems of the above indicated type has the limit

$$c_{\text{out}}(t) \sim \tfrac{1}{2}A \operatorname{erfc}\left\{-\frac{t-\mu}{\sigma\sqrt{2}}\right\} \qquad (n \to \infty) \tag{2.44}$$

In contaminant transport, the step response corresponds to the breakthrough curve.

Although it is interesting to know whether or not a propagating signal will approach the Gaussian curve asymptotically, practical experience with groundwater contaminants indicates that, on a field scale, plumes are often considerably skewed. The Gaussian limit, if it exists, has apparently not been reached yet, because the number of systems passed was still too small. One may hope, however, that skew plumes can also be characterized by a limited number of parameters. Put in other words: one may hope for a skew limit, that is reached before the Gaussian limit appears. That such a limit does indeed exist, is shown in the appendix to this chapter. The expression derived there turns out to be an asymptotic expansion that goes by the name of *Edgeworth* (Cramér, 1970, p 86). Stated in our terms, this expansion reads

$$c_{\text{out}}(t) \sim \frac{A}{\sqrt{2\pi\sigma^2}} \cdot$$

$$\cdot \left[1 - \left\{ \frac{1}{3!} \overset{1}{\gamma}\sigma^3 \frac{d^3}{dt^3} \right\} + \left\{ \frac{1}{4!} \overset{2}{\gamma}\sigma^4 \frac{d^4}{dt^4} + \frac{1}{2!} \left(\frac{1}{3!} \overset{1}{\gamma}\sigma^3 \right)^2 \frac{d^6}{dt^6} \right\} - \dots \right] \exp \left\{ - \frac{(t-\mu)^2}{2\sigma^2} \right\}$$

$$(n \to \infty) \tag{2.45}$$

where μ, σ^2 and A (which is not typical of Edgeworth's expansion) are defined by (2.32), (2.33) and (2.37), respectively. Moreover,

$$\overset{1}{\gamma}\sigma^3 = \sum \overset{1}{\gamma}_i \sigma_i^3 \tag{2.46}$$

$$\overset{2}{\gamma}\sigma^4 = \sum \overset{2}{\gamma}_i \sigma_i^4 \tag{2.47}$$

The derivatives occurring between the braces of (2.45) are to be interpreted as operators acting on the exponential function. Notice that $\overset{1}{\gamma}\sigma^3$ and $\overset{2}{\gamma}\sigma^4$ are proportional to the number of systems passed by the signal. Especially, when the systems are interpreted as identical sections along a straight stream tube, we have

$$\overset{1}{\gamma}\sigma^3 :: x \tag{2.48}$$

and

$$\overset{2}{\gamma}\sigma^4 :: x \tag{2.49}$$

The addition of a third derivative to the Gaussian function causes the impulse response to become skew, as illustrated by Figure 2.5. The terms containing the fourth and sixth derivatives tend to sharpen the peak and to produce longer tails.

It is of some interest to point out how the terms containing the derivatives behave as n increases. Introducing the variable

$$T = \frac{t-\mu}{\sigma} \tag{2.50}$$
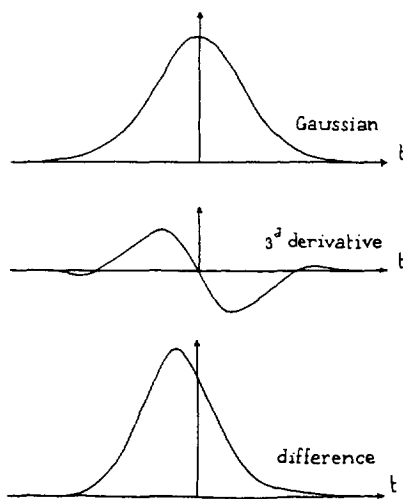
Figure 2.5   *Effect of 3^d derivative in (2.45) on the output signal.*

we find from (2.45) that

$$c_{\text{out}}(T) \sim \frac{A}{\sqrt{2\pi\sigma^2}} [1 + \{\tfrac{1}{6}\overset{1}{\gamma}H_3(T)\} + \{\tfrac{1}{24}\overset{2}{\gamma}H_4(T) + \tfrac{1}{72}(\overset{1}{\gamma})^2 H_6(T)\} + \dots].$$
$$\cdot \exp\left(-\frac{T^2}{2}\right) \qquad (n \to \infty) \tag{2.51}$$

where $H_n(T)$ is the nth order Hermite polynomial, defined by

$$\frac{d^n}{dT^n} e^{-T^2/2} = (-1)^n H_n(T) e^{-T^2/2} \tag{2.52}$$

(Cramér, 1970, p 87). In particular,

$$
\begin{aligned}
H_0(T) &= 1 \\
H_1(T) &= T \\
H_2(T) &= T^2 - 1 \\
H_3(T) &= T^3 - 3T \\
H_4(T) &= T^4 - 6T^2 + 3 \\
H_5(T) &= T^5 - 10T^3 + 15T \\
H_6(T) &= T^6 - 15T^4 + 45T^2 - 15
\end{aligned}
\tag{2.53}
$$

We infer from (2.33), (2.46) and (2.47) that $\overset{1}{\gamma} :: \sqrt{n}$ and $\overset{2}{\gamma} :: 1/n$. Therefore, in (2.51), the term containing $\overset{1}{\gamma}$ fades at rate $1/\sqrt{n}$ and the term containing $\overset{2}{\gamma}$ and

$(\frac{1}{\gamma})^2$ fades at rate $1/n$. Higher order terms of Edgeworth's expansion fade ever faster as n increases.

There exists an alternative expansion to Edgeworth's by the name of *Gram-Charlier* (Cramér, 1970, p 87), which, in our terms, reads

$$c_{\text{out}}(t) = \frac{A}{\sqrt{2\pi\sigma^2}}\left\{1 + \frac{c_3}{3!}H_3(T) + \frac{c_4}{4!}H_4(T) + \ldots\right\}\exp\left(-\frac{T^2}{2}\right) \qquad (2.54)$$

(The factor A is not characteristic of Gram-Charlier's series either). The coefficients c_i are defined by

$$c_i = \frac{\sigma}{A}\int_{-\infty}^{\infty} H_i(T)c_{\text{out}}(T)dT \qquad (2.55)$$

The formal correctness of (2.54) is easily established by use of the orthogonality properties of the Hermite polynomials:

$$\frac{1}{\sqrt{2\pi}}\int_{-\infty}^{\infty} H_i(T)H_j(T)e^{-T^2/2}dT = i! \qquad \text{if } i = j$$
$$\frac{1}{\sqrt{2\pi}}\int_{-\infty}^{\infty} H_i(T)H_j(T)e^{-T^2/2}dT = 0 \qquad \text{if } i \neq j \qquad (2.56)$$

The two expansions have been shown by Cramér to be rearrangements of one another. Only Edgeworth's series has proper asymptotic properties: the persistence of terms, as $n \to \infty$, is in the order of appearance in (2.45).

The formulation of Gram and Charlier suggests that any function can be expressed in the form (2.54). Alas, the convergence properties of (2.54) are rather poor and the practical value of Gram-Charlier's expansion is, in this respect, limited (Von Mises, 1964, p 137). By way of illustration, Figure 2.6 gives approximations of the block-function by Gram-Charlier's series, using 10, 100, and 1000 terms. Although, in this example, convergence is slow, the solution tends to approach the proper limit. We have also experimented with (2.54) to model dispersive transport according to the classical differential equation of dispersion (which is to be introduced in the next chapter). There, we found the solution to diverge after a certain number of terms were included, the number being smaller the closer we came to the source of pollution.

Figure 2.6 *The block-function, approached by Gram-Charlier's series, using 10, 100, and 1000 terms.*

As to the coefficients c_3 and c_4 of (2.54), it follows from (2.55) and (2.56) that $c_3 = \overset{1}{\gamma}$ and $c_4 = \overset{2}{\gamma}$, so the beginning of Gram-Charlier's series reads

$$c_{\text{out}}(T) = \frac{A}{\sqrt{2\pi\sigma^2}} \left\{ 1 + \tfrac{1}{6}\overset{1}{\gamma}H_3(T) + \tfrac{1}{24}\overset{2}{\gamma}H_4(T) + \ldots \right\} \exp\left(-\frac{T^2}{2} \right) \quad (2.57)$$

which is to be compared with (2.51). For later use we mention that the step responses (breakthrough curves) corresponding to (2.51) and (2.57) are

$$c_{\text{out}}(T) \sim \tfrac{1}{2}A\,\text{erfc}\left(-\frac{T}{\sqrt{2}} \right)$$

$$-\frac{A}{\sqrt{2\pi}} \left[\left\{ \tfrac{1}{6}\overset{1}{\gamma}H_2(T) \right\} + \left\{ \tfrac{1}{24}\overset{2}{\gamma}H_3(T) + \tfrac{1}{72}(\overset{1}{\gamma})^2 H_5(T) \right\} + \cdots \right] \exp\left(\frac{T^2}{2} \right)$$

$$(n \to \infty) \quad\quad\quad\quad\quad\quad (2.58)$$

and

$$c_{\text{out}}(T) = \tfrac{1}{2}A\,\text{erfc}\left(\frac{T}{\sqrt{2}} \right) - \frac{A}{\sqrt{2\pi}} \left\{ \tfrac{1}{6}\overset{1}{\gamma}H_2(T) + \tfrac{1}{24}\overset{2}{\gamma}H_3(T) + \cdots \right\} \exp\left(-\frac{T^2}{2} \right)$$

$$(2.59)$$

respectively.

Both Edgeworth's and Gram-Charlier's series are used in statistics to describe non-Gaussian frequency distributions. For that purpose the series are truncated after the first few terms, because higher order terms are increasingly difficult to obtain accurately from measuring data, which are always subject to some scattering. An example of the use of Edgeworth's series in the field of hydrology is Chatwin (1980), who fitted longitudinal dispersion data that showed a definite non-Gaussian behavior. The Gram-Charlier expansion was recently used by Van Mazijk et al. (1989) to model pollution of the Rhine river.

Using (2.53) and the orthogonality property (2.56), it can be verified that truncation of Edgeworth's expansion and Gram-Charlier's series at the dots in (2.51) and (2.54), respectively, does not influence the mean μ, the standard deviation σ, the skewness $\overset{1}{\gamma}$ nor the excess $\overset{2}{\gamma}$ of $c_{\text{out}}(T)$. The functions represented by the truncated series, however, are no longer unconditionally unimodal. They may even become negative on some intervals of T. Barton and Dennis (1952) investigated the conditions on $\overset{1}{\gamma}$ and $\overset{2}{\gamma}$, under which positive definiteness and unimodality are secured. We have extended their analysis a little, because positive definiteness seems to be too strict a condition for practical purposes: slightly negative values at the tip or at the toe of an impulse response function may be acceptable, considering that the series are approximations anyway (Chatwin, 1980). Our results are shown in Figure 2.7 for the Gram-Charlier series, and in Figure 2.8 for Edgeworth's expansion.

Let us first consider Figure 2.7. Generally speaking, the graph of $c_{\text{out}}(T)$, calculated by means of the truncated series of Gram-Charlier, may show negative
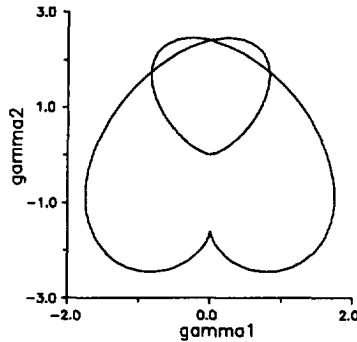
Figure 2.7   *Combinations of $\overset{1}{\gamma}$ and $\overset{2}{\gamma}$ for which the second derivative of the truncated series of Gram-Charlier vanishes.*
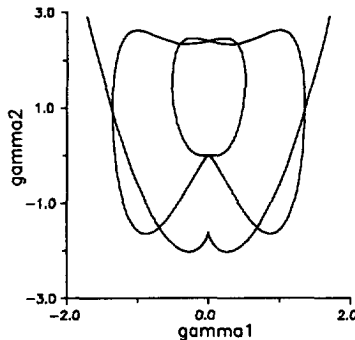
Figure 2.8   *Combinations of $\overset{1}{\gamma}$ and $\overset{2}{\gamma}$ for which the second derivative of the truncated series of Edgeworth vanishes.*

parts and dips. We have depicted in Figure 2.7 those combinations of $\overset{1}{\gamma}$ and $\overset{2}{\gamma}$ for which the graph of $c_{\text{out}}(T)$ has at least one point of inflexion with zero gradient. Crossing one of the curves of Figure 2.7, by varying $\overset{1}{\gamma}$ and $\overset{2}{\gamma}$ continuously, there appears or disappears a dip in the corresponding graph of $c_{\text{out}}(T)$. It turns out that there are no dips in the negative parts of $c_{\text{out}}(T)$ if the image of $(\overset{1}{\gamma}, \overset{2}{\gamma})$ falls within the smaller heart-shaped region of Figure 2.7. Hence, in that case, $c_{\text{out}}(T)$ can have no negative parts at all and must be positive definite there. If the image of $(\overset{1}{\gamma}, \overset{2}{\gamma})$ falls within the bigger heart-shaped region, then $c_{\text{out}}(T)$ turns out to have no dips in its positive parts. Consequently, $c_{\text{out}}(T)$ is positive definite and unimodal if $(\overset{1}{\gamma}, \overset{2}{\gamma})$ lies within the intersection of the two hearts. The interpretation of Figure 2.8, which goes for the truncated Edgeworth's expansion, is fully similar. It appears that the region of unimodality and positive

definiteness is very limited indeed. Chatwin (1980), being somewhat less strict, recommends to stay within the region where both $\overset{1}{\gamma}$ and $\overset{2}{\gamma}$ are at most one. It is our experience that $\overset{2}{\gamma}$ may vary up to four, before the use of Edgeworth's expansion or Gram-Charlier's series for the purpose of data fitting becomes really questionable. Unfortunately, values of $\overset{1}{\gamma}$ and $\overset{2}{\gamma}$ encountered in contaminant transport are frequently found to be much higher. As $\overset{1}{\gamma}$ and $\overset{2}{\gamma}$ decrease with the distance travelled, the expressions (2.58) and (2.59) become eventually useful to describe breakthrough curves at some distance from a spill. As such, they are an improvement, indeed, of the Gaussian limit (2.36). As will be seen in the next chapter, it is possible, in many problems of contaminant transport, to express $\overset{1}{\gamma}$ and $\overset{2}{\gamma}$ as functions of the distance of transportation. In such cases, the distance from the source of contamination at which Edgeworth's expansion or Gram-Charlier's series start to be applicable, can be determined beforehand.

Using Gram-Charlier or Edgeworth in this fashion guarantees correctness of the first four moments. There is no guarantee that higher order moments are not far off. It would be more satisfactory, therefore, to have a criterion that tells us when (that is: at what distance from a source of pollution) the contribution of higher order moments becomes negligible. We leave this question for future research.

2.6 Other ways to describe breakthrough profiles

The rather frustrating breakdown of the skew convolutional limits of Section 2.5 at shorter distances from the source urges us to look for alternative ways to describe dispersive transport of groundwater. Two of them are discussed in the current section.

What we did (or, rather, attempted to do) in the last section was, essentially: to describe an impulse response function approximately in terms of its first moments. The motivating idea is that we sometimes know the moments of an impulse response, while the impulse response itself is unknown or hard to calculate. The "problem of moments" is a classical one, put forward by such famous mathematicians as Chebyshev, Markov, and Stieltjes, and elaborated by many others. A concise historical review can be found in the introduction to Shohat and Tamarkin (1943). The problem of moments is concerned with the conditions under which a sequence of real quantities M_0, M_1, M_2, ... determines a distribution. The results can be used to approximate a breakthrough curve by a staircase function. (This is equivalent, of course, to approximating an impulse response function by a series of pulses). Von Mises (1964) gives a very clear account of the appealing procedure, of which we highlight some of the particulars.

Assume that the first $2m$ moments M_0 through M_{2m-1} of an impulse response function $c(t)$ are given. We want to find the m-pulse distribution that has precisely these moments. The abcissa of the pulses are a_1, $a_2, \ldots, a_m$ and their

magnitudes are $A_1, A_2, \ldots, A_m$. This problem can be shown to have a unique solution, that is: the a_i and A_i are single valued and the A_i are non-negative. The following equations hold:

$$M_k = \int t^k c(t)dt = \sum_{i=1}^{m} a_i^k A_i \qquad k = 0, 1, \ldots, 2m-1 \qquad (2.60)$$

which set suffices to solve for the a_i and A_i. Although (2.60) has a highly non-linear appearance, Von Mises presents a nice maneuver that changes the problem into a linear alternative. The equations of (2.60) are multiplied by some constants and combined to give

$$\int P(t)c(t)dt = \sum_{i=1}^{m} P(a_i)A_i \qquad (2.61)$$

Here, $P(t)$ is any polynomial in t, whose order is not higher than $(2m-1)$. If we introduce the polynomial of order m,

$$\omega(t) = (t - a_1)(t - a_2) \ldots (t - a_m) = t^m + \sum_{i=0}^{m-1} c_i t^i \qquad (2.62)$$

we can use for $P(t)$ any of the expressions

$$\omega(t), \ t\omega(t), \ t^2\omega(t), \ldots, \ t^{m-1}\omega(t) \qquad (2.63)$$

Since each of these expressions vanishes if one of the a_i is introduced for t, it is seen that with these choices for $P(t)$, the right-hand term of (2.61) vanishes. Consequently, the left-hand term must vanish also. This means that, with $j = 0, 1, \ldots, m-1$

$$0 = \int t^j \omega(t)c(t)dt = \int \left\{ t^{m+j} + \sum_{i=0}^{m-1} c_i t^{i+j} \right\} c(t)dt$$

$$= M_{m+j} + \sum_{i=0}^{m-1} c_i M_{i+j} \qquad (2.64)$$

In matrix form:

$$\begin{bmatrix} M_0 & M_1 & \cdots & M_{m-1} \\ M_1 & M_2 & \cdots & M_m \\ \vdots & \vdots & \vdots & \\ M_{m-1} & M_m & \cdots & M_{2m-2} \end{bmatrix} \begin{bmatrix} c_0 \\ c_1 \\ \vdots \\ c_{m-1} \end{bmatrix} = - \begin{bmatrix} M_m \\ M_{m+1} \\ \vdots \\ M_{2m-1} \end{bmatrix} \qquad (2.65)$$

The square matrix is of the Toeplitz-type, for which very efficient numerical routines are readily available (Press et al., 1992). The relations between the

c_i and the a_i follow from (2.62). Once the a_i have been found, the A_i can be computed from the first m equations of (2.60), which in matrix form read

$$
\begin{bmatrix}
1 & 1 & \cdots & 1 \\
a_1 & a_2 & \cdots & a_m \\
\vdots & \vdots & & \vdots \\
a_1^{m-1} & a_2^{m-1} & \cdots & a_m^{m-1}
\end{bmatrix}
\begin{bmatrix}
A_1 \\
A_2 \\
\vdots \\
A_m
\end{bmatrix}
=
\begin{bmatrix}
M_1 \\
M_2 \\
\vdots \\
M_m
\end{bmatrix}
\tag{2.66}
$$

Here we meet with a Vandermonde matrix, which can also be handled very efficiently (Press et al., 1992). The whole procedure is now neatly presented by just two matrix equations of special types. Although Von Mises's method converges theoretically to the true breakthrough curve, we will see in the next chapter that (in our applications) numerical problems start to occur from the twentieth moment or so, the reason being that higher order moments can assume large values indeed. Figure 2.9 gives an example of a breakthrough curve, approximated by a staircase function, using twenty-two moments. Twenty-two moments yield eleven steps. Not all of them differ significantly from zero, so that the approximation looks rather crude.
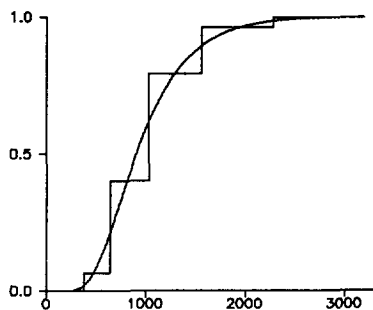
Figure 2.9 *A breakthrough curve approximated by a staircase function.*

Figure 2.9 shows that the true breakthrough curve cuts all of the steps and rises of the staircase. This is not a coincidence: Von Mises proves this to be a rule. In fact, the steps and rises are cut almost in the middle, such that the middle points give a fair impression of the breakthrough curve. This is illustrated by Figure 2.10. As the staircase function converges to the true breakthrough curve, this must also be true for the middle points.

Unlike the series of Gram-Charlier and Edgeworth, Von Mises' method shows no tendency to degenerate near the source, but the number of midpoints that can be evaluated there without numerical problems, tends to be small.

We now take quite another point of view, noticing one more time that any convolutional process can, in a way, be regarded as a model of dispersive
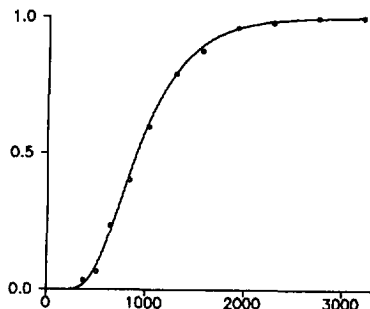
Figure 2.10   *The same breakthrough curve as in Figure 2.9, approx-imated by the midpoints of the steps and rises.*
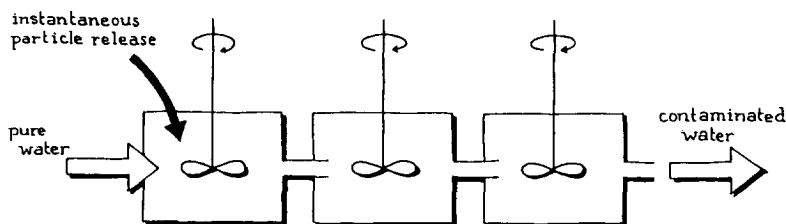
Figure 2.11   *The mixing reservoirs model.*

groundwater transport, thanks to the existence of the Gaussian limit. Neverthe-less, models that show at least some analogy, however crude, to the mechanism of groundwater transport, are likely to do a better job than models that don't. They may produce the correct breakthrough curve before the Gaussian limit is reached. In other words: some of the moments of order three and up may as-sume the correct values before their effect on the shape of the breakthrough curve becomes negligible. A very simple model of this kind is the mixing reservoirs model (Figure 2.11), that has the mixing of particles in common with dispersion of groundwater. It is supposed that all particles entering a reservoir are instan-taneously and completely mixed therein, which can be achieved by constant and thorough stirring of the reservoir contents. The impulse response of a single mixing reservoir is well known to be

$$\theta(t) = ae^{-at} \qquad (t \geq 0) \tag{2.67}$$

where a is a reservoir characteristic. The response of the nth reservoir is found by n-fold convolution of $\theta(t)$:

$$\theta_n(t) = \frac{a^n t^{n-1}}{(n-1)!} e^{-at} \qquad (t \geq 0) \tag{2.68}$$

Regarded as a function of t, (2.68) is a distribution function, known as the gamma-distribution (Von Mises, 1964, p 248). $\theta_n(t)$ is also a distribution function if considered as a function of n, known as Poisson's distribution (Von Mises, [1964] p 138). $\theta_n(t)$ approaches a Gauss-curve of t if n approaches infinity. $\theta_n(t)$ approaches a Gauss-curve of n if t approaches infinity. Although, in the model of Figure 2.11, n is a discrete number, it is possible to interpolate smoothly between any two integer values, if $(n-1)!$ is generalized to $\Gamma(n)$ (Abramowitz and Stegun, 1964, p 255):

$$\theta_n(t) = \frac{a^n t^{n-1}}{\Gamma(n)} e^{-at} \qquad (t \geq 0) \tag{2.69}$$

We intend to use (2.69) not so much as a model of dispersion, as well as an approximative function to describe dispersive groundwater transport, just as we did with the truncated series of Edgeworth and Gram-Charlier, in Section 2.5. As such, the degrees of freedom of (2.69) are very scarce: two parameters, a and n, allow only for the matching of the mean and the standard deviation. Yet we are especially interested in matching the skewness. A third degree of freedom can be introduced by allowing for a shift along the t-axis:

$$\theta_n(t) = \frac{a^n (t-b)^{n-1}}{\Gamma(n)} e^{-a(t-b)} \qquad (t \geq b) \tag{2.70}$$

(This function is understood to be zero if $t < b$). In the shape (2.70) $\theta_n(t)$ is known as the Pearson type III distribution. It is not mentioned as such in Von Mises (1964), but the reader can be referred to almost any textbook on statistics, for instance Haan (1986), p 119. Its characteristics are

$$\mu = \frac{n}{a} + b \tag{2.71}$$

$$\sigma = \frac{\sqrt{n}}{a} \tag{2.72}$$

$$\frac{1}{\gamma} = \frac{2}{\sqrt{n}} \tag{2.73}$$

and inversely:

$$a = \frac{2}{\frac{1}{\gamma}\sigma} \tag{2.74}$$

$$n = \frac{4}{(\frac{1}{\gamma})^2} \tag{2.75}$$

$$b = \mu - \frac{2\sigma}{\frac{1}{\gamma}} \tag{2.76}$$

The breakthrough curve corresponding to Pearson-III is the so called incomplete gamma function (Abramowitz and Stegun, 1964, p 260), shifted along the time

axis $(t \rightarrow t - b)$. Figure 2.12 gives an impression of the general behavior of the implete gamma function for increasing values of n. We will see in the next chapter that Pearson type III is a most useful function to model dispersive groundwater flow, if the first three moments are given. In anticipation of the next chapter we note that the mixing process according to this model is non-Fickian. The "dispersive" flux in any point depends on the upstream concentration gradient, whereas the dispersive flux according to Fick's law would be proportional to the central gradient. In addition there is no upstream transport, as there is in Fickian dispersion.
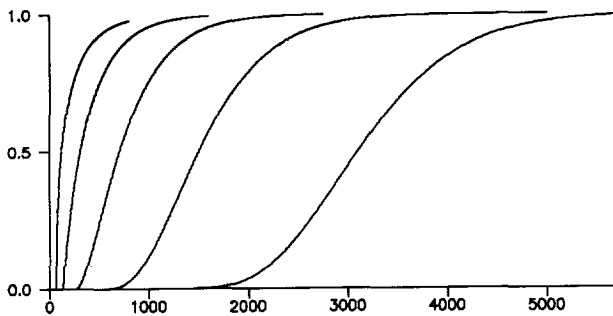

Figure 2.12   *General behavior of breakthrough curves derived from
                   the Pearson type III distribution. Horizontal axis: time.
                   Vertical axis: dimensionless concentration.*

The gamma distribution (not Pearson type III) has been proposed earlier by Jury (Jury and Roth, 1990) as a model of dispersion, along with the log-normal distribution. Jury speaks of Travel Time Probability Density Functions instead of impulse responses. He regards the Travel Time PDF as an integral soil property, to be measured in the field.

This place seems to be as good as any to make some additional remarks on concentrations and contaminant breakthrough. We have not given a definition, but concentration is intuitively understood to be an amount of particles per unit of volume. The exact place of the particles within the volume does not occur in this definition. In flow through heterogeneous media the exact place of the particles does matter. For instance, if all particles are located in an immobile zone, a groundwater sample would show zero concentration. The situation is less evident, and the more confusing , if the groundwater velocity varies from place to place. It is important, therefore, to distinguish between *volume-averaged* and *flux-averaged* concentrations. (The ratio of the two might be useful as a parameter to characterize a degree of mixing. Mixing can be said to be complete if the volume averaged concentration equals the flux averaged concentration, i.e. if their ratio is one). Our illumination of the convolution-concept by means of Figure 2.1 may have raised the suggestion that, for the principle to apply, mixing

must be complete at the points where a signal is transferred from one system to the next. This is not necessarily the case, as the following example shows.

Suppose that an originally straight front of some intruding contaminant is split up into two parts after travelling a distance l. (Figure 2.13). One part, having width p, travels on at velocity v_1, and the other part, having width q, travels on at velocity v_2. Suppose that the process repeats itself every time another distance l has been covered, thus producing ever thinner fingers. Although highly stylized, this is not at all unlike the way actual fronts progress through heterogeneous media. For comparison Figure 2.14 shows the deformation of a moving front in a heterogeneous medium that we will examine in more detail in Chapter 4.
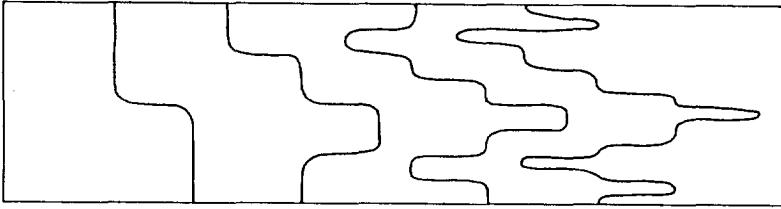
Figure 2.13 *Breaking up of a front according to the binomial process.*
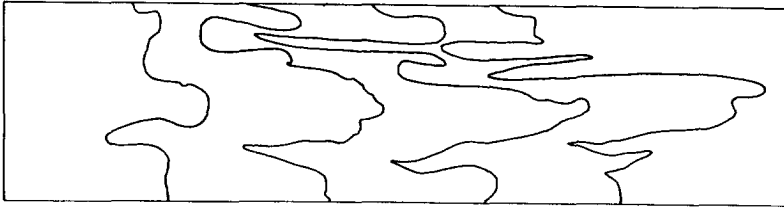
Figure 2.14 *Breaking up of a front in the heterogeneous medium to be introduced in Chapter 4. (Courtesy J. C. Panda, Univ. of Minn.)*

The breakthrough curve at a distance nl from the origin is a staircase function, whose steps are given by the binomial distribution:

$$c_j = \binom{n}{j} p^{n-j} q^i \qquad (j = 0, n) \tag{2.77}$$

(Von Mises, 1964, p 168). The breakthrough time of the jth step is given by

$$t_j = (n - j)\frac{l}{v_p} + j\frac{l}{v_q} \tag{2.78}$$

As (2.77) is a distribution function the convolution principle applies and the Central Limit Theorem guarantees convergence to the Gaussian limit, although complete mixing is achieved only asymptotically.

2.7 The bank groundwater plant in retrospect

Although we did not yet refer to the bank groundwater plant, all conclusions drawn in this chapter apply to bank groundwater as well. Unlike equal sections along a straight stream tube, the subsystems depicted in Figure 1.3 were seen to be quite dissimilar. The Central Limit Theorem in its general form pertains to series of systems with different impulse responses, though, and the Gaussian-like response of the composite system, that we described in the introduction to this thesis, turns out to be in no way coincidental. It is not necessary, therefore, to model the subsystems in much detail, in order to obtain a good idea of the impulse response of the plant as a whole. Crude models, that yield mean travel times and variances and, possibly, skewnesses of subsystems are sufficient. Even if they would not yield a complete picture of the breakthrough curve, they give exact information on its first three moments.

There is nothing in the proof of the Central Limit Theorem that requires the subsystems to be physically alike. If the water company would be interested in the risks of norm violation at a consumer's tap, following a hazardous spill in the catchment area of the river, the chain of subsystems could be extended straightforwardly to include, say, leakage from a nuclear power plant, overland flow, dispersive transport by the river, flow through the purification plant and transport through the distribution network. The longer the chain, the more likely the response is to become fully Gaussian and the less sense there is in modeling the subsystems in great detail.

2.8 Appendix

2.8.1 *Introduction*

This appendix can be omitted at first reading of the thesis. It contains a heuristic proof that, under certain conditions, a series of linear systems with impulse response functions of different shapes must produce an impulse response function that tends to assume the Gaussian shape. We end up with an expression that applies already in an earlier stage, when the Gaussian limit has not yet been reached. (As a matter of fact, this expression turns out to be Edgeworth's expansion, as already presented in Section 2.5). In the course of the derivation, certain conditions are imposed on the shapes of the admissible impulse response functions. They are summarized and discussed from a point of view of contaminant transport. In addition, we also consider parallel series of linear systems. In

$\bar{\theta}_1(\omega)$	$\bar{\theta}_2(\omega)$	$\cdots\cdots\cdots$	$\bar{\theta}_n(\omega)$
$\bar{\theta}_1(0)$	$\bar{\theta}_1(0)$	$\cdots\cdots\cdots$	$\bar{\theta}_n(0)$
$\dfrac{\omega}{1!}\bar{\theta}_1'(0)$	$\dfrac{\omega}{1!}\bar{\theta}_2'(0)$	$\cdots\cdots\cdots$	$\dfrac{\omega}{1!}\bar{\theta}_1'(0)$
$\dfrac{\omega}{21!}\bar{\theta}_1''(0)$	$\dfrac{\omega}{2!}\bar{\theta}_2''(0)$	$\cdots\cdots\cdots$	$\dfrac{\omega}{2!}\bar{\theta}_n''(0)$
$\vdots$	$\vdots$		$\vdots$
$\vdots$	$\vdots$		$\vdots$

Table 2.1 *Terms of the Taylor series of $\bar{\theta}_1(\omega)$*

order to enhance the presentation of this somewhat long-winded section, we use the Halmos symbol ▮ to mark the end of a logical unit, such as a conclusion of an argument or a remark.

2.8.2 *Conditions under which a series of linear systems produce a Gaussian impulse response*

Our starting point is (2.5), which upon Fourier transformation gave (2.6). (Notice that it is implicitly assumed that the impulse response functions are Fourier transformable indeed). Without loss of generality one may assume that $c_{\text{in}}(t)$ is Dirac's delta, so $\bar{c}_{\text{in}}(\omega) = 1$ and (2.6) assumes the simplified form

$$\bar{c}_{\text{out}}(\omega) = \bar{\theta}_1(\omega) \cdot \bar{\theta}_2(\omega) \ldots \bar{\theta}_n(\omega) \tag{A.1}$$

The functions in the right-hand side of this equation are expanded in their Taylor series. (The Taylor series of $\bar{\theta}_i(\omega)$ reads

$$\bar{\theta}_i(\omega) = \bar{\theta}_i(0) + \frac{\omega}{1!}\bar{\theta}_i'(0) + \frac{\omega^2}{2!}\bar{\theta}_i''(0) + \ldots$$

so the following approach is confined to impulse response functions whose Fourier transforms show no singularities at $w = 0$. This is another assumption to be kept in mind).

Multiplication of n Taylor series yields a new power series of ω, the first terms of which are easily found:

$$T_0 = \bar{\theta}_1(0) \cdot \bar{\theta}_2(0) \ldots \bar{\theta}_n(0) \tag{A.2}$$

$$T_1 = \frac{\omega}{1!}\{\bar{\theta}_1'(0)\bar{\theta}_2(0) \ldots \bar{\theta}_n(0)$$
$$+ \{\bar{\theta}_1(0)\bar{\theta}_2'(0) \ldots \bar{\theta}_n(0)$$
$$\vdots$$
$$+ \{\bar{\theta}_1(0)\bar{\theta}_2(0) \ldots \bar{\theta}_n'(0)\} \tag{A.3}$$

The following terms, however, become increasingly complex. Therefore, we take recourse to a shorthand notation. The functions in the right-hand side of (A.1) are lined up in the diagram of Table 2.1, along with the terms of their Taylor series. A shorthand version of this table is shown in Table 2.2.

	$\bar{\theta}_1$	$\bar{\theta}_2$	$\cdots$	$\bar{\theta}_n$
1	0	0	$\cdots$	0
$\omega/1!$	1	1	$\cdots$	1
$\omega^2/2!$	2	2	$\cdots$	2
.	.	.		.
.	.	.		.
.	.	.		.
$\omega^r/r!$	r	r	$\cdots$	r
.	.	.		.
.	.	.		.
.	.	.		.

Table 2.2   *Shorthand version of table 2.1*

Any term occurring in the power series of the product $\bar{\theta}_1 \cdot \bar{\theta}_2 \ldots \bar{\theta}_n$ can now be represented by a numerical string, which is formed by picking numbers from Table 2.2, going from left to right. For example, the string $[1\,0\,3\,\ldots\,]$ stands for

$$[1\,0\,3\,\ldots] = \frac{\omega}{1!}\bar{\theta}'_1(0) \cdot \bar{\theta}_2(0) \cdot \frac{w^3}{3!}\bar{\theta}'''_3(0)\ldots \tag{A.4}$$

As there are n functions in the right-hand side of (A.1), all strings in Table 2.2 contain n digits. A little thought makes clear that, when the digits of a string add up to r, then the string contributes to the coefficient of w^r. For instance $[1\,0\,3\,0\,0\,\ldots\,0]$ contributes to the coefficient of $\omega^{1+3} = \omega^4$. In more detail, the contribution of this string contains a factor

$$\frac{\omega}{1!} \cdot \frac{\omega^3}{3!}$$

and one needs to keep track of the denominators in this expression, too. ∎

As we intend to group the strings of Table 2.2 according to powers of ω, it is natural to ask: which strings contribute to the coefficient of, say, ω^3? And, moreover, how many such strings are there? It is clear that the number 3 can be *partitioned* in different ways:

$$\begin{aligned} 3 &= 1 + 1 + 1 \\ &= 1 + 2 \\ &= 2 + 1 \\ &= 3 \end{aligned}$$

In fact, there exist 2^{3-1} partitions. The strings belonging to the first partition contain three ones and $(n-3)$ zeros. Their contributions share a common factor

$(\omega/1!)^3$. According to the definition of binomial coefficients, there are $\binom{n}{3}$ such strings. They look like

$$[1\,1\,1\,0\,0\,0\ldots], \ [1\,1\,0\,1\,0\,0\ldots], \ [1\,1\,0\,0\,1\,0\ldots], \ \text{etc.}$$

The strings belonging to the second partition contain one 1 and one 2, and $(n-2)$ zeros. Here, the number 1 should always stay to the left of the number 2. Their contributions share a common factor $(\omega/1! \cdot \omega^2/2!)$ and there are $\binom{n}{2}$ such strings. They look like

$$[1\,2\,0\,0\,0\,0\ldots], \ [1\,0\,2\,0\,0\,0\ldots], \ [1\,0\,0\,2\,0\,0\ldots], \ \text{etc.}$$

The strings belonging to the third partition are similar; only the numbers 1 and 2 change places. The last partition, finally, yields strings that contain only one 3 and $(n-1)$ zeros. Their contributions share a common factor $(\omega^3/3!)$ and their number is $\binom{n}{1}$. ∎

The above is easily generalized: if one considers ω^r, then there exist 2^{r-1} partitions. The number of digits differing from zero range from 1 to r. If a partition contains k such digits, $1 \le k \le r$, then there belong $\binom{n}{k}$ strings to that particular partition, where n is the number of functions $\bar{\theta}_i$.

To become less abstract, the product of the Taylor series of n functions has been worked out in Table 2.3. The resulting n-digit strings are grouped according to powers of ω. The table has been truncated after ω^4. It can easily be extended to higher powers of ω, but the current table is believed to give a good idea of what the coefficient of an arbitrary power of ω will look like. ∎

As centralized moments are useful characteristics of an impulse response function, we decide to proceed our analysis in terms of centralized impulse response functions. This is conveniently accomplished in the Fourier domain, as

$$\int_{-\infty}^{+\infty} \theta(t-\mu)e^{i\omega t}dt = e^{i\omega\mu}\int_{-\infty}^{+\infty} \theta(t)e^{i\omega t}dt = e^{i\omega\mu}\bar{\theta}(\omega)$$

and thus

$$\bar{\theta}(\omega) = e^{-i\omega\mu}\overset{c}{\bar{\theta}}(\omega) \tag{A.5}$$

where $\overset{c}{\bar{\theta}}(\omega)$ is the Fourier transform of the centralized impulse response function. Hence, it follows that (A.1) can be written as

$$\bar{c}_{\text{out}}(\omega) = e^{i\omega\sum_1^n \mu_i}\overset{c}{\bar{\theta}}_1(\omega) \cdot \overset{c}{\bar{\theta}}_2(\omega)\ldots\overset{c}{\bar{\theta}}_r(\omega) \tag{A.6}$$

By centralization, the first derivatives of $\overset{c}{\bar{\theta}}_i(\omega)$, evaluated at $\omega = 0$, become zero. Now table 2.3, if applied to centralized functions, cleans up considerably: all strings containing at least one digit 1 become zero. The reduced table is shown

power of ω	# of partitions	# of strings	strings look like	common factors
0	—	$\binom{n}{0}$	$[0000\cdot\cdot]$	1
1	$2^{1-1}=1$	$\binom{n}{1}$	$[1000\cdot\cdot][0100\cdot\cdot]$ etc	$\dfrac{\omega}{1!}$
2	$2^{2-1}=1$	$\binom{n}{1}$	$[2000\cdot\cdot][0200\cdot\cdot]$ etc	$\dfrac{\omega^2}{2!}$
		$\binom{n}{2}$	$[1100\cdot\cdot][1010\cdot\cdot]$ etc	$\left(\dfrac{\omega}{1!}\right)^2$
3	$2^{3-1}=4$	$\binom{n}{1}$	$[3000\cdot\cdot][0300\cdot\cdot]$ etc	$\dfrac{\omega^3}{3!}$
		$\binom{n}{2}$	$[2100\cdot\cdot][2010\cdot\cdot]$ etc	$\dfrac{\omega^2}{2!}\dfrac{\omega}{1!}$
		$\binom{n}{2}$	$[1200\cdot\cdot][1020\cdot\cdot]$ etc	$\dfrac{\omega}{1!}\dfrac{\omega^2}{2!}$
		$\binom{n}{3}$	$[1110\cdot\cdot][1101\cdot\cdot]$ etc	$\left(\dfrac{\omega}{1!}\right)^3$
4	$2^{4-1}=8$	$\binom{n}{1}$	$[4000\cdot\cdot][0400\cdot\cdot]$ etc	$\dfrac{\omega^4}{4!}$
		$\binom{n}{2}$	$[3100\cdot\cdot][3010\cdot\cdot]$ etc	$\dfrac{\omega^3}{3!}\dfrac{\omega}{1!}$
		$\binom{n}{2}$	$[2200\cdot\cdot][2020\cdot\cdot]$ etc	$\left(\dfrac{\omega^2}{2!}\right)^2$
		$\binom{n}{2}$	$[1300\cdot\cdot][1030\cdot\cdot]$ etc	$\dfrac{\omega}{1!}\dfrac{\omega^3}{3!}$
		$\binom{n}{3}$	$[2110\cdot\cdot][2101\cdot\cdot]$ etc	$\dfrac{\omega^2}{2!}\left(\dfrac{\omega}{1!}\right)^2$
		$\binom{n}{3}$	$[1210\cdot\cdot][1201\cdot\cdot]$ etc	$\dfrac{\omega}{1!}\dfrac{\omega^2}{2!}\dfrac{\omega}{1!}$
		$\binom{n}{3}$	$[1120\cdot\cdot][1102\cdot\cdot]$ etc	$\left(\dfrac{\omega}{1!}\right)^2\dfrac{\omega^2}{2!}$
		$\binom{n}{4}$	$[1111\cdot\cdot][11101\cdot]$ etc	$\left(\dfrac{\omega}{1!}\right)^4$

Table 2.3   *Elaboration of the product of n Taylor series (truncated after ω^4)*

as Table 2.4. For future purposes, this table has been extended up to the eighth

power of ω. ∎

It is seen from the column "# of strings" that some partitions contribute more to a particular power of ω than others do. As a matter of fact,

$$\frac{\binom{n}{r}}{\binom{n}{r-1}} = \frac{n}{r} \qquad (A.7)$$

which shows that a group of $\binom{n}{r}$ strings will contain infinitely more strings than a group of $\binom{n}{r-1}$ strings, as $n \to \infty$. In Table 2.4 the groups of strings have been lined up in order of increasing magnitude, for each power of ω. It becomes clear that, for even powers of ω, strings containing only second derivatives outnumber all the others if $n \to \infty$. Their number is $\binom{n}{\frac{r}{2}}$, where r is the power of ω. Odd powers of ω become dominated in number by strings that contain second derivatives and just one third derivative. Their number is $\binom{n}{\frac{r-1}{2}}$. ∎

In order to be more specific, let us attach an order of magnitude to each group of strings. It has already been assumed that all Taylor series involved converge. Then each of them must have a largest coefficient. From these n coefficients we pick again the largest one, which has magnitude $\mathcal{A}$, say. Now we are able to indicate upperbounds for the groups of strings in Table 2.4. This has been worked out in Table 2.5. ∎

One may notice that

$$\frac{1}{n^r} \binom{n}{r} \leq \frac{1}{r!} \qquad (A.8)$$

the right-hand value being approached if $n \to \infty$. Accounting for this, Table 2.5 has been reworked in terms of powers of $\omega\sqrt{n}$ rather than ω. (see Table 2.6). ∎

It appears from the last column of Table 2.5 that terms involving odd powers of $\omega\sqrt{n}$ tend to disappear if n increases. So, if the product of n Taylor series is expressed as a power series of $\omega\sqrt{n}$, the result tends to become a function that is symmetric about the origin. This interesting conclusion is not definite, though, because we did not indicate lower bounds of the coefficient of ω^r. One can still think of series of linear systems that will never yield a symmetrical output signal. This is the case, for instance, if none of the impulse response functions has non-zero even centralized moments. We purposely exclude such cases by requiring the impulse response functions to be non-negative, which guarantees the existence of positive even centralized moments of any order. Under this restriction we may rightly conclude that the product tends to become a symmetrical function. (Our restriction is justified in view of the application that we have in mind, i.e., transport of contaminants through porous media. Negative impulse response functions would imply the existence of negative concentrations, which seems to be a physical impossibility). ∎

power of ω	# of partitions	# of strings	strings look like	common factors
0	--	$\binom{n}{0}$	$[0000\cdot\cdot]$	1
2	1	$\binom{n}{1}$	$[2000\cdot\cdot][0200\cdot\cdot]$ etc	$\dfrac{\omega^2}{2!}$
3	1	$\binom{n}{1}$	$[3000\cdot\cdot][0300\cdot\cdot]$ etc	$\dfrac{\omega^3}{3!}$
4	2	$\binom{n}{1}$	$[4000\cdot\cdot][0400\cdot\cdot]$ etc	$\dfrac{\omega^4}{4!}$
		$\binom{n}{2}$	$[2200\cdot\cdot][2020\cdot\cdot]$ etc	$\left(\dfrac{\omega^2}{2!}\right)^2$
5	3	$\binom{n}{1}$	$[5000\cdot\cdot][0500\cdot\cdot]$ etc	$\dfrac{\omega^5}{5!}$
		$\binom{n}{2}$	$[3200\cdot\cdot][3020\cdot\cdot]$ etc	$\dfrac{\omega^3}{3!}\dfrac{\omega^2}{2!}$
		$\binom{n}{2}$	$[2300\cdot\cdot][2030\cdot\cdot]$ etc	$\dfrac{\omega^2}{2!}\dfrac{\omega^3}{3!}$
6	5	$\binom{n}{1}$	$[6000\cdot\cdot][0600\cdot\cdot]$ etc	$\dfrac{\omega^6}{6!}$
		$\binom{n}{2}$	$[4200\cdot\cdot][4020\cdot\cdot]$ etc	$\dfrac{\omega^4}{4!}\dfrac{\omega^2}{2!}$
		$\binom{n}{2}$	$[2400\cdot\cdot][2040\cdot\cdot]$ etc	$\dfrac{\omega^2}{2!}\dfrac{\omega^4}{4!}$
		$\binom{n}{2}$	$[3300\cdot\cdot][3030\cdot\cdot]$ etc	$\left(\dfrac{\omega^3}{3!}\right)^2$
		$\binom{n}{3}$	$[2220\cdot\cdot][2202\cdot\cdot]$ etc	$\left(\dfrac{\omega^2}{2!}\right)^3$
7	8	$\binom{n}{1}$	$[7000\cdot\cdot][0700\cdot\cdot]$ etc	$\dfrac{\omega^7}{7!}$
		$\binom{n}{2}$	$[5200\cdot\cdot][5020\cdot\cdot]$ etc	$\dfrac{\omega^5}{5!}\dfrac{\omega^2}{2!}$
		$\binom{n}{2}$	$[2500\cdot\cdot][2050\cdot\cdot]$ etc	$\dfrac{\omega^2}{2!}\dfrac{\omega^5}{5!}$
		$\binom{n}{2}$	$[4300\cdot\cdot][4030\cdot\cdot]$ etc	$\dfrac{\omega^4}{4!}\dfrac{\omega^3}{3!}$
		$\binom{n}{2}$	$[3400\cdot\cdot][3040\cdot\cdot]$ etc	$\dfrac{\omega^3}{3!}\dfrac{\omega^4}{4!}$

		$\binom{n}{3}$	[3220··][3202··] etc	$\dfrac{\omega^3}{3!}\left(\dfrac{\omega^2}{2!}\right)^2$
		$\binom{n}{3}$	[2320··][2302··] etc	$\dfrac{\omega^2}{2!}\,\dfrac{\omega^3}{3!}\,\dfrac{\omega^2}{2!}$
		$\binom{n}{3}$	[2230··][2203··] etc	$\left(\dfrac{\omega^2}{2!}\right)^2\dfrac{\omega^3}{3!}$
8	13	$\binom{n}{1}$	[8000··][0800··] etc	$\dfrac{\omega^8}{8!}$
		$\binom{n}{2}$	[6200··][6020··] etc	$\dfrac{\omega^6}{6!}\,\dfrac{\omega^2}{2!}$
		$\binom{n}{2}$	[2600··][2060··] etc	$\dfrac{\omega^2}{2!}\,\dfrac{\omega^6}{6!}$
		$\binom{n}{2}$	[5300··][5030··] etc	$\dfrac{\omega^5}{5!}\,\dfrac{\omega^3}{3!}$
		$\binom{n}{2}$	[3500··][3050··] etc	$\dfrac{\omega^3}{3!}\,\dfrac{\omega^5}{5!}$
		$\binom{n}{2}$	[4400··][4040··] etc	$\left(\dfrac{\omega^4}{4!}\right)^2$
		$\binom{n}{3}$	[3320··][3302··] etc	$\left(\dfrac{\omega^3}{3!}\right)^2\dfrac{\omega^2}{2!}$
		$\binom{n}{3}$	[3230··][3203··] etc	$\dfrac{\omega^3}{3!}\,\dfrac{\omega^2}{2!}\,\dfrac{\omega^3}{3!}$
		$\binom{n}{3}$	[2330··][2303··] etc	$\dfrac{\omega^2}{2!}\left(\dfrac{\omega^3}{3!}\right)^2$
		$\binom{n}{3}$	[4220··][4202··] etc	$\dfrac{\omega^4}{4!}\left(\dfrac{\omega^2}{2!}\right)^2$
		$\binom{n}{3}$	[2420··][2402··] etc	$\dfrac{\omega^2}{2!}\,\dfrac{\omega^4}{4!}\,\dfrac{\omega^2}{2!}$
		$\binom{n}{3}$	[2240··][2204··] etc	$\left(\dfrac{\omega^2}{2!}\right)^2\dfrac{\omega^4}{4!}$
		$\binom{n}{4}$	[2222··][22202·] etc	$\left(\dfrac{\omega^2}{2!}\right)^4$

Table 2.4   *Elaboration of the product of n Taylor series of functions with zero first derivative (truncated after ω^4)*

There is another interesting feature to be noticed from Table 2.6. It appears that some groups of strings disappear faster than others, as n increases. This finding will be of use later in this appendix. ∎

power of ω	upperbound for the coefficient of ω^r
0	$\binom{n}{0}$
2	$\binom{n}{1}|A|$
3	$\binom{n}{1}|A|$
4	$\binom{n}{1}|A| + \binom{n}{2}|A|^2$
5	$\binom{n}{1}|A| + 2\binom{n}{2}|A|^2$
6	$\binom{n}{1}|A| + 3\binom{n}{2}|A|^2 + \binom{n}{3}|A|^3$
7	$\binom{n}{1}|A| + 4\binom{n}{2}|A|^2 + 3\binom{n}{3}|A|^3$
8	$\binom{n}{1}|A| + 5\binom{n}{2}|A|^2 + 6\binom{n}{3}|A|^3 + \binom{n}{4}|A|^4$

Table 2.5 *Upper bounds for the coefficients of ω^r ($r = 0, 2, 3, \dots$).*
A is the term of largest magnitude from any of the
Taylor series of $\overset{c}{\theta}_i(\omega)$

Going back from Table 2.6 to Table 2.4 we find that the non-vanishing terms in the power series of $\omega\sqrt{n}$ derive from the last groups of strings of the even powers of ω. These groups are entirely composed of zeros and twos. We recall that the zeros stand for the areas of the impulse response functions $\theta_i(t)$, which were 1 by assumption. The twos stand for the second derivatives of $\overset{c}{\theta}_i(\omega)$ evaluated at $\omega = 0$. Therefore, the non-vanishing coefficient of $(\omega\sqrt{n})^{2r}$ ($r = 1, 2, \dots$) is given by

$$\left(\frac{1}{2!}\right)^r * \{\text{sum of all possible products of } r \text{ second derivatives } \overset{c}{\theta}_i''(0)\} \blacksquare \quad \text{(A.9)}$$

We will now outline the proof of a useful theorem (Section 2.8.6): If x_i ($i = 1, n$) are n numbers, then

$$\lim_{n \to \infty} \frac{(x_1 + x_2 + \dots + x_n)^r}{r! \sum \underbrace{x_i x_j \dots x_k}_{\substack{r \text{ factors} \\ i,j,\dots,k=1,n \\ i \neq j \neq \dots \neq k}}} = 1 \quad \text{(A.10)}$$

power of $\omega\sqrt{n}$	upper bound for the coefficient of $(\omega\sqrt{n})^r$	$\lim\limits_{n\to\infty}$
0	1	1
2	$|A|$	$|A|$
3	$\dfrac{1}{\sqrt{n}}|A|$	0
4	$\dfrac{1}{n}|A| + \dfrac{1}{2!}|A|^2$	$\dfrac{1}{2!}|A|^2$
5	$\dfrac{1}{n\sqrt{n}}|A| + \dfrac{2}{2!\sqrt{n}}|A|^2$	0
6	$\dfrac{1}{n^2}|A| + \dfrac{3}{2!n}|A|^2 + \dfrac{1}{3!}|A|^3$	$\dfrac{1}{3!}|A|^3$
7	$\dfrac{1}{n^2\sqrt{n}}|A| + \dfrac{4}{2!n\sqrt{n}}|A|^2 + \dfrac{3}{3!\sqrt{n}}|A|^3$	0
8	$\dfrac{1}{n^3}|A| + \dfrac{5}{2!n^2}|A|^2 + \dfrac{6}{3!n}|A|^3 + \dfrac{1}{4!}|A|^4$	$\dfrac{1}{4!}|A|^4$

Table 2.6 *Upper bounds for the coefficients of $(\omega\sqrt{n})^r$ $(r = 0, 2, 3, \ldots)$*

for any fixed integer r.

Elaboration of the numerator yields $n!$ products of r factors. There are

$$O(n) \text{ products of the form } \quad x_i^r \qquad\qquad (i = 1, n)$$

$$O(n^2) \text{ products of the form } \quad \frac{r!}{r_1!r_2!}x_i^{r_1}x_j^{r_2} \qquad \begin{pmatrix} i, j = 1, n; i \neq j \\ r_1 + r_2 = r \end{pmatrix}$$

$$O(n^3) \text{ products of the form } \quad \frac{r!}{r_1!r_2!r_3!}x_i^{r_1}x_j^{r_2}x_k^{r_3} \quad \begin{pmatrix} i, j, k = 1, n; i \neq j \neq k \\ r_1 + r_2 + r_3 = r \end{pmatrix}$$

$$\vdots$$

$$O(n^r) \text{ products of the form } \quad r!\,\underbrace{x_i x_j \ldots x_k}_{r \text{ factors}} \qquad \begin{pmatrix} i, j, k = 1, n; \\ i \neq j \neq \cdots \neq k \end{pmatrix}$$

The denominator of the fraction in the left-hand side of (A.10) equals the sum of the last mentioned products. As this group of products outnumbers all the others, as $n \to \infty$, by at least one order it follows that the limit expressed by (A.10) equals 1 indeed. ∎

We are now able to replace (A.9) by

$$\left(\frac{1}{2!}\right)^r \cdot \frac{1}{r!} \cdot \left(\text{ sum of all second derivatives } \overset{c}{\bar{\theta}}_i^n(0)\right)^r \tag{A.11}$$

(This step implies the introduction of an error whose *relative* magnitude tends to zero if $n \to \infty$). ∎

Intermezzo:

There exists a direct relation between the moments of $\theta(t)$, defined by (2.23), and the derivatives that occur in the Taylor series of $\bar{\theta}(\omega)$. In order to see this, write (2.23) in the form

$$M_r = \frac{\lim_{\omega \to 0} \int_{-\infty}^{+\infty} t^r \theta(t) e^{i\omega t} dt}{\lim_{\omega \to 0} \int_{-\infty}^{+\infty} \theta(t) e^{i\omega t} dt} \tag{A.12}$$

Integrating by parts it is found that

$$M_r = (-i)^r \frac{\bar{\theta}^{(r)}(0)}{\bar{\theta}(0)} \tag{A.13}$$

where $\bar{\theta}^{(r)}(0)$ indicates the rth derivative of $\bar{\theta}(\omega)$, evaluated at $\omega = 0$. ∎

On basis of (A.13), with $\bar{\theta}(0) = 1$, the second derivatives $\overset{c}{\bar{\theta}}_i''(0)$ equal minus the second centralized moments of $\theta_i(t)$, which by definition of variance equal $-\sigma_i^2$. So (A.11) can in turn be replaced by

$$\left(\frac{1}{2!}\right)^r \cdot \frac{1}{r!} \left\{ \sum_1^n (-\sigma_i^2) \right\}^r ∎ \tag{A.14}$$

Using this expression and (A.6) we finally arrive at the Taylor series expansion of $\bar{c}_{\text{out}}(\omega)$:

$$\bar{c}_{\text{out}}(\omega) \sim e^{i\omega \sum_1^n \mu_i} \cdot \left\{ 1 - \frac{1}{2}\omega^2 \sum_1^n \sigma_i^2 + \frac{1}{2!}\left(\frac{1}{2}\omega^2 \sum_1^n \sigma_i^2\right)^2 \right.$$

$$\left. - \frac{1}{3!}\left(\frac{1}{2}\omega^2 \sum_1^n \sigma_i^2\right)^3 + \frac{1}{4!}\left(\frac{1}{2}\omega^2 \sum_1^n \sigma_i^2\right)^4 - \ldots \right\} \quad (n \to \infty) \tag{A.15}$$

or

$$\bar{c}_{\text{out}}(\omega) \sim e^{i\omega \sum_1^n \mu_i} \cdot e^{-\frac{1}{2}\omega^2 \sum_1^n \sigma_i^2} \quad (n \to \infty) \tag{A.16}$$

Upon Fourier inversion it follows that

$$\boxed{c_{\text{out}}(t) \sim \frac{1}{\sqrt{2\pi\sigma^2}} \exp\left\{ -\frac{(t-\mu)^2}{2\sigma^2} \right\} \quad (n \to \infty)} \tag{A.17}$$

which is a Gaussian curve indeed, with

$$\text{mean } \mu = \sum_1^n \mu_i \qquad (A.18)$$

and

$$\text{variance } \sigma^2 = \sum_1^n \sigma_i^2 \qquad (A.19)$$

So the mean of the Gaussian limit is just the sum of the means of the impulse responses of the systems passed, and the variance is just the sum of their variances.

∎

Tracing back our steps, it is seen that the following assumptions have been made as to the individual systems:
1) they be mathematically linear, in order that the superposition principle hold,
2) their impulse responses have unit area,
3) the impulse responses be Fourier transformable,
4) all derivatives of their Fourier transforms exist at $\omega = 0$,
5) the impulse response functions be positive or zero everywhere.

The first assumption is essential as the convolution principle constitutes the core of the proof of existence of a Gaussian limit.

Assumption 2 is a mere convenience. As will be seen in Section 2.8.4 the condition can be relaxed, in order to yield limits for systems with decay, amplification and internal sources or sinks. These limits are Gaussian, too.

Assumption 3 holds whenever the area of the impulse response function is finite. This adds no new restrictions to those imposed by assumption 2.

Assumptions 4 and 5 seem to be the most intriguing ones. They are probably necessary to obtain the Gaussian limit. The convolutional principle may still apply, however, if the conditions set by these assumptions are not met. One may expect the existence of simple limits for such systems, too, although they are unlikely to be Gaussian. As an example, consider the transfer of changes in groundwater potential through a heterogeneous porous medium. In the one-dimensional case such a medium can be represented by a series of systems having different geohydrological properties. The Fourier transformed impulse response of a particular system out of the series might be given by

$$\bar{\theta}_i(\omega) = A_i e^{-x\sqrt{i\alpha_i\omega}} + (1 - A_i)e^{x\sqrt{i\alpha_i\omega}} \qquad (A.20)$$

where x is a measure of distance while A_i and α_i are characteristics of the system. The convolution principle applies, and the impulse response has unit area, but $\bar{\theta}_i(\omega)$ has no derivative of any order at $\omega = 0$. Consequently, there exists no Taylor series expansion and the method used in this chapter fails. It is nevertheless expected on physical grounds that a limit exist as $n \rightarrow \infty$,

although it will not be a Gaussian limit. Even more challenging is a series where "Gaussian" and "non-Gaussian" systems alternate. Being of interest to the theory of flow through heterogeneous media, these problems can probably be tackled by Laurent series instead of Taylor series. We will not pursue them any further, however, as they are beyond the scope of this thesis. ∎

2.8.3 *Skew-Gaussian convolutional limits*

As stated in the preceding section, plumes of contaminants often show definite tails, even at distances of hundreds of meters from their sources. In this section we will search for limits that show a skewed shape. Use will be made of an extension of theorem (A.10) (Section 2.8.6):

$$\lim_{n \to \infty} \frac{(y_1 + y_2 + \cdots + y_n)(x_1 + x_2 + \cdots + x_n)^{r-1}}{\underbrace{\sum y_i x_j \ldots x_k}_{\substack{r \text{ factors} \\ i,j,\ldots,k=1,n \\ i \neq j \neq \cdots \neq k}}} = 1 \tag{A.21}$$

As we already noticed from Table 2.6, some of the vanishing groups of strings disappear faster than others, as a signal travels through a series of linear systems. The ones to persist longest fade at rate $1/\sqrt{n}$, and they appear to be present in the coefficients of odd powers of $\omega\sqrt{n}$ only. Going back to table 2.4 it is found that these strings are made up of one three and a varying number of twos and zeros. Their contributions to $\bar{c}_{out}(\omega)$ share a common factor $\left(\frac{\omega^2}{2!}\right)^{r-1}\frac{\omega^3}{3!}$ $r = 1, 2, 3, \ldots$). Moreover, there are r partitions producing strings of one three and a varying number of twos and zeros. In view of (A.21) these contributions can be replaced by

$$r \left(\frac{\omega^2}{2!}\right)^{r-1} \frac{\omega^3}{3!} \frac{1}{r!} \left(\sum_1^n \overset{c}{\bar{\theta}}_i'''(0)\right) \left(\sum_1^n \overset{c}{\bar{\theta}}_i''(0)\right)^{r-1} \tag{A.22}$$

as $n \to \infty$. (This step, once again, implies the introduction of an error whose relative magnitude tends to zero as $n \to \infty$.) By virtue of (A.13) and (2.29) one has $\overset{c}{\bar{\theta}}_i''(0) = -\sigma_i^2$ and $\overset{c}{\bar{\theta}}_i''' = -i\overset{1}{\gamma}_i\sigma_i^3$, so (A.22) gives

$$\left(\frac{\omega^2}{2!}\right)^{r-1} \frac{\omega^3}{3!} \frac{1}{(r-1)!} \left(\sum_1^n -i\overset{1}{\gamma}_i\sigma_i^3\right) \left(\sum_1^n -\sigma_i^2\right)^{r-1} \tag{A.23}$$

which upon summation over r yields

$$-\frac{i\omega^3}{3!} \sum_1^n \gamma_i\sigma_i^3 \exp\left(-\frac{1}{2!}\omega^2 \sum_1^n \sigma_i^2\right) \tag{A.24}$$

Decentralization of this expression adds a multiplicative factor $\exp(i\omega \sum_1^n \mu_i)$ (see [A.6]). Fourier inversion finally gives

$$-\frac{1}{3!} \sum_1^n \overset{1}{\gamma}_i\sigma_i^3 \frac{d^3}{dt^3} \left\{ \frac{1}{\sqrt{2\pi \sum_1^n \sigma_i^2}} \cdot \exp\left\{-\frac{(t - \sum_1^n \mu_i)^2}{2 \sum_1^n \sigma_i^2}\right\} \right\} \tag{A.25}$$

This is the contribution of the terms that fade at rate $1/\sqrt{n}$, which has to be added to the Gaussian limit (A.17) in order to obtain a limit that is reached in an earlier phase of the transport process, before the Gaussian develops:

$$c_{\text{out}}(t) \sim \frac{1}{\sqrt{2\pi\sigma^2}}\left\{1 - \frac{1}{3!}\overset{1}{\gamma}\sigma^3\frac{d^3}{dt^3}\right\}\exp\left\{-\frac{(t-\mu)^2}{2\sigma^2}\right\} \quad (n \to \infty) \qquad (A.26)$$

This limit has the same mean and variance as (A.17). Moreover, it has skewness

$$\overset{1}{\gamma} = \frac{1}{\sigma^3}\sum_1^n \overset{1}{\gamma_i}\sigma_i^3 \qquad (A.27)$$

Still earlier limiting shapes may be obtained in a similar fashion. For instance, addition of the terms that fade at rate $1/n$ (see Table 2.6) gives (Section 2.8.7):

$$c_{\text{out}}(t) \sim \frac{1}{\sqrt{2\pi\sigma^2}}\left\{1 - \frac{1}{3!}\overset{1}{\gamma}\sigma^3\frac{d^3}{dt^3} + \frac{1}{4!}\overset{2}{\gamma}\sigma^4\frac{d^4}{dt^4} + \frac{1}{2!}\left(\frac{1}{3!}\overset{1}{\gamma}\sigma^3\right)^2\frac{d^6}{dt^6}\right\}\cdot$$
$$\cdot \exp\left\{-\frac{(t-\mu)^2}{2\sigma^2}\right\} \quad (n \to \infty) \qquad (A.28)$$

which has excess

$$\overset{2}{\gamma} = \frac{1}{\sigma^4}\sum_1^n \overset{2}{\gamma_i}\sigma_i^4 \qquad (A.29)$$

The newly added terms tend to broaden the peak and to shorten the tails of the output signal. The series (A.28) can be extended further by induction (subsection 2.8.8).

2.8.4 *Convolutional limits for parallel series of systems*

Up to this subsection the transferred signal was essentially a scalar function of time. A possible physical interpretation of this assumption is that two consecutive systems are interconnected at a single point through which all the material carrying the signal has to pass. Although many systems of practical importance exhibit this feature, the case of dispersive groundwater flow seems to be more complicated. Two consecutive sections along a stream tube are usually interconnected at several points and the signal transferred between them may differ from one point to another. Moreover, the output signal at a particular point of exit may be related to input signals at more than one point of entrance. Such cases induce us to consider a signal as a vector whose elements are functions of time.

In order to add dimensionality to our discourse, we now consider parallel series of linear systems that allow for transverse interaction (Figure 2.15). The output signals $\overset{i}{c}_{\text{out}}$ depend on all input signals $\overset{i}{c}_{\text{in}}$, and the transformation is effected by all impulse responses in between. In order to guide our thoughts,

examine the coupled system shown in Figure 2.16. For this simple arrangement the relation between input signals and output signals is given by

$$\begin{cases} \overset{1}{c}_{out}(t) = \int \overset{1}{c}_{in}(t - \tau)\theta_{11}(\tau)d\tau + \int \overset{2}{c}_{in}(t - \tau)\theta_{12}(\tau)d\tau \\ \overset{2}{c}_{out}(t) = \int \overset{1}{c}_{in}(t - \tau)\theta_{21}(\tau)d\tau + \int \overset{2}{c}_{in}(t - \tau)\theta_{22}(\tau)d\tau \end{cases} \tag{A.30}$$

which upon Fourier transformation gives

$$\begin{cases} \overset{1}{\bar{c}}_{out}(\omega) = \overset{1}{\bar{c}}_{in}(\omega) \cdot \bar{\theta}_{11}(\omega) + \overset{2}{\bar{c}}_{in}(\omega) \cdot \bar{\theta}_{12}(\omega) \\ \overset{2}{\bar{c}}_{out}(\omega) = \overset{1}{\bar{c}}_{in}(\omega) \cdot \bar{\theta}_{21}(\omega) + \overset{2}{\bar{c}}_{in}(\omega) \cdot \bar{\theta}_{22}(\omega) \end{cases} \tag{A.31}$$

or, in matrix notation

$$\begin{bmatrix} \overset{1}{\bar{c}}_{out} \\ \overset{2}{\bar{c}}_{out} \end{bmatrix} = \begin{bmatrix} \bar{\theta}_{11} & \bar{\theta}_{12} \\ \bar{\theta}_{21} & \bar{\theta}_{22} \end{bmatrix} \begin{bmatrix} \overset{1}{\bar{c}}_{in} \\ \overset{2}{\bar{c}}_{in} \end{bmatrix} \tag{A.32}$$

or

$$\bar{c}_{out} = \mathcal{A}\bar{c}_{in} \tag{A.33}$$

Here, $\bar{c}_{in}$ and $\bar{c}_{out}$ are vectors, while $\mathcal{A}$ is a 2 × 2 matrix. We will call this the *transfer matrix* of the system. This concept is easily extended to a system of m coupled subsystems. Notice that the matrix $\mathcal{A}$ then becomes three-diagonal.
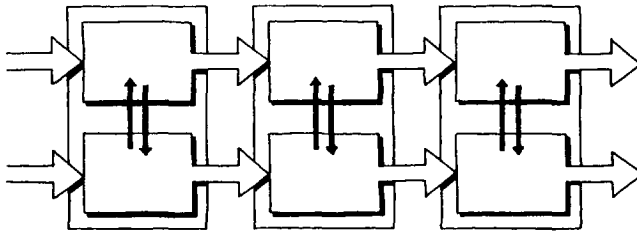
Figure 2.15 *Parallel series of systems with transverse interaction.*
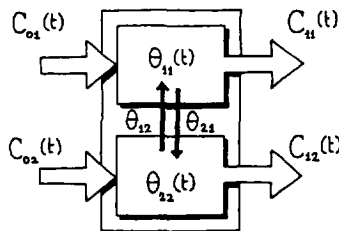
Figure 2.16 *Two parallel systems.*

We are now to find an expression for the output signal in case n such coupled systems are placed in series.

In a first approach, suppose all n coupled systems have the same transfer matrix $\mathcal{A}$. Then the Fourier transformed output signal is given by

$$\bar{c}_{\text{out}} = \mathcal{A}^n \bar{c}_{\text{in}} \tag{A.34}$$

The vector $\bar{c}_{\text{in}}$ can be represented by a linear sum of eigenvectors of $\mathcal{A}$:

$$\bar{c}_{\text{in}} = e_1 + e_2 + \ldots e_m \tag{A.35}$$

By definition of eigenvalue,

$$\mathcal{A} e_i = \lambda_i e_i \tag{A.36}$$

where λ_i is any eigenvalue of $\mathcal{A}$ and e_i is the corresponding eigenvector. So

$$\bar{c}_{\text{out}} = \lambda_1^n e_1 + \lambda_2^n e_2 + \cdots + \lambda_m^n e_m \tag{A.37}$$

Without loss of generality one may assume that λ_1 is the dominant eigenvalue of $\mathcal{A}$. Now write (A.37) in the form

$$\bar{c}_{\text{out}} = \lambda_1^n \left\{ e_1 + \left(\frac{\lambda_2}{\lambda_1} \right)^n e_2 + \ldots \left(\frac{\lambda_m}{\lambda_1} \right)^n e_m \right\} \tag{A.38}$$

then it follows that

$$\bar{c}_{\text{out}} \sim \lambda_1^n e_1 \qquad (n \to \infty) \tag{A.39}$$

This is a classical result of linear algebra, due to Von Mises, which in the present context has some interesting consequences:

* It says that any input signal vector (having finite moments) is eventually converted into the dominant eigenvector of $\mathcal{A}$. So only the strength of the output signal depends on the input signal; not the ratio between its elements.
* As λ_1 is composed of a finite number of Fourier transformed impulse responses, it follows that λ_1 has the properties formulated at the end of Section 2.8.8. If λ_1 has the desired properties, then the Fourier inverse of λ_1^n will show the limit derived in the foregoing sections, as $n \to \infty$.
* *That conclusion, however, applies equally to the other λ_i. Referring to (A.37) we conclude that the output signal consists (eventually) of a series of Gauss-curves. The Gauss-curves associated with the non-dominant eigenvalue decay rapidly, as compared to the one associated with the dominant eigenvalue.*
* *We hasten to emphasize that a decayed Gauss-curve may have a non-zero area. Applied to contaminant transport, this means that the remaining Gauss-curve (the one associated with the dominant eigenvalue) does not necessarily carry all of the contaminant. The rest forms a very long tail of near-zero concentration.*

Notice that the elements of c_{out} are not necessarily identical. This is because the elements of e_1 will not be identical in general (see [A.39]). Each element of e_1 adds its own characteristics to those of λ_1^n. As $n \to \infty$, however, their individual contributions will be negligible, so the elements of $c_{out}(t)$ will eventually approach the same shape.

A more complicated case arises if the transfer matrices are not identical. Let us call them $\mathcal{A}_1, \mathcal{A}_2, \ldots, \mathcal{A}_n$. If there is repetition, such that $\mathcal{A}_i = \mathcal{A}_{k+i} = \mathcal{A}_{2k+i} \ldots$ ($i = 1, k - 1$, k being some integer) then one may define a matrix $\mathcal{B} = \mathcal{A}_1 \cdot \mathcal{A}_2 \ldots \mathcal{A}_{k-1}$, and the preceding analysis applies with respect to $\mathcal{B}$.

We will now regard the case of a non-repetitive series of transferring parallel systems. Equation (A.30) can be written in matrix form as

$$\begin{bmatrix} \overset{1}{c}_{out}(t) \\ \overset{2}{c}_{out}(t) \end{bmatrix} = \int \begin{bmatrix} \theta_{11}(\tau)\theta_{12}(\tau) \\ \theta_{21}(\tau)\theta_{22}(\tau) \end{bmatrix} \begin{bmatrix} \overset{1}{c}_{in}(t - \tau) \\ \overset{2}{c}_{in}(t - \tau) \end{bmatrix} d\tau \qquad (A.40)$$

or

$$c_{out}(t) = \int \Theta(\tau)c_{in}(t - \tau)d\tau \qquad (A.41)$$

The extension to m parallel systems is obvious. Analogous to (2.5) the action of a series of n parallel systems can be described by a multiple convolution integral

$$c_{out}(t) = \iint \cdots \int \Theta_1(\tau_2 - \tau_1) \cdot \Theta_2(\tau_3 - \tau_2) \ldots \Theta_n(t - \tau_n)c_{in}(\tau_1)d\tau_1 d\tau_2 \ldots d\tau_n \qquad (A.42)$$

where the Θ_i are now matrices while c_{in} and c_{out} are vectors. By assumption, the elements of the matrices Θ_i are non-negative. Non-negative matrices possess peculiar properties, for instance the product matrix

$$P = \lim_{n \to \infty} \Theta_1 \cdot \Theta_2 \cdot \ldots \Theta_n \qquad (A.43)$$

was found to have linearly dependent rows and linearly dependent columns, such that all eigenvalues of P are zero, except for one. (An exceptional case occurs if the Θ_i are all unit matrices, which corresponds physically to parallel series of systems without transverse interaction). This limiting behavior is usually apparent already after a few matrix multiplications, as is illustrated by the following arbitrary numerical example:

$$\begin{bmatrix} 1 & 2 & 3 \\ 3 & 2 & 1 \\ 4 & 3 & 2 \end{bmatrix} \begin{bmatrix} 3 & 1 & 5 \\ 2 & 2 & 4 \\ 1 & 3 & 3 \end{bmatrix} \begin{bmatrix} 5 & 1 & 4 \\ 3 & 8 & 2 \\ 1 & 5 & 1 \end{bmatrix} \begin{bmatrix} 1 & 3 & 2 \\ 2 & 4 & 3 \\ 6 & 1 & 1 \end{bmatrix} \begin{bmatrix} 9 & 2 & 8 \\ 7 & 5 & 3 \\ 6 & 1 & 7 \end{bmatrix} = \begin{bmatrix} 25,666 & 10,050 & 20,122 \\ 26,462 & 10,278 & 20,798 \\ 39,494 & 15,360 & 31,028 \end{bmatrix} \qquad (A.44)$$

As can be seen, the rows of the product matrix are (almost) non-integral multiples of each other and so are the columns. Such a matrix P can be written as

$$P = \lambda e \times e^{-1} \qquad (A.45)$$

where λ is the non-zero eigenvalue and e is the corresponding eigenvector. By e^{-1} we mean the inverse of e, such that the inner product

$$e^{-1} \cdot e = 1 \qquad (A.46)$$

The cross in (A.45) denotes the matrix product of e and e^{-1}. Now suppose that one has r matrices P_i that have the same properties as P in (A.45). Then their product can be written as

$$P_1 \cdot P_2 \ldots P_r = \lambda_1 \cdot \lambda_2 \ldots \lambda_r \cdot (e_1 \times e_1^{-1})(e_2 \times e_2^{-1}) \ldots (e_r \times e_r^{-1}) \qquad (A.47)$$

Returning to equation (A.42), it is always possible to write the product $\Theta_1 \cdot \Theta_2 \cdot \ldots \Theta_n$ as the product of r matrices P_i ($r \ll n$) that have property (A.45) if $n \to \infty$:

$$c_{\text{out}}(t) = \iint \cdots \int P_1 \cdot P_2 \ldots P_r c_{\text{in}} d\tau_1 d\tau_2 \ldots d\tau_n \qquad (A.48)$$

or, using (A.47)

$$c_{\text{out}}(t) = \iint \cdots \int \lambda_1 \cdot \lambda_2 \ldots \lambda_r \cdot (e_1 \times e_1^{-1})(e_2 \times e_2^{-1}) \ldots (e_r \times e_r^{-1}) c_{\text{in}} d\tau_1 d\tau_2 \ldots d\tau_n \qquad (A.49)$$

or

$$c_{\text{out}}(t) = \iint \cdots \int \lambda_1 \cdot \lambda_2 \ldots \lambda_r (e_1^{-1} \cdot e_2)(e_2^{-1} \cdot e_3) \ldots (e_r^{-1} \cdot c_{\text{in}}) e_1 d\tau_1 d\tau_2 \ldots d\tau_n \qquad (A.50)$$

Notice that the product $\lambda_1 \cdot \lambda_2 \ldots \lambda_r (e_1^{-1} \cdot e_2)(e_2^{-1} \cdot e_3) \ldots (e_r^{-1} \cdot c_{\text{in}})$ is a product of scalar functions. It follows, therefore, that the elements of $c_{\text{out}}(t)$ are given by a multiple convolution product of scalar functions. By virtue of the preceding sections their limits will be skew-Gaussian as n and r tend to infinity while $n \gg r$. Although the elements of e_1 will not be equal in general, their contributions to the convolution products become negligible as $n \to \infty$. So all elements of $c_{\text{out}}(t)$ will eventually obtain the same shape.

Two additional conclusions can be drawn:
* The index 1 in (A.50) refers to the last series of parallel systems that have been passed by the signal. As the signal travels on, the vector e_1 will be replaced by a new vector, possibly with completely different elements. This means that the limiting shape of $c_{\text{out}}(t)$ will, in general, not be approached in a smooth manner.
* Rearrangement of the order of the matrices P_i in (A.48) has no influence on the shape of $c_{\text{out}}(t)$ because the matrices P_i commute by virtue of (A.45).

Rearrangement of the matrices Θ_i in (A.42), however, may influence the shape of $c_{\text{out}}(t)$. Carried to porous media, this means that rearrangement of groups of inhomogeneities may not influence the shape of a plume, while rearrangement of individual inhomogeneities may.

To conclude this subsection we note that we considered only finite vectors.

2.8.5 *Conclusion and final remarks*

We were able to explain why a signal of finite duration, which passes through a series of linear systems, tends to attain a skew-Gaussian shape. Our demonstration applies only to systems that obey the conditions listed in Section 2.8.2. The subsystems considered for the bank groundwater plant mentioned in Chapter 1 apparently are in this class. One of the imposed conditions can easily be relaxed: it is not strictly necessary that the impulse response functions have unit area. If their areas are unequal to one, the systems show gain or loss: besides altering the shape of a signal they amplify or dampen it. Especially the last phenomenon occurs frequently in groundwater flow, due to interactions of contaminants with the soil matrix or because of their natural decay. The occurrence of gain or loss changes the analysis of Section 2.8.2 just slightly. The only necessary intervention is to divide the functions $\overset{c}{\theta}_i(\omega)$ in (A.6) by $\overset{c}{\theta}_i(0)$ and to multiply (A.18) by $\prod_{i=1}^{n} \overset{c}{\theta}_i(0)$ to make up for it, where $\overset{c}{\theta}_i(0)$ is the area of the impulse response of the ith system. The same goes for the skew limits of Section 2.8.3.

The parameters μ, σ^2, $\overset{1}{\gamma}\sigma^3$ and $\overset{2}{\gamma}\sigma^4$ are all proportional to n, the number of systems passed. If the systems are identical then n is proportional to the distance between an observation point and the point where the signal is generated. (One might think of contaminant transport along a stream tube in a uniform flow field). Calling this distance x we get

$$\mu :: x \tag{A.51}$$

$$\sigma :: \sqrt{x} \tag{A.52}$$

$$\overset{1}{\gamma} :: 1/\sqrt{x} \tag{A.53}$$

$$\overset{2}{\gamma} :: 1/x \tag{A.54}$$

The multiplicative factor $\prod_{i=1}^{n} \overset{c}{\theta}_i(0)$ behaves differently. This factor can be written as

$$\prod_{i=1}^{n} \overset{c}{\theta}_i(0) = e^{\sum_{1}^{n} \ln \overset{c}{\theta}_i(0)} \tag{A.55}$$

which for identical systems gives

$$\prod_{i=1}^{n} \overset{c}{\theta}_i(0) = e^{\frac{x}{l} \ln A} \tag{A.56}$$

where A is the area of the impulse response function and l is the length of a single system. So in case of gain or loss a signal is amplified ($A > 1$) or dampened ($A < 1$) exponentially. Using (A.51) through (A.54) and (A.56) the skew-Gaussian limits can be expressed as functions of x and t. The remaining parameters have to be regarded as medium constants.

In general, the parameters μ, σ^2, $\overset{1}{\gamma}\sigma^3$ and $\overset{2}{\gamma}\sigma^4$ of the convolutional limit are just the <u>sum</u> of the corresponding parameters of the component systems: $\mu = \sum \mu_i$, etc. The area of the impulse response of the composite system equals the <u>product</u> of the areas of the impulse responses of the component systems. In the conservative case, without amplification or decay, this area is one.

The conditions listed in Section 2.8.2, to which the component systems are subjected, are merely mathematical. The individual systems may, therefore, be of completely different physical composure. In fact, there is even no restriction that requires the system to be physical...

2.8.6 *Derivation of (A.10)*

We want to show that

$$\lim_{n \to \infty} \frac{(x_1 + x_2 + \cdots + x_n)^r}{r! \underbrace{\sum x_i x_j \ldots x_k}_{\substack{r \text{ factors} \\ i,j,\ldots,k=1,n \\ i \neq j \neq \cdots \neq k}}} = 1 \qquad (A.57)$$

for a fixed integer r. Here, x_i ($i = 1, n$) are arbitrary numbers and i, j, k, r, n are integers. According to Abramowitz and Stegun (1964), p 823, one has

$$(x_1 + x_2 + \cdots + x_n)^r = \frac{r!}{r_1! r_2! \ldots r_n!} x_1^{r_1} x_2^{r_2} \ldots x_n^{r_n} \qquad (A.58)$$

$$\text{summed over } r_1 + r_2 + \cdots + r_n = r$$

The number of products in the right-hand side of (A.58) depends obviously on n and r. We can distinguish between different groups of products, having different dimensions:

. there are n products of the form $1! x_i^r$ ($i = 1, n$).

. there are $n(n-1)$ products of the form $2! x_i^{r-1} x_j$ ($i, j = 1, n; i \neq j$) if $r-1 \neq 1$ and there are $\binom{n}{2}$ such products if $r - 1 = 1$. In both cases the dimension of this group has order n^2.

. it follows likewise that the dimension of the group of products involving three different x_i has order n^3, etc.

. the group of products of the form $r! \underbrace{x_i x_j \ldots x_k}_{\substack{r \text{ factors} \\ i,j,\ldots,k=1,n \\ i \neq j \neq \cdots \neq k}}$ has dimension $\binom{n}{r}$, which is

of the order n^r.

This last group exceeds all others in magnitude by at least one order, if $n \to \infty$. After summing its members the group can be identified with the denominator of (A.57). It follows that the limit expressed by (A.57) must equal 1 indeed. ∎

As it is known from analysis that

$$\lim_{n \to \infty} f(n) \cdot \lim_{n \to \infty} g(n) = \lim_{n \to \infty} f(n)g(n) \tag{A.59}$$

theorem (A.57) can be extended to give

$$\lim_{n \to \infty} \frac{(y_1 + y_2 + \cdots + y_n)^{r_1}(x_1 + x_2 + \cdots + x_n)^{r_2}}{r_1! r_2! \underbrace{\sum y_i y_j \ldots y_k}_{\substack{r_1 \text{ factors} \\ i,j,\ldots,k,s,t,\ldots,u=1,n \\ i \neq j \neq \cdots \neq k \\ s \neq t \neq \cdots \neq v}} \underbrace{\sum x_s x_t \ldots x_u}_{r_2 \text{ factors}}} = 1 \tag{A.60}$$

Notice that the denominator has dimension $\binom{n}{r_1}\binom{n}{r_2}$, which is of the order $n^{r_1+r_2}$. In a similar way as we proved (A.57) it can be shown that

$$\lim_{n \to \infty} \frac{r_1! r_2! \underbrace{\sum y_i y_j \ldots y_k}_{\substack{r_1 \text{ factors} \\ i,j,\ldots,k,s,t,\ldots,u=1,n \\ i \neq j \neq \cdots \neq k \\ s \neq t \neq \cdots \neq v}} \underbrace{\sum x_s x_t \ldots x_u}_{r_2 \text{ factors}}}{(r_1 + r_2)! \underbrace{\sum y_i y_j \ldots y_k x_s x_t \ldots x_u}_{\substack{r_1 \text{ factors} \qquad r_2 \text{ factors} \\ i,j,\ldots,k,s,t,\ldots,u=1,n \\ i \neq j \neq \cdots \neq k \neq s \neq t \neq \cdots \neq v}}} = 1 \tag{A.61}$$

The denominator of (A.61) has dimension $\binom{n}{r_1+r_2}$ which is also of the order $n^{r_1+r_2}$. It can be shown that the difference between the denominators of (A.57) and (A.61) is of the order $n^{r_1+r_2-1}$. Using (A.59) once again it follows from (A.60) and (A.61) that

$$\lim_{n \to \infty} \frac{(y_1 + y_2 + \cdots + y_k)^{r_1}(x_1 + x_2 + \cdots + x_n)^{r_2}}{(r_1 + r_2)! \underbrace{\sum y_i y_j \ldots y_k x_s x_t \ldots x_u}_{\substack{r_1 \text{ factors} \qquad r_2 \text{ factors} \\ i,j,\ldots,k,s,t,\ldots,u=1,n \\ i \neq j \neq \cdots \neq k \neq s \neq t \neq \cdots \neq v}}} = 1 \tag{A.62}$$

which we used in Section 2.8.3 to derive the skew-Gaussian limit (A.26). ∎

2.8.7 *Derivation of (A.28)*

In order to derive the skew-Gaussian limit (A.28) we notice that the next groups of terms to be taken into account are composed of strings containing one four and a varying number of twos and zeros, together with those containing two

threes and a varying number of zeros (compare tables 2.6 and 2.4). These are the groups of terms that fade at rate $\frac{1}{n}$. Put in other words: their dimensions are of order r^{n-1}. When we derived the limits (A.17) and (A.26) we used (A.57) to replace $\sum x_i x_j \ldots x_k$ by $\frac{1}{r!}(x_1 + x_2 + \cdots + x_n)^r$, thereby introducing an error of order r^{n-1}. As this error itself has the same order of magnitude as the groups of terms that we want to include now, it is not allowed to exploit (A.57) once again. We will now derive a more accurate expression to replace $\sum x_i x_j \ldots x_k$ by. ∎

Using (A.58) we have

$$
(x_1 + x_2 + \cdots + x_n)^r = r! \sum \underbrace{x_i x_j \ldots x_k}_{\substack{r \text{ factors} \\ i,j,\ldots,k=1,n \\ i \neq j \neq \cdots \neq k}} +
$$

$$
+ \frac{r!}{2!} \sum \underbrace{x_i^2 x_j \ldots x_k}_{\substack{r-1 \text{ factors} \\ i,j,\ldots,k=1,n \\ i \neq j \neq \cdots \neq k}} + O(n^{r-2}) \tag{A.63}
$$

so

$$
\sum \underbrace{x_i x_j \ldots x_k}_{\substack{r \text{ factors} \\ i,j,\ldots,k=1,n \\ i \neq j \neq \cdots \neq k}} = \frac{1}{r!}(x_1 + x_2 + \cdots + x_n)^r -
$$

$$
\frac{1}{2!} \sum \underbrace{x_i^2 x_j \ldots x_k}_{\substack{r-1 \text{ factors} \\ i,j,\ldots,k=1,n \\ i \neq j \neq \cdots \neq k}} + O(n^{r-2}) \tag{A.64}
$$

For the present purpose the right-hand side is accurate enough to replace the expression $\sum x_i x_j \ldots x_k$. The shape of the second term is not very convenient, though. Using the same argument one gets

$$
\sum \underbrace{x_i^2 x_j \ldots x_k}_{\substack{r-1 \text{ factors} \\ i,j,\ldots,k=1,n \\ i \neq j \neq \cdots \neq k}} = \frac{x_1^2}{(r-2)!}(x_2 + x_3 + \cdots + x_n)^{r-2}
$$

$$
+ \frac{x_2^2}{(r-2)!}(x_1 + x_3 + \cdots + x_n)^{r-2}
$$

$$
\vdots
$$

$$
+ \frac{x_n^2}{(r-2)!}(x_1 + x_2 + \cdots + x_{n-1})^{r-2} + O(n^{r-2}) \tag{A.65}
$$

or

$$\underbrace{\sum x_i^2 x_j \dots x_k}_{\substack{r-1 \text{ factors} \\ i,j,\dots,k=1,n \\ i\neq j \neq \cdots \neq k}} = \frac{1}{(r-2)!}(x_1^2 + x_2^2 + \cdots + x_n)^2(x_1 + x_2 + \cdots + x_n)^{r-2} + O(n^{r-2})$$

(A.66)

(The step from (A.65) to (A.66) introduces an additional error of the order n^{r-2}, which does not change the order of the total error). Substitution of (A.66) in (A.64) gives finally:

$$\underbrace{\sum x_i x_j \dots x_k}_{\substack{r \text{ factors} \\ i,j,\dots,k=1,n \\ i\neq j \neq \cdots \neq k}} = \frac{1}{r!}(x_1 + x_2 + \cdots + x_n)^r -$$

$$\frac{1}{2!(r-2)!}(x_1^2 + x_2^2 + \cdots + x_n^2)(x_1 + x_2 + \cdots + x_n)^{r-2} + O(n^{r-2}) \quad \text{(A.67)}$$

The first term in the right-hand side has already been taken into account in the limits (A.17) and (A.26). Only the effect of the second term has to be included in the sequel. ∎

We now proceed to the derivation of (A.28). The strings containing one four and a variable number of zeros share a common factor $\left(\frac{\omega^2}{2!}\right)^{r-1}\frac{\omega^4}{4!}$ ($r = 1, 2, 3, \dots$), as can be seen from table 2.4. Moreover, there are r partitions producing strings of one four and a varying number of zeros. Using (A.62) in the form (A.21) we find that the contribution of these strings to $\bar{c}_{out}(\omega)$ is

$$r\left(\frac{\omega^2}{2!}\right)^{r-1}\frac{\omega^4}{4!}\frac{1}{r!}\left(\sum_1^n \overset{c}{\bar{\theta}_i^{iv}}(0)\right)\left(\sum_1^n \overset{c}{\bar{\theta}_i''}(0)\right)^{r-1}$$

(A.68)

which can be replaced by

$$\left(\frac{\omega^2}{2!}\right)^{r-1}\frac{\omega^4}{4!}\frac{1}{(r-1)!}\left(\sum_1^n(\overset{2}{\bar{\gamma}_i}+3)\sigma_i^4\right)\left(\sum_1^n -\sigma_i^2\right)^{r-1}$$

(A.69)

Here, use is made of (A.13), (2.24), and (2.26). Summing over r gives

$$\frac{\omega^4}{4!}\left(\sum_1^n(\overset{2}{\bar{\gamma}_i}+3)\sigma_i^4\right)\exp\left(-\frac{1}{2!}\omega^2\sum_1^n\sigma_i^2\right)$$

(A.70)

Decentralization adds a multiplicative factor $\exp(i\omega\sum_1^n\mu_i)$, see (A.6). Fourier inversion then yields

$$\frac{1}{4!}\left(\sum_1^n(\overset{2}{\bar{\gamma}_i}+3)\sigma^4\right)\frac{d^4}{dt^4}\left\{\frac{1}{\sqrt{2\pi\sum_1^n\sigma_i^2}}\exp\left\{-\frac{(t-\sum_1^n\mu_i)^2}{2\sum_1^n\sigma_i^2}\right\}\right\}$$

(A.71)

The strings containing two threes and a varying number of twos and zeros share a common factor $\left(\frac{\omega^2}{2!}\right)^{r-2}\left(\frac{\omega^3}{3!}\right)^2$ $(r = 2, 3, 4, \ldots)$, see table 2.4. Moreover, there are $\binom{r}{2}$ partitions producing such strings. Using (A.62) in the form

$$\lim_{n\to\infty} \frac{(y_1 + y_2 + \cdots + y_n)^2 (x_1 + x_2 + \cdots + x_n)^{r-2}}{r! \underbrace{\sum y_i y_j x_k \ldots x_l}_{\substack{r \text{ factors} \\ i,j,k,\ldots,l=1,n \\ i\neq j\neq k\neq\cdots\neq l}}} = 1 \qquad (A.72)$$

it is found that the contributions of these strings to $\bar{c}_{\text{out}}(\omega)$ is

$$\binom{r}{2}\left(\frac{\omega^2}{2!}\right)^{r-2}\left(\frac{\omega^3}{3!}\right)^2 \frac{1}{r!}\left(\sum_1^n \bar{\theta}_i'''(0)\right)^2 \left(\sum_1^n \bar{\theta}_i''(0)\right)^{r-2} \qquad (A.73)$$

which can be replaced by

$$\frac{1}{2!}\left(\frac{\omega^2}{2!}\right)^{r-2}\left(\frac{\omega^3}{3!}\right)^2 \frac{1}{(r-2)!}\left(\sum_1^n -i\frac{1}{1}\gamma_i\sigma_i^3\right)^2 \left(\sum_1^n -\sigma_i^2\right)^{r-2} \qquad (A.74)$$

where we made use of (A.13), (2.24), and (2.25). Summing over r gives

$$\frac{1}{2!}\left(\frac{-i\omega^3}{3!}\sum_1^n \gamma_i\sigma_i^3\right)^2 \exp\left(-\frac{1}{2!}\omega^2\sum_1^n \sigma_i^2\right)^2 \qquad (A.75)$$

Decentralization once again adds a factor $\exp(i\omega\sum_1^n \mu_i)$ and Fourier inversion yields

$$\frac{1}{2!}\left(\frac{1}{3!}\sum_1^n \gamma_i\sigma_i^3\right)^2 \frac{d^6}{dt^6}\left\{\frac{1}{\sqrt{2\pi\sum_1^n \sigma_i^2}}\exp\left\{-\frac{(t-\sum_1^n \mu_i)^2}{2\sum_1^n \sigma_i^2}\right\}\right\} \qquad (A.76)$$

At last we consider the contribution of the second term in the right-hand side of (A.67) to $\bar{c}_{\text{out}}(\omega)$. Tracing back the steps that led to (A.17) this contribution is found to be given by

$$-\left(\frac{\omega^2}{2!}\right)^r \frac{1}{2!(r-2)!}\left(\sum_1^n (\bar{\theta}_i''(0))^2\right)\left(\sum_1^n \bar{\theta}_i''(0)\right)^{r-2} \qquad (A.77)$$

$(r = 2, 3, 4, \ldots)$, which can be replaced by

$$-\frac{1}{2!}\left(\frac{\omega^2}{2!}\right)^2 \left(\sum_1^n \sigma_i^4\right)\frac{1}{(r-2)!}\left(\frac{\omega^2}{2!}\right)^{r-2}\left(\sum_1^n -\sigma_i^2\right)^{r-2} \qquad (A.78)$$

where use is made of (A.13) and (2.24). Summing over r gives

$$-\frac{1}{2!}\left(\frac{\omega^2}{2!}\right)^2\left(\sum_1^n \sigma_i^4\right)\exp\left(-\frac{1}{2!}\omega^2\sum_1^n\sigma_i^2\right) \tag{A.79}$$

Decentralization and Fourier inversion yields

$$-\left(\frac{1}{2!}\right)^3\left(\sum_1^n\sigma_i^4\right)\frac{d^4}{dt^4}\left\{\frac{1}{\sqrt{2\pi\sum_1^n\sigma_i^2}}\exp\left\{-\frac{(t-\sum_1^n\mu_i)^2}{2\sum_1^n\sigma_i^2}\right\}\right\} \tag{A.80}$$

In summary, the contribution to $\bar{c}_{\rm out}(t)$, consisting of (A.71), (A.76), and (A.80), reads

$$\left\{\frac{1}{4!}\left(\sum_1^n\overset{2}{\gamma}_i\sigma_i^4\right)\frac{d^4}{dt^4}+\frac{1}{2!}\left(\frac{1}{3!}\sum_1^n\overset{1}{\gamma}_i\sigma_i^3\right)^2\frac{d^6}{dt^6}\right\}\cdot$$
$$\cdot\frac{1}{\sqrt{2\pi\sum_1^n\sigma_i^2}}\exp\left\{-\frac{(t-\sum_1^n\mu_i)^2}{2\sum_1^n\sigma_i^2}\right\} \tag{A.81}$$

This has to be added to the skew-Gaussian limit in order to obtain a still earlier limit:

$$c_{\rm out}(t)\sim\frac{1}{\sqrt{2\pi\sigma^2}}\left\{1-\frac{1}{3!}\overset{1}{\gamma}\sigma^3\frac{d^3}{dt^3}+\frac{1}{4!}\overset{2}{\gamma}\sigma^4\frac{d^4}{dt^4}\right.$$
$$\left.\frac{1}{2!}\left(\frac{1}{3!}\overset{1}{\gamma}\sigma^3\right)^2\frac{d^6}{dt^6}\right\}\exp\left\{-\frac{(t-\mu)^2}{2\sigma^2}\right\}\qquad(n\to\infty) \tag{A.82}$$

where $\mu=\sum_1^n\mu_i$, $\sigma^2=\sum_1^n\sigma_i^2$, $\overset{1}{\gamma}=\frac{1}{\sigma^3}\sum_1^u\overset{1}{\gamma}_i\sigma_i^3$ and $\overset{2}{\gamma}=\frac{1}{\sigma^4}\sum_1^n\overset{2}{\gamma}_i\sigma_i^4$. ∎

2.8.8 *Extension of convolutional limit (A.28) by induction*

It may be clear by now that we can refine the skew convolutional limit ever further by successively including the terms that decay at rate $1/n\sqrt{n}$, $1/n^2$, etc. The amount of algebra however, although being elementary, becomes soon prohibitive. On the other hand, the process is purely mechanical. One may expect, therefore, that new terms can be deducted from former terms by induction. Lining up the terms of various order that we have obtained already, we get Table 2.7.

The term of order two is zero as a result of centralization. We remember from subsection 2.8.3 that the third order term was made up of all strings of Table 2.4 containing one three and a varying number of twos and zeros. They give rise to the term $-\frac{\overset{1}{\gamma}\sigma^3}{3!}\frac{d^3}{dt^3}$ in the skew convolutional limit (Table 2.7). Likewise, the term of fourth order was made up of all strings containing one four and a varying number of twos and zeros, together with all strings containing two threes and

order of term	rate of growth/decay	appearance of term
1	n	1
2	$\sqrt{n}$	0
3	$\dfrac{1}{\sqrt{n}}$	$-\dfrac{\overset{1}{\gamma}\sigma^3}{3!}\dfrac{d^3}{dt^3}$
4	$\dfrac{1}{n}$	$\dfrac{\overset{2}{\gamma}\sigma^4}{4!}\dfrac{d^4}{dt^4}+\dfrac{1}{2!}\left(\dfrac{\overset{1}{\gamma}\sigma^3}{3!}\right)^2\dfrac{d^6}{dt^6}$

Table 2.7 *First four terms of the skew convolutional limit*

a varying number of twos and zeros (subsection 2.8.7). They yield the terms $\frac{\overset{2}{\gamma}\sigma^4}{4!}\frac{d^4}{dt^4}$ and $\frac{1}{2!}\left(\frac{\overset{1}{\gamma}\sigma^3}{3!}\right)\frac{d^6}{dt^6}$, resp. (Table 2.7). The fifth order term must be made up of all strings in Table 2.4 that contain one five along with a varying number of twos and zeros, one four and one three along with a varying number of twos and zeros, and three threes along with a varying number of twos and zeros. By analogy with the terms of orders three and four we expect the fifth order term in the skew convolutional limit to become

$$-\frac{\overset{3}{\gamma}\sigma^5}{5!}\frac{d^5}{dt^5}-\frac{\overset{1}{\gamma}\sigma^3\overset{2}{\gamma}\sigma^4}{3!\,4!}\frac{d^7}{dt^7}-\frac{1}{3!}\left(\frac{\overset{1}{\gamma}\sigma^3}{3!}\right)^3\frac{d^9}{dt^9} \qquad (A.83)$$

Proceeding this way, the sixth term will be

$$\frac{\overset{4}{\gamma}\sigma^6}{6!}\frac{d^6}{dt^6}+\frac{1}{2!}\left(\frac{\overset{2}{\gamma}\sigma^4}{4!}\right)^2\frac{d^8}{dt^8}+\frac{\overset{1}{\gamma}\sigma^3\overset{3}{\gamma}\sigma^4}{3!\,4!}\frac{d^8}{dt^8}$$

$$+\frac{1}{2!}\left(\frac{\overset{1}{\gamma}\sigma^3}{3!}\right)^2\frac{\overset{2}{\gamma}\sigma^4}{4!}\frac{d^{10}}{dt^{10}}+\frac{1}{4!}\left(\frac{\overset{1}{\gamma}\sigma^3}{3!}\right)^4\frac{d^{12}}{dt^{12}} \qquad (A.84)$$

and so on. To cut the reasoning short, we have the following rule of induction, which requires no consulting of tables:
To construct the nth order term,
   1) form all products

$$\frac{\overset{i}{\gamma}\sigma^{i+2}}{(i+2)!}\cdot\frac{\overset{j}{\gamma}\sigma^{j+2}}{(j+2)!}\cdots\frac{\overset{k}{\gamma}\sigma^{k+2}}{(k+2)!}\frac{d^s}{dt^s}$$

such that $i+j+\cdots+k=n-2$. It is not required that $i\neq j\neq\cdots\neq k$. The order s of the derivative is $s=(i+2)+(j+2)+\cdots+(k+2)$.

2) if $\frac{\dot{\gamma}\sigma^{i+2}}{(i+2)!}$ occurs r times, then multiply the product by $\frac{1}{r!}$.

3) the sign in front of the product is plus if s is even, else minus.

4) sum all products to find the nth order term of the convolutional limit. ∎

CHAPTER 3: APPLICATION TO 1-DIMENSIONAL CONTAMINANT TRANSPORT

3.1 Aim of the chapter

The breakthrough formulas, presented in the previous chapter, will presently be applied to transport through porous media. Our prime interest is in one-dimensional transport under conditions of steady flow. Most of the problems to be considered allow for exact analytical solutions, although the expressions may become quite complicated at times. It is our aim to replace them by a simpler, uniform (albeit approximative) approach, that has a wider range of application and is easy to implement in existing computer programs.

3.2 A note on the history of dispersion research

This thesis considers only longitudinal dispersive transport, i.e. we neglect dispersion in directions perpendicular to the main direction of flow. As almost every self-respecting groundwater model seems to deal with a three-dimensional formulation of the problem, we feel a need to justify our choice and we will do so by historical arguments.

The development of the theory of dispersion has always been hampered by scarcity of field data. The reason is plain to see: groundwater flows very slowly under natural conditions, displacing itself only one to several meters a year. It was never easy to realize costly long lasting field experiments on a practical scale, especially in a time when the need of a clean and healthy environment had not yet attracted political action. Early dispersion research struggled with a lack of funds. Experiments focussed on simple column models in laboratory environments, filled with homogeneous sand. Their test setups derived immediately from chemical reactors. As a matter of fact a good deal of the theory of dispersive flow in porous media has its origin in the field of chemistry, where it received considerable attention in the period following World War II. Bear (in De Wiest, 1969) presented the state of the art in the field of groundwa-

ter flow at the end of the nineteen sixties. It appears from his account that the notion of 'macro dispersion' had not yet evolved. 'Hydrodynamical' dispersion was attributed to velocity differences on a pore scale or even within pores. The conceptual models at the time speculated on mixing effects in increasingly complex arrays of capillary tubes, leading to the notion of dispersion as a fully three dimensional process, requiring a tensorial formulation. Realizing that it would never become possible to know the exact three-dimensional structure of a pore channel system, researchers introduced statistical approaches to the problem. Theories bloomed, in contrast to experimental evidence, which remained confined to the laboratory. It was generally agreed that the coefficient of dispersion was proportional to the velocity, the constant of proportionality (α_L for dispersion in the direction of flow and α_T for transverse dispersion) having the order of the grain size. It lasted until about 1970 before the first field evidence showed up that, in order to match theoretical to real breakthrough curves, the proportionality constant had to be chosen several to many orders of magnitude bigger than that. It was conjectured that macroscopic heterogeneities of real aquifers were the cause. They, too, were likely to never lend themselves to be exactly known, opening up a whole new field of research to statisticians. The stochastic approach to groundwater flow became a discipline in its own right. If ever science showed a tendency to prosper in the absence of measuring data, it is in the field of dispersive groundwater transport. While stochastians scaled up their theories, numerical modelers scaled up the dispersion tensor, putting considerable effort in 3-D formulations that would keep numerical dispersion within acceptable bounds. Both stochasticians and modelers remained vague, however, as to the magnitudes of the elements of the dispersion tensor, keeping practical hydrologists in suspense. Many field observations on dispersion *have* been reported, but their reliability must be questioned in most cases (Gelhar et al., 1985; Gelhar et al., 1992). It became a popular practice to choose the transverse dispersivities one third of the longitudinal value. Only recently began the results of well controlled experiments on a scale of practical interest to penetrate the literature, notably in the journal Water Resources Research. The best known and best controlled full scale test sites are those at Borden Air Force Base, Ontario (Mackay et al., 1986; Freyberg, 1986; Sudicky, 1986; Rajaram and Gelhar, 1991) and on Cape Cod, Massachusetts (LeBlanc et al., 1991; Garabedian et al., 1991). Another test of interest is being conducted at Jutland, Denmark (Jensen et al., 1993). (The references are not exhaustive and research at these sites is still going on). Although the hydrological conditions at the various sites are quite different, the tests are very conclusive as to the importance of longitudinal dispersion relative to transverse dispersion. In all cases it was found that transverse dispersion in the vertical direction has only the order of molecular diffusion, corresponding with a proportionality constant α_T of ca .001 m. This finding emerged earlier from a quite different test setup by Molz and Widdowson (1988). The longitudinal proportionality constant α_L was 100 (Borden), 500 (Cape Cod) and 900 (Jutland) times as big. Transverse dispersion measured in the horizontal plane was 10 times (Borden), 10 times (Cape Cod) and 2 times (Jutland) as big as

the vertical transverse dispersion. This kind of dispersion is difficult to assess, as the width of a plume of contaminant may contract and expand depending on local heterogeneities and non-steady flow conditions. It may be meaningful, in this respect, the the Danish test site is very homogeneous as compared to the other two, allowing for a more accurate estimate.

In conclusion, there is evidence that for engineering practice dispersion is *at most* a two-dimensional phenomenon. A one-dimensional (i.e. longitudinal) approach can be expected to suffice in many cases of practical interest.

3.3 Moments and cumulants

All methods to be discussed in this chapter require knowledge of the central moments (or alternative characteristics) of breakthrough curves, up to some order, given a differential equation. They can be obtained in many ways, most of which become quite laborious if more than the first few moments are needed. We will learn in this chapter that three or four moments suffice for our purpose, but we will be able to draw that conclusion only after considering moments of any order.

One method of obtaining them seems to be particularly geared to dispersion-like problems. This method will be applied in the subsequent sections, the present section being preparative.

A definition of moments was given by equation (2.24). An equivalent alternative was stated in Appendix 2.8, equations (A.12) and (A.13), where moments were related to the coefficients of the Taylor series of the Fourier-transformed function in question. Let that function be $c(t)$ and let us assume that it describes the concentration of a conservative (i.e. non decaying) contaminant, following an event of instantaneous pollution. Denoting its Fourier transform by $\bar{c}(i\omega)$, the Taylor series reads

$$\bar{c}(i\omega) = 1 + \frac{i\omega}{1!}\bar{c}'(0) + \frac{(i\omega)^2}{2!}\bar{c}''(0) + \cdots \tag{3.1}$$

where accents denote differentiation with respect to $i\omega$. The nth moment corresponds to the coefficient of $(i\omega)^n/n!$ in this series:

$$M_n = \left\{ \frac{d^n \bar{c}(i\omega))}{d(i\omega)^n} \right\}_{\omega=0} \tag{3.2}$$

For reasons explained in any textbook on mathematical statistics (e.g. Stuart and Ord, 1987), moments are not always the most convenient candidates to characterize - in our case - plumes of contaminant. *Cumulants* offer an attractive alternative. They are defined similar to moments, the difference being that the Taylor series is taken of $\ln\{\bar{c}(i\omega)\}$ rather than $\bar{c}(i\omega)$. This leads us to the formal

relation

$$\exp\left(\sum_{n=1}^{\infty} K_n \frac{(i\omega)^n}{n!}\right) = \sum_{n=0}^{\infty} M_n \frac{(i\omega)^n}{n!} \tag{3.3}$$

where K_n is the nth cumulant. Notice that K_0 is absent, because $\ln 1 = 0$. The set of equations (3.3) is triangular and can be solved explicitly for M_n to yield the recursive relation

$$\frac{M_n}{n!} = \sum_{i=1}^{n} \frac{i}{n} \frac{M_{n-i}}{(n-i)!} \frac{K_i}{i!} \tag{3.4}$$

or, inversely

$$\frac{K_n}{n!} = \frac{M_n}{n!} - \sum_{i=1}^{n-1} \frac{i}{n} \frac{M_{n-i}}{(n-i)!} \frac{K_i}{i!} \tag{3.5}$$

These expressions are convenient for programming, if one needs to calculate moments from cumulants and vice versa. Unlike moments, there exist no such things as central cumulants: cumulants are invariant under centralization, except for K_1, which vanishes then. Thus, central moments are calculated from cumulants by

$$\frac{\overset{c}{M}_n}{n!} = \sum_{i=2}^{n} \frac{i}{n} \frac{\overset{c}{M}_{n-i}}{(n-i)!} \frac{K_i}{i!} \tag{3.6}$$

We met in Section 2.4 with still other characteristics, the skewness $\overset{1}{\gamma}$ and the excess $\overset{2}{\gamma}$. These are simply scaled cumulants, defined by

$$\overset{n}{\gamma} = \frac{K_{n+2}}{(K_2)^{\frac{1}{2}n+1}} \tag{3.7}$$

The use of cumulants will be demonstrated while discussing the classical model of dispersive groundwater flow, the Convection Dispersion Equation (CDE).

3.4 Flux-averaged versus volume-averaged concentrations

Until now we refrained from giving an exact definition of concentration, and there really was no need to go beyond intuition. At this point, however, we can no longer sidestep the issue.

Two types of concentration appear in the literature, namely flux-averaged concentration c_F and volume-averaged (or "resident") concentration c_R (Kreft and Zuber, 1978). The difference between the two was not recognized from the onset and constituted a source of confusion among early researchers in this field. The importance of the topic surmounts the academic level and the outcome has a bearing on practical questions concerning the design of test setups to assess soil parameters through tracer experiments.

Let us consider a stream tube in a porous medium, with cross sectional area S. Suppose that part of the fluid particles that cross $S(x)$ at a judicious point x_0 along the longitudinal x-axis is tagged. (We will refer to the tagged particles as "solute"). The *flux-averaged* concentration is then defined by

$$c_F = \frac{\sum n_i v_i}{\sum v_i} \tag{3.8}$$

where v_i is the velocity component perpendicular to S of the ith fluid particle. The operator n_i is a tagger, having value one if the ith particle is tagged, and zero otherwise. The summation is taken over all N particles that pass S per unit of time. Alternatively, (3.8) can be written as

$$c_F = \frac{\sum n_i v_i / N}{\sum v_i / N} = \frac{1}{v} \frac{\sum n_i v_i}{N} \tag{3.9}$$

where v is the mean velocity (perpendicular to S) of all fluid particles. Changing from velocity v to flux q we get

$$q c_F = \frac{\theta}{N} \sum n_i v_i \tag{3.10}$$

The product $q c_F$ is the *total solute flux*, being the tagged part of q. θ is the porosity of the porous matrix. Form a practical point of view, c_F might be the concentration of some contaminant in a groundwater sample taken from a monitoring well.

In contrast to (3.8) the *volume-averaged* or resident concentration is defined by

$$c_R = \frac{\sum n_i v}{\sum v_i} = \frac{1}{v} \frac{\sum n_i v}{N} \tag{3.11}$$

This concentration can be interpreted as the relative number of tagged particles n_i / N that *would have* crossed S per unit of time, if all fluid particles had the mean velocity v. Changing to flux again:

$$q c_R = \frac{\theta}{N} \sum n_i v \tag{3.12}$$

The product $q c_R$ is called *convective solute flux*. From a practical point of view, c_R might be the concentration of some contaminant in the groundwater extracted from a soil sample that was taken without disturbing its water content.

In general, the total solute flux differs in magnitude from the convective solute flux. The difference is termed dispersive solute flux. By analogy to Fick's law of diffusion, this type of flux is supposed to be proportional to the spatial gradient of c_R, such that

$$q c_F = q c_R - \theta D \frac{\partial c_R}{\partial x} \tag{3.13}$$

where D is the longitudinal dispersion constant. Relation (3.13) seems to have been introduced by Danckwerts (1953). The analogy to Fick's law lacks any physical ground and has been questioned ever since. Fortunately, the asymptotic behavior of the model is correct: it produces Gaussian breakthrough curves at large distances from a source of contamination, and we saw in Chapter 2 that this is a necessary requirement if one is to model convolutional groundwater transport. But then again, numerous alternative models could do the same. Still the Fickian model is almost exclusively used, which must be attributed to its mathematical charms.

Adding to (3.13) the mass balance relation

$$-\frac{\partial q c_F}{\partial x} = \theta \frac{\partial c_R}{\partial t} \tag{3.14}$$

it is easily found that

$$D \frac{\partial^2 c_R}{\partial x^2} - v \frac{\partial c_R}{\partial x} = \frac{\partial c_R}{\partial t} \tag{3.15}$$

which is the (one-dimensional version of the) classical Convection Dispersion Equation (CDE). Elementary rearrangement of terms shows that c_F equally satisfies the CDE. Both types of concentration are therefore equally fit to describe dispersive groundwater flow. It is clear from (3.13), however, that they cannot at the same time obey the same boundary conditions. Consequently, if a given problem is solved in terms of c_R, the resulting solution will differ from the equivalent solution in terms of c_F. (Parker and van Genuchten, 1987). We will illustrate this for a few cases, whose solution we need anyway.

3.5 The classical Convection Dispersion Equation

The dimensionless form of the CDE (3.15) is

$$\frac{\partial^2 c}{\partial X^2} - \frac{\partial c}{\partial X} = \frac{\partial c}{\partial T} \tag{3.16}$$

where

$$X = \frac{x v}{D} \tag{3.17}$$

and

$$T = \frac{v^2 t}{D} \tag{3.18}$$

It is common use, in one-dimensional flow, to set

$$D = \alpha_L v \tag{3.19}$$

where α_L is supposed to be a constant, independent of velocity. This would change (3.17) and (3.18) into

$$X = \frac{x}{\alpha_L} \tag{3.20}$$

$$T = \frac{vt}{\alpha_L} \tag{3.21}$$

α_L is called 'longitudinal dispersivity'. The first problem to tackle is an infinite medium (say a column) which at $T = 0$ contains a solute at concentration 1 in the negative half $X < 0$ and pure water in the positive half $X > 0$. To complete the mathematical statement of the problem, we add $c = \frac{1}{2}$ at $T = 0$, $X = 0$ (Kreft and Zuber, 1978). Clearly, the boundary condition at $X = 0$ is in terms of volume-averaged concentration c_R and the solution of this problem (which is well known [Crank, 1957]) must also be in c_R:

$$c_R = \tfrac{1}{2}\mathrm{erfc}\left(\frac{X - T}{2\sqrt{T}}\right) \tag{3.22}$$

This is fine for undisturbed soil samples. For groundwater samples we need c_F, which can be obtained from (3.22) by means of (3.13). The dimensionless form of (3.13) is

$$c_F = c_R - \frac{\partial c_R}{\partial X} \tag{3.23}$$

We derive from (3.22) and (3.23)

$$c_F = \tfrac{1}{2}\mathrm{erfc}\left(\frac{X - T}{2\sqrt{T}}\right) + \frac{1}{4\sqrt{\pi T}}\exp\left\{-\frac{(X - T)^2}{4T}\right\} \tag{3.24}$$

Figure 3.1 gives a comparison of the two solutions. The graphs show a slight shift in time, which may be of importance if samples are taken close to the source (think of column experiments in a laboratory setting). It can also be seen that there is some upstream dispersion, notably in the beginning. As this cannot happen in actual porous media, because - apart from some Brownian motion - fluid particles move only downstream, solutions (3.22) and (3.24) are not ideal for modelling dispersive groundwater transport.

In order to prevent backflow at the source, it is common practice to set $c_F = 1$ at $X = 0$, for all values of time T. (This does not improve the model, of course. It only conceals one of its shortcomings). We now have a problem in terms of c_F, whose well known solution reads

$$c_F = \tfrac{1}{2}\mathrm{erfc}\left(\frac{X - T}{2\sqrt{T}}\right) + \tfrac{1}{2}e^X\mathrm{erfc}\left(\frac{X + T}{2\sqrt{T}}\right) \tag{3.25}$$

(Rifai et al., 1956). Relation (3.23) is not so convenient to obtain c_R from c_F. However, conservation of mass ensures that

$$q\int_0^t c_F dt' = \theta \int_x^\infty c_R dx' \tag{3.26}$$
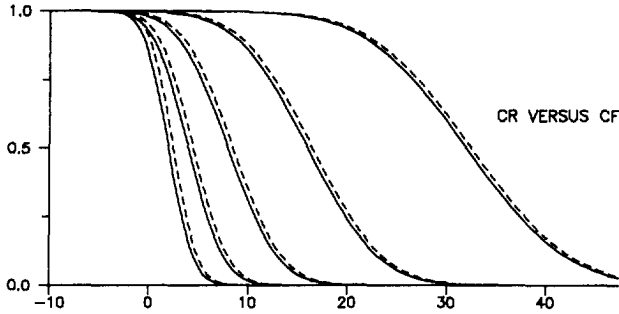
Figure 3.1   *Volume-averaged (drawn) versus flux-averaged (dotted) concentrations in an infinite column. Dimensionless time = 2, 4, 8, 16, 32. Horizontal axis: dimensionless distance. Vertical axis: dimensionless concentration.*

(In words, this relation states that all mass flowed past x can be found between X and ∞). Reworked and put in dimensionless variables:

$$c_R = -\int_0^T \frac{\partial c_F}{\partial X} dT' \tag{3.27}$$

(Kreft and Zuber, 1978). It follows now from (3.25) that

$$c_R = \tfrac{1}{2}\mathrm{erfc}\left(\frac{X-T}{2\sqrt{T}}\right) - \frac{1}{2}e^X \mathrm{erfc}\left(\frac{X+T}{2\sqrt{T}}\right).$$

$$.(1+X+T) + \sqrt{\frac{T}{\pi}}\exp\left\{-\frac{(X-T)^2}{4T}\right\} \tag{3.28}$$

(Danckwerts, 1953). These two solutions are compared in Figure 3.2. There appears a remarkable jump in c_R at $X = 0$, which is easy to understand mathematically (see [3.23]) but harder to grasp physically. This point was discussed at some length by Parker and Van Genuchten (1984, 1985, 1986), Dagan and Bresler (1985), and Kreft and Zuber (1986), without reaching a convincing conclusion, except for the statement that the model does not apply close to the source. In spite of that, (3.25) is most commonly used to interpret tracer experiments. As Parker and Van Genuchten stress, it has at least the property that it preserves mass. We will therefore concentrate on (3.25), when we look for approximate solutions to the CDE in the next section.

The CDE can be easily extended to take first order decay into account. Equation (3.15) then changes into

$$D\frac{\partial^2 c}{\partial x^2} - v\frac{\partial c}{\partial x} = \frac{\partial c}{\partial t} + \lambda c \tag{3.29}$$
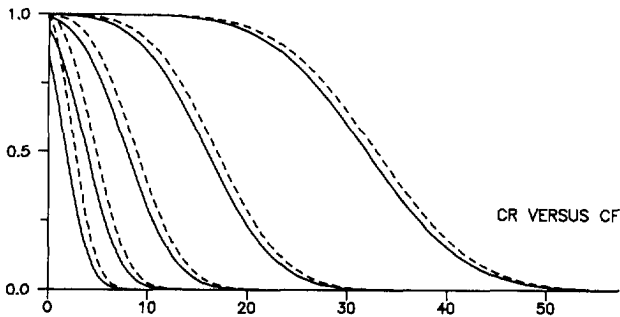
Figure 3.2   *Volume-averaged (drawn) versus flux-averaged (dotted)*
concentrations in a semi-infinite column. Dimension-
less time = 2, 4, 8, 16, 32. Horizontal axis: dimension-
less distance. Vertical axis: dimensionless concentra-
tion.

(Lapidus and Amundson, 1952) where λ is the characteristic decay constant of the solute. Changing to dimensionless variables (3.20) and (3.21) and making the substitution

$$c^* = c \, e^{\lambda^* t} \tag{3.30}$$

with

$$\lambda^* = \frac{\alpha_L \lambda}{v} \tag{3.31}$$

the CDE reappears:

$$\frac{\partial^2 c^*}{\partial X^2} - \frac{\partial c^*}{\partial X} = \frac{\partial c^*}{\partial T} \tag{3.32}$$

It makes no physical sense to look for a solution of (3.31) analogous to the infinite column (3.22), as that would require infinite concentrations at $X \to -\infty$. The analogue of the semi-infinite column (3.25) is physically possible (Bear, 1969), and reads:

$$c_F = \tfrac{1}{2} e^{\frac{1}{2} X(1-\beta)} \text{erfc}\left(\frac{X - \beta T}{2\sqrt{T}}\right) + \tfrac{1}{2} e^{\frac{1}{2} X(1+\beta)} \text{erfc}\left(\frac{X + \beta T}{2\sqrt{T}}\right) \tag{3.33}$$

where

$$\beta = \sqrt{1 + 4\alpha_L \lambda / v} \tag{3.34}$$

The literature on dispersive flow is extremely rich and there exist numerous extensions of the CDE to account for more complicated forms of decay, various kinds of sorption, stagnant zones, etc. It is not our aim to give an overview, though, and the above suffices for the purpose of this work (although we will briefly touch upon the subject of sorption in the section on Strack's dispersion equation).

3.6 Various approximate solutions to the CDE

3.6.1 *Moments and cumulants of the CDE*

In order to apply the approximate methods of Chapter 2, we need either the central moments or the cumulants of $c(X, T)$, and we want to obtain them not from an existing solution, but from the differential equation (3.16) (because, in more complicated cases, solutions may not always be at hand). Taking the Fourier-transform of (3.16) we find that

$$\frac{d^2\bar{c}}{dX^2} - \frac{d\bar{c}}{dX} = -i\omega\bar{c} \tag{3.35}$$

which has the general solution

$$\bar{c} = A_{12}\exp\left\{\tfrac{1}{2}X \pm \tfrac{1}{2}X\sqrt{1-4i\omega}\right\} \tag{3.36}$$

A_1 and A_2 are unknown constants, that can be solved from the requirement that the solution be mass preserving. The amount of mass carried by (3.36) is given by $\bar{c}(\omega = 0)$. (Notice that $\bar{c}(\omega = 0)$ is equal to the zero$^{\text{th}}$ moment M_0, according to [3.2]). Setting this amount equal to unity, it follows that

$$1 = A_{12}\exp\{\tfrac{1}{2}X \pm \tfrac{1}{2}X\} \tag{3.37}$$

which is satisfied only if $A_1 = 0$ and $A_2 = 1$. Thus

$$\bar{c} = \exp\left\{\tfrac{1}{2}X - \tfrac{1}{2}X\sqrt{1-4i\omega}\right\} \tag{3.38}$$

To obtain cumulants, we take the logarithm of (3.38):

$$\ln\bar{c} = \tfrac{1}{2}X - \tfrac{1}{2}X\sqrt{1-4i\omega} \tag{3.39}$$

and consider the Taylor series of $\ln\bar{c}$. Noting that

$$\sqrt{1+a} = 1 + \tfrac{1}{2}\frac{a}{1!} - \frac{1}{2^2}\frac{a^2}{2!} + \frac{1.3}{2^3}\frac{a^3}{3!} - \frac{1.3.5}{2^4}\frac{a^4}{4!} + \cdots \tag{3.40}$$

we find

$$\ln\bar{c} = X(i\omega) + \tfrac{1}{2}X\sum_{n=2}^{\infty}2^n\frac{(i\omega)^n}{n!}\prod_{i=2}^{n}(2i-3) \tag{3.41}$$

By definition, the cumulants are the coefficients of $(i\omega)^n/n!$ in this expression (see Section 3.3), thus

$$K_1 = X \tag{3.42}$$

$$K_n = 2^{n-1}X\prod_{i=2}^{n}(2i-3) \qquad n = 2, 3, 4, \ldots \tag{3.43}$$

from which the central moments are obtained by means of (3.6). The skewness $\overset{1}{\gamma}$ and excess $\overset{2}{\gamma}$ are also easily pulled from (3.43), cf. (3.7). For future reference we mention that

$$\mu = X \tag{3.44}$$

$$\sigma = \sqrt{2X} \tag{3.45}$$

$$\overset{1}{\gamma} = \sqrt{18/X} \tag{3.46}$$

$$\overset{2}{\gamma} = 30/X \tag{3.47}$$

(It is to be noted that these expressions are dimensionless, hence μ and σ are in dimensionless time (3.21). Their dimension-bearing counterparts are, therefore, $\mu = x/v$ and $\sigma = \sqrt{2\alpha_L x}/v$, resp. This remark does <u>not</u> apply to $\overset{1}{\gamma}$ and $\overset{2}{\gamma}$, who remain dimensionless. Their counterparts read $\sqrt{18\alpha_L/x}$ and $30\alpha_L/x$, resp.) It is a nice feature of cumulants that they are proportional to X, the distance travelled by the plume. This suggests that they can be calculated moving along a stream line, just like the mean travel time is calculated in conventional piston flow models.

Notice that the above method of calculating moments via cumulants works so well, because of the exponential form of (3.38), which is characteristic of dispersion-like problems.

3.6.2 *Edgeworth and Gram-Charlier*

When we discussed the series of Edgeworth and Gram-Charlier in Section 2.5, we noticed already that they do not converge unconditionally. Unfortunately, divergence occurs when applied to dispersive groundwater flow. This is illustrated for Gram-Charlier's series by Figure 3.3. Drawn lines are obtained by (2.59), taking 1 to 5 terms into account. The dotted lines are calculated from (3.25). In case of one term the breakthrough curve is the error-function, which is the Gaussian limit. Inclusion of the second term, that contains the skewness $\overset{1}{\gamma}$, gives an improvement over the Gaussian, but addition of the excess $\overset{2}{\gamma}$ marks the onset of divergence.

Edgeworth's expansion behaves more fashionable, but does not converge either (Figure 3.4). Its better performance is due to the fact that Edgeworth grouped his terms in order of decreasing importance, making his approach preferable for our purpose.

Divergence does not render the method useless. After all, the series are asymptotically correct, which means that X can always be chosen large enough so that convergence *is* obtained. On the other hand, the approach breaks down at shorter distances from the source, when the plume is still very skew. This is shown by Figure 3.5, which gives the asymptotic behavior of both series, truncated after three terms. The figure confirms the superiority of Edgeworth's expansion.
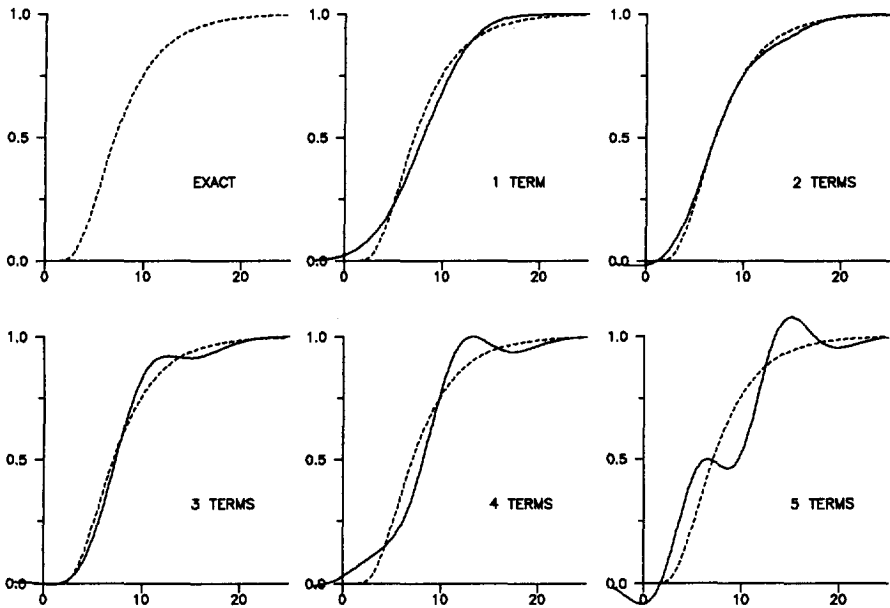
Figure 3.3   *Convergence and subsequent divergence of Gram-Charlier's series, applied to the Convection Dispersion equation. Horizontal axis: dimensionless time (vt/α_L). Vertical axis: dimensionless concentration. The distance from the origin is chosen such as to make the skewness $\overset{1}{\gamma} = 1.5$.*

In Section 2.5 we took some pain to indicate conditions under which the truncated series of Edgeworth and Gram-Charlier produce positive definite and unimodal responses (see Figures 2.7 and 2.8). These conditions are clearly violated by the examples in Figures 3.3 and 3.4, because the breakthrough curves labelled "3 terms" have negative parts. In fact, it follows from (3.46) and (3.47) that

$$\overset{2}{\gamma} = \tfrac{5}{3}(\overset{1}{\gamma})^2 \tag{3.48}$$

which is a parabola in the $(\overset{1}{\gamma}, \overset{2}{\gamma})$-plane. This curve touches the smaller heart-shaped region of Figure 2.7 only in the origin $\overset{1}{\gamma} = \overset{2}{\gamma} = 0$. Consequently, the impulse response will never become fully non-negative, unless $X \to \infty$. The situation is only slightly better for Edgeworth's expansion, Figure 2.8. Nevertheless, Figure 3.5 suggests that Edgeworth's approach is useful if $\overset{1}{\gamma} \leq 1$. In case of the CDE this occurs at dimensionless distances (x/α_L) bigger than 16.

The literature seems to be not unanimous as to a criterion for convergence of Edgeworth's expansion. Kendall (Stuart and Ord, 1987) refers to old work by
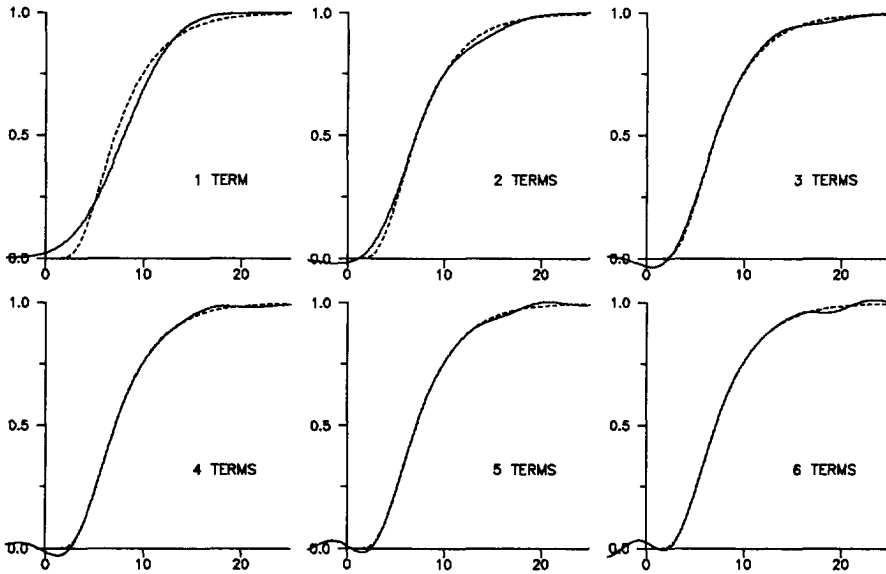
Figure 3.4   *Convergence and subsequent divergence of Edgeworth's expansion, applied to the Convection Dispersion Equation. Horizontal axis: dimensionless time (vt/α_L). Vertical axis: dimensionless concentration. The distance from the origin is chosen such as to make the skewness $\overset{1}{\gamma} = 1.5$.*

Cramér and Galbrun, dating back to 1925 and earlier, to state that the integral

$$\int_{-\infty}^{\infty} |c(T)| \exp\left\{\frac{(T-X)^2}{4X}\right\} d(T-X) \tag{3.49}$$

must exist, in order for $c(T)$ to have a converging expansion. On the other hand, there is a somewhat younger book by Von Mises (1931), that requires the integral

$$\int_{-\infty}^{\infty} \left|\frac{c(T)}{T-X}\right| \exp\left\{\frac{(T-X)^2}{4X}\right\} d(T-X) \tag{3.50}$$

to be finite. The latter criterion is clearly stricter than the former. Be that as it may, both conditions indicate that the tail of $c(X,T)$ must decay at rate $\exp(-T^2/4X)$, whereas the actual rate of decay is only $\exp(-T/4)$, as can be inferred from (3.25).

    The oscillations of Edgeworth's expansion can to some extent be moved away from the region of interest by choosing a proper weighing function to multiply
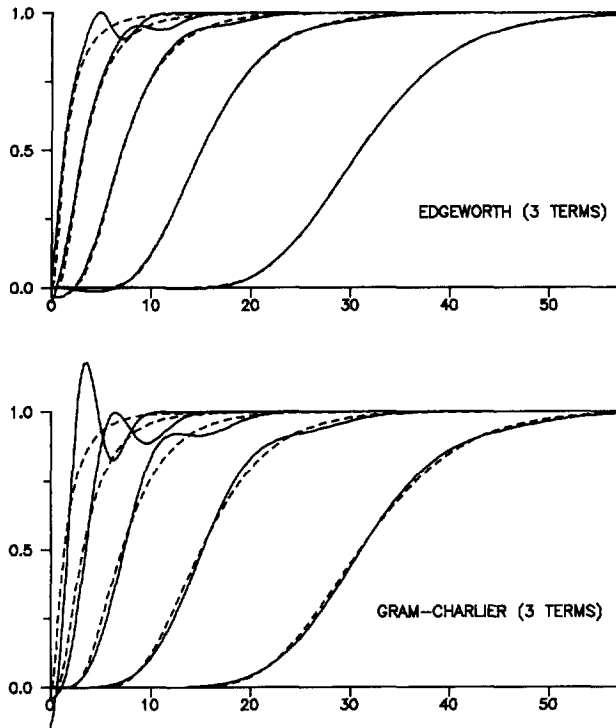
Figure 3.5   *Asymptotic convergence of Gram-Charlier's series (first three terms) and Edgeworth's expansion (first three terms) to an exact solution of the Convection Dispersion equation. Horizontal axis: dimensionless time (vt/α_L). Vertical axis: dimensionless concentration. Dimensionless distances from the origin: 2, 4, 8, 16, 32. The corresponding values of the skewness $\frac{1}{\gamma}$ are 3, 2.12, 1.5, 1.06 and .75.*

$c(X,T)$ by. Figure 3.6 shows Edgeworth's expansion applied to $c(X,T) * T^2$, times a proper constant to make the zero[th] moment equal one. (The result of the expansion was divided, of course, by the same weighing function to produce the figure). The oscillations are actually quite heavy but they occur outside the interval that we are interested in. They were polished away to obtain Figure 3.6. There may exist better weighing functions, but the choice is seriously limited by the practical requirement that they may not complicate the calculation of cumulants. All things considered, this procedure seems to work, but the polishing step is far from elegant and we feel not secure that the result will be sufficiently foolproof to be incorporated in a complex groundwater model.
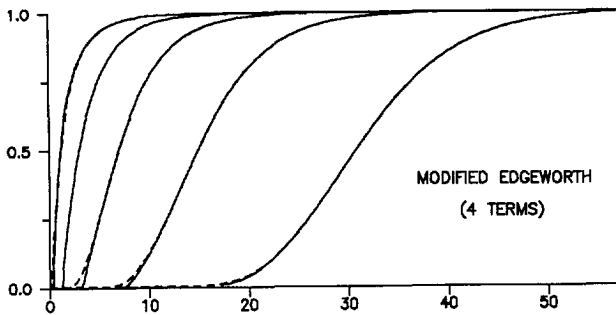
Figure 3.6   *Edgeworth's expansion using a weighing function. Os-*
cillations before breakthrough are not shown. All spec-
ifications conform Figure 3.5.

3.6.3 *Von Mises*

For sake of brevity we indicate the staircase function approach, described in
Section 2.6, by the name of Von Mises, although we are not sure whether or not he
was the originator. Figure 3.7 presents exact solutions to the CDE according to
(3.25), approached by the midpoints of the steps and rises of staircase functions,
using the moments of Subsection 3.6.1. Each two extra dots in a breakthrough
curve require evaluation of two more moments, which is an easy task in itself.
However, the numerical accuracy of the matrix manipulations that come with the
method becomes problematic when the number of moments exceeds twenty or so.
Special programming techniques may raise this bound, but the set of points to
approximate the exact breakthrough curves by will nevertheless remain sparse.
All the same, they give a fair idea of the shape of the curves.
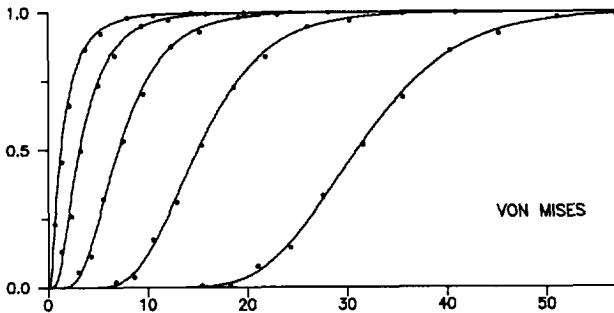
Figure 3.7   *Von Mises' approximation of breakthrough curves ap-*
plied to the CDE. Drawn lines are exact. All specifica-
tions conform Figure 3.5.

3.6.4 *Pearson III*

The mixing reservoirs model, leading to the Pearson type III distribution function, was also presented in Section 2.6. Applied to solute transport, Pearson III characterizes an impulse response whose corresponding breakthrough curve is the incomplete gamma function (Abramowitz and Stegun, 1964, p 260), shifted along the time axis. Press et al. (1989) discuss efficient algorithms, including a FORTRAN function-routine. Pearson III contains just three parameters, equations (2.74) to (2.76), that can be related to the CDE through (3.44) to (3.46). The performance of the shifted incomplete gamma function is shown in Figure 3.8. The approximation appears to be slightly off at the beginning of breakthrough.
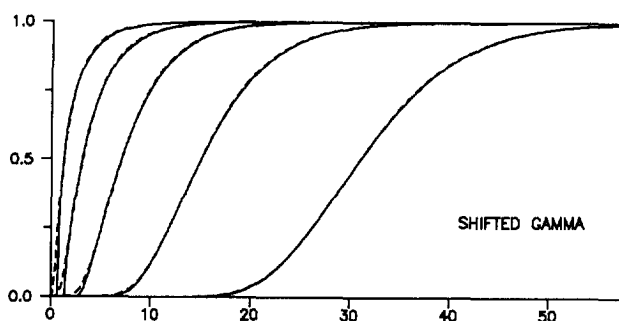
Figure 3.8 *Exact solutions to the CDE approximated by the shifted incomplete gamma function. All specifications conform Figure 3.5.*

On the other hand, the results are very robust and show no tendency to degenerate. Their evaluation, moreover, is highly efficient, considering that only three moments of the CDE are needed. Physically speaking, this variation on the mixing reservoirs model is apparently closely related to the diffusive model underlying the CDE. A marked difference is the theoretical breakthrough time of the first solute particle, which is zero for the CDE and $\mu - 2\sigma/\overset{1}{\gamma}$ for Pearson III. There are also marked differences in the shape of the breakthrough curves very close to the source ($x < \alpha_L$) where Pearson III has a steep front (Figure 3.9). From a practical point of view this need not be alarming, because at short distances the CDE is a poor model itself. The deficiency at the front appears to be mitigated if the skewness $\overset{1}{\gamma}$ is somewhat reduced. In Figure 3.10 we multiplied $\overset{1}{\gamma}$ by 0.8. The improvement goes at the expense of the former perfect fit later on, but the whole evokes a well balanced impression.

We stress that, in this application, we did not introduce the mixing reservoirs model as a model of dispersive groundwater flow. Rather did we use the resulting incomplete gamma function as an approximate solution to the CDE, which is
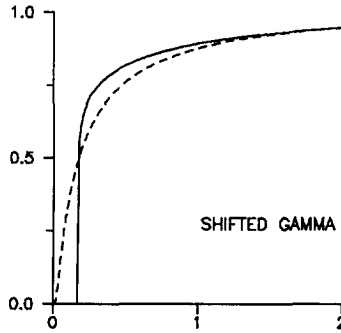
Figure 3.9   *Difference between CDE and Pearson III close to the source* $(x = 0.5\alpha_L)$.
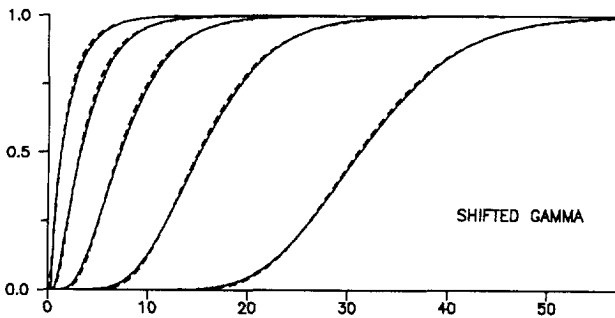
Figure 3.10   *Same as Figure 3.8, with a slightly reduced skewness.*

therefore the actual model, from which the parameters of the incomplete gamma function derive.

3.6.5 *Decay*

The decaying case (3.29) is interesting by the fact that its zero[th] order moment declines during transport of the plume. We saw in Section 2.5 that this does not preclude the existence of a Gaussian limit. *Moments and cumulants must be scaled by M_0, however, and the resulting approximative solution has to be multiplied by M_0*. We illustrate the procedure briefly.

The Fourier transform of (3.29) reads

$$\frac{d^2 \bar{c}}{dX^2} - \frac{d\bar{c}}{dX} = -i\omega\bar{c} + \lambda^*\bar{c} \tag{3.51}$$

where X and T are dimensionless. The parameter λ^* (being dimensionless either) is given by (3.31). The solution of the semi-infinite case, analogous to Subsection

3.6.1, is

$$\bar{c}_F(X, i\omega) = e^{\frac{1}{2}X}e^{-\frac{1}{2}X\sqrt{1-4(i\omega-\lambda^*)}} \tag{3.52}$$

if we choose $\bar{c}_F(0,0) = 1$ (because that corresponds to the boundary condition at $X = 0$ of the non-decaying analogue). By definition

$$M_0 = \bar{c}_F(X, 0) = e^{\frac{1}{2}X(1-\beta)} \tag{3.53}$$

where β has the same meaning as in the exact solution (3.33) of this problem:

$$\beta = \sqrt{1 + 4\lambda^*} \tag{3.54}$$

The scaled version of (3.52) reads

$$\frac{\bar{c}_F(X, i\omega)}{M_0} = e^{\frac{1}{2}X\beta}e^{-\frac{1}{2}X\sqrt{\beta^2-4i\omega}} \tag{3.55}$$

from which we obtain the following expression for the cumulants

$$K_1 = \frac{X}{\beta} \tag{3.56}$$

$$K_n = X\frac{2^{n-1}}{\beta^{2n-1}}\prod_{i=2}^{N}(2i-3) \tag{3.57}$$

(compare [3.42] and [3.43]). From this we derive the following dimensionless forms of μ, σ, $\overset{1}{\gamma}$, and $\overset{2}{\gamma}$

$$\mu = \frac{X}{\beta} \tag{3.58}$$

$$\sigma = \frac{1}{\beta}\sqrt{\frac{2X}{\beta}} \tag{3.59}$$

$$\overset{1}{\gamma} = \sqrt{\frac{18}{\beta X}} \tag{3.60}$$

$$\overset{2}{\gamma} = \frac{30}{\beta X} \tag{3.61}$$

(compare [3.44] to [3.47] and notice the remark following these equations). It is interesting to notice that the mean occurs earlier than in the non-decaying case, a phenomenon that we already experienced with the bank groundwater plant in Chapter 1 (see Figure 1.4).

Figure 3.11 shows approximations to the exact solution (3.33), by Edgeworth's expansion, Von Mises' method, and the incomplete gamma function,
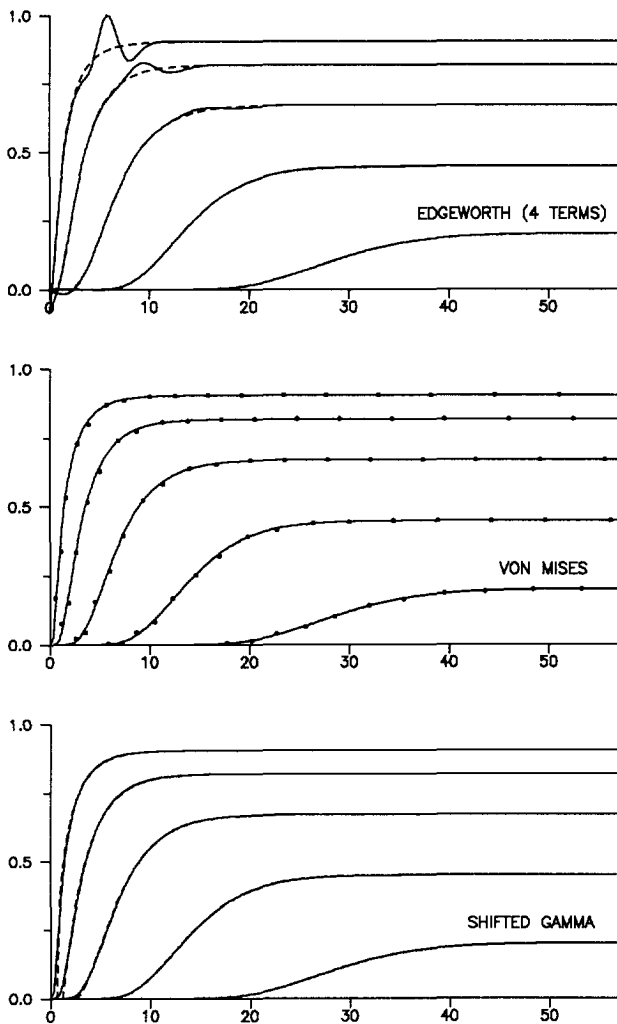
Figure 3.11   *Various approximations to the CDE with decay term. In this example $\beta = 1.1$. All specifications conform Figure 3.5.*

resp. We need not comment on this figure, because the characteristics of the various methods are not different from what we found in the non-decaying case.

3.7 Strack's dispersion equation

The CDE predicts the presence of contaminated particles at any distance from the source, right at the instant of contamination. Strack (1992) considers this a major objection. In order to overcome the problem he proposed to add a kind of inertia term to Fick's law of diffusion, changing it from

$$q_d = -D\frac{\partial c}{\partial x} \qquad (3.62)$$

to

$$q_d = -D\frac{\partial c}{\partial x} - \beta\frac{\partial q_d}{\partial t} \qquad (3.63)$$

where q_d is the dispersive solute flux. As before, D is the longitudinal dispersion constant, which equals $\alpha_L v$ in one-dimensional flow (compare [3.19]. β is a new constant (not to be mixed up with the β-coefficient that we used to characterize decay in previous sections)! This parameter controls the propagation velocity of the solute front. (Strack's derivations are actually fully three-dimensional, allowing for curvilinear stream lines. We confine ourselves to a simplified account of Strackian dispersion along a straight stream line). Notice that addition of the new term in (3.63) makes it possible to have a finite flux q_d, even if the gradient $\partial c/\partial x$ becomes infinite. Like Fick's law, the new term is merely phenomenological; there are no underlying thermodynamical concepts.

From the discussion in Section 3.4 we infer that the concentration in (3.63) is volume-averaged:

$$q_d = -D\frac{\partial c_R}{\partial x} - \beta\frac{\partial q_d}{\partial t} \qquad (3.64)$$

Similar to (3.13) we obtain the following expression for the total solute flux:

$$qc_F = qc_R + \theta q_d = qc_R - \theta D\frac{\partial c_R}{\partial x} - \theta\beta\frac{\partial q_d}{\partial t} \qquad (3.65)$$

where q is the fluid flux and θ is the effective porosity. The concentration in the left-hand term of (3.65) is flux-averaged. The mass balance is unaltered by Strack's assumption:

$$-\frac{\partial qc_F}{\partial x} = \theta\frac{\partial c_R}{\partial t} \qquad (3.66)$$

Elimination of q and q_d from (3.64) through (3.66) shows that

$$\alpha_L v\frac{\partial^2 c_R}{\partial x^2} - v\frac{\partial c_R}{\partial x} = \frac{\partial c_R}{\partial t} + \beta v\frac{\partial^2 c_R}{\partial x\partial t} + \beta\frac{\partial^2 c_R}{\partial t^2} \qquad (3.67)$$

and likewise for c_F. Changing to dimensionless variables $X = x/\alpha_L$ and $T = vt/\alpha_L$:

$$\frac{\partial^2 c}{\partial X^2} - \frac{\partial c}{\partial X} = \frac{\partial c}{\partial T} + \lambda\left(\frac{\partial^2 c}{\partial X\partial T} + \frac{\partial^2 c}{\partial T^2}\right) \qquad (3.68)$$

for both c_R and c_F, where

$$\lambda = \frac{\beta v}{\alpha_L} \tag{3.69}$$

The next chapter presents experimental evidence that $\beta :: 1/v$, so that λ is a constant, not depending on velocity. Equation (3.68) turns into the CDE if $\lambda = 0$. On the other hand, when λ becomes infinitely large, (3.68) turns into

$$\frac{\partial^2 c}{\partial X \partial T} + \frac{\partial^2 c}{\partial T^2} = 0 \tag{3.70}$$

which describes piston flow. It is thus seen that Strack's model balances neatly between the two classical models of contaminant transport.

Solutions in terms of c_F can be recast in terms of c_R by the mass balance relation

$$c_R = -\int_0^T \frac{\partial c_F}{\partial X} dT' \tag{3.71}$$

which is nothing but a restatement of (3.66). Notice that (3.71) is identical to (3.27). In the CDE-case we had also an easy relation (3.23) to transform solutions in terms of c_R into solutions in terms of c_F. The equivalent expression is somewhat less convenient in the present case:

$$c_F + \lambda \frac{\partial c_F}{\partial T} = c_R + \lambda \frac{\partial c_R}{\partial T} - \frac{\partial c_R}{\partial X} \tag{3.72}$$

This relation follows from (3.64) and (3.65).

A standard classification technique shows easily that Strack's dispersion equation (3.68) is of the hyperbolic type. Hyperbolic differential equations allow for a transformation of the independent variables to so called characteristics, along which the equation itself assumes a particularly simple form. This is the basis for a numerical solution scheme, which has been extensively explored as part of the LCMR-project. The results are reported elsewhere (Fairbrother, 1992). In this thesis we employ the Laplace-transform technique, to solve two simple problems that can be regarded as extensions of the problems discussed in Section 3.5 for the CDE.

The first problem is that of an infinite column, which at $T = 0$ contains a solute at concentration 1 in the negative half $X < 0$ and pure water in the positive half $X > 0$. The concentration is set equal to .5 at $T = 0$, $X = 0$. It is shown in Appendix 3.10.1 that this problem yields the following solution in terms of c_R:

a) if $T \leq X$ then

$$c_R(X,T) = \frac{\lambda}{2\sqrt{\lambda(\lambda+4)}} e^{-a} I_0\{\sqrt{a^2 - b^2}\}$$
$$+ \tfrac{1}{2} e^{-b} + \tfrac{1}{2} b \int_b^c \frac{e^{-\tau}}{\sqrt{\tau^2 - b^2}} I_1\{\sqrt{\tau^2 - b^2}\} d\tau \tag{3.73}$$

b) if $T \geq X$ then

$$c_R(X,T) = \frac{\lambda}{2\sqrt{\lambda(\lambda+4)}} e^{-a} I_0\{\sqrt{a^2 - b^2}\}$$

$$+ 1 - \tfrac{1}{2}e^{-b} - \tfrac{1}{2}b \int_b^c \frac{e^{-\tau}}{\sqrt{\tau^2 - b^2}} I_1\{\sqrt{\tau^2 - b^2}\} d\tau \qquad (3.74)$$

where

$$a = \frac{2T}{\lambda(\lambda+4)} \qquad (3.75)$$

$$b = \left| \frac{X - T}{\sqrt{\lambda(\lambda+4)}} \right| \qquad (3.76)$$

$$c = \frac{T(2+\lambda) - \lambda X}{\lambda(\lambda+4)} \qquad (3.77)$$

This solution applies only on intervals of time where the lower bound b of the integral does not exceed the upper bound c. The concentration is either zero (in the downstream part of the column) or one (in the upstream part) if this condition is not met. The concentration jumps at dimensionless time

$$T_f = \tfrac{1}{2}X\{\sqrt{\lambda(\lambda+4)} - \lambda\} \qquad (3.78)$$

if $X > 0$, and at

$$T_t = -\tfrac{1}{2}X\{\sqrt{\lambda(\lambda+4)} + \lambda\} \qquad (3.79)$$

where the subscripts f and t stand for front and tail, respectively. The characteristic behavior of the solution is better inferred from concentration profiles (c_R vs X) than from breakthrough curves. Figure 3.12 gives a few examples. One may notice that the fronts and the tails are not symmetrically located with respect to the mean.

Equations (3.73) and (3.74) are the counterparts of solution (3.22) of the CDE (compare Figure 3.1). Expressions for flux-averaged concentrations c_F analogous to (3.24) can be found straight forwardly. We will not present them here, because they are rather inconvenient and the infinite model is not so useful as a model of dispersive solute transport, because it shows backflow at the source. We will focus on the semi-infinite column instead.

Appendix 3.10.2 presents a solution of Strack's differential equation (3.68) for c_F, in case of a semi-infinite column which has originally zero concentration. At $T = 0$ the value of c_R is suddenly raised to 1 and kept constant ever after. The expression reads

$$c_F(X,T) = e^{\frac{1}{2}X - ab} + a e^{\frac{1}{2}X} \int_b^c \frac{e^{-a\tau}}{\sqrt{\tau^2 - a^2}} I_1\{\sqrt{\tau^2 - a^2}\} d\tau \qquad (3.80)$$
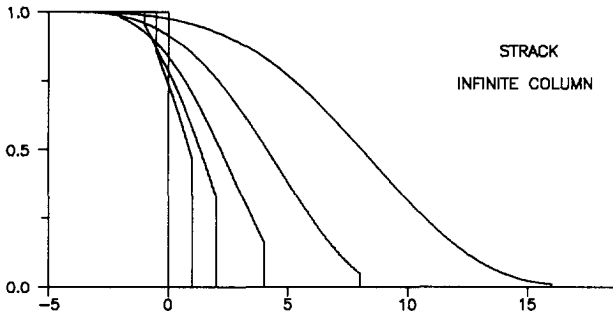
Figure 3.12   *Some concentration profiles in an infinite column according to Strack's dispersion equation, for $\lambda = 0.5$. The profiles correspond to $T = 0., 0.5, 1., 2., 4$ and 8. Horizontal axis: dimensionless distance. Vertical axis: dimensionless concentration.*

where

$$a = \tfrac{1}{2}(\lambda + 2) \tag{3.81}$$

$$b = \frac{X}{\sqrt{\lambda(\lambda + 4)}} \tag{3.82}$$

$$c = \frac{2T + \lambda X}{\lambda(\lambda + 4)} \tag{3.83}$$

The solution applies when $b \leq c$, c_F being zero if this condition is not met. There occurs a concentration jump at dimensionless time

$$T_f = \tfrac{1}{2}X\{\sqrt{\lambda(\lambda + 4)} - \lambda\} \tag{3.84}$$

which propagates at dimensionless velocity

$$v_f = \tfrac{1}{2}\left(\sqrt{1 + \tfrac{4}{\lambda}} + 1\right) \tag{3.85}$$

Notice that T_f is exactly the same as in the case of the infinite column. The tail is forced, however, to remain at $X = 0$. Figure 3.13 gives a number of concentration profiles for the same value of λ and the same times as in Figure 3.12. In addition, Figure 3.14 shows some typical breakthrough curves (c_F vs T), compared with solutions of the CDE. This figure gives a fair impression of how λ affects breakthrough behavior.

It is shown in Appendix 3.10.3 that the cumulants of Strack's dispersion equation, semi-infinite column case, are

$$K_1 = X \tag{3.86}$$

$$K_n = \tfrac{1}{2}X A_n \tag{3.87}$$
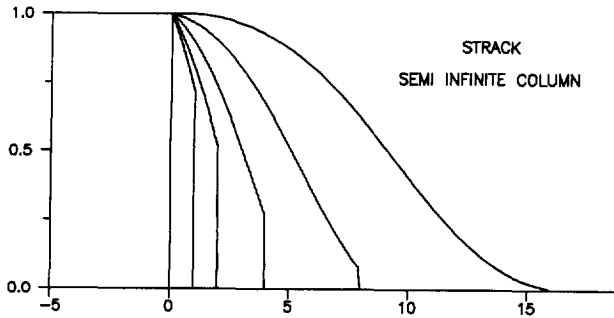
Figure 3.13 *Some concentration profiles in a semi-infinite column according to Strack's dispersion equation. All specifications conform Figure 3.12.*
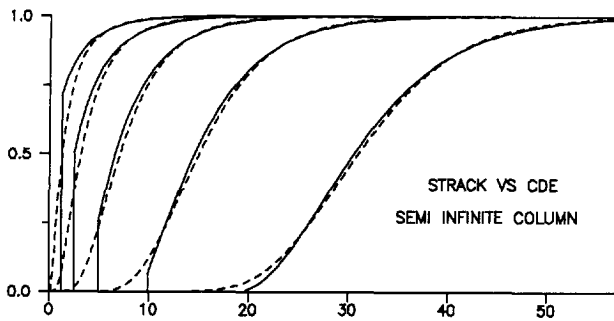
Figure 3.14 *Some breakthrough curves in a semi-infinite column according to Strack's dispersion equation for $\lambda = 1$. Dotted lines are solutions to the CDE. All specifications conform Figure 3.5.*

where

$$\frac{A_n}{n!} = \frac{1}{2n} \sum_{i=1}^{n} \frac{A_{n-i}}{(n-i)!} \frac{\{\lambda^i + (\lambda+4)^i\}}{i!}$$

$$A_0 = 1$$

$$(3.88)$$

The $\overset{i}{\gamma}$ that are needed to apply Edgeworth's method of approximation can be obtained from the cumulants by means of (3.7). Since we saw that it makes no sense to use more than 3 terms, we can explicitly state that the dimensionless

forms of μ, σ, $\overset{1}{\gamma}$, and $\overset{2}{\gamma}$ are

$$\mu = X \tag{3.89}$$

$$\sigma = \sqrt{2X} \tag{3.90}$$

$$\overset{1}{\gamma} = \frac{3(\lambda + 2)}{\sqrt{2X}} \tag{3.91}$$

$$\overset{2}{\gamma} = \frac{6(\lambda^2 + 4\lambda + 5)}{X} \tag{3.92}$$

These expressions turn into (3.44) to (3.47) if $\lambda = 0$, as they should do. Von Mises' method requires central moments of various orders, which can be calculated by (3.6). The parameters of Pearson III, applied to Strack's differential equation, are found through (2.74) to (2.76):

$$a = \frac{2}{3\lambda + 6} \tag{3.93}$$

$$n = \frac{8X}{(3\lambda + 6)^2}$$

$$b = \frac{3\lambda + 2}{3\lambda + 6} X \tag{3.95}$$

Edgeworth's approximation, Von Mises' approach and the shifted incomplete gamma function (the latter labeled 'Pearson III') are shown by Figure 3.15. The superiority of the shifted incomplete gamma function shows once more. In fact, the approximation looks not worse than Figure 3.8, although the curves are much skewer. Edgeworth's approximation is clearly inferior and starts to become useful only at $X = 64$. Von Mises' approach is not too bad, but it fails to reflect the typical steep front behavior of Strack's breakthrough curves, close to the source.

3.8 Strack's dispersion equation, inclusive of decay and sorption

Strack Strack [1994], Strack and Fairbrother [1994]) extended his equation to include first order decay and linear rate dependent sorption. We treat the 1-D case in this section, before passing on to the more general case. The basic equations, from which Strack's differential equation derives, are
1) Mass balance of sorbing phase:

$$\frac{\partial c_s}{\partial t} = \kappa_1 c_R - \kappa_2 c_s - \nu c_s \tag{3.96}$$

2) Mass balance of sorbing + moving phases:

$$-\frac{\partial q c_F}{\partial x} = \theta \frac{\partial (c_R + c_s)}{\partial t} + \nu (c_R + c_s) \tag{3.97}$$
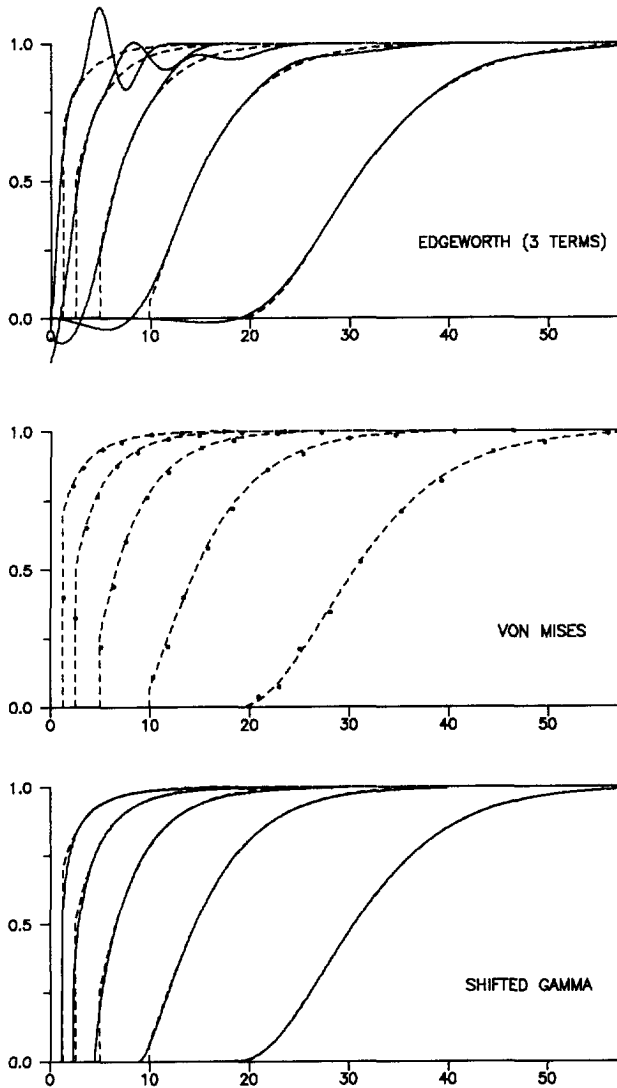
Figure 3.15   *Various approximations to Strack's dispersion equation for $\lambda = 1$. Dotted lines are exact. All specification conform Figure 3.5, except for the skewnesses, which are 4.5, 3.18, 1.59 and 1.13, respectively.*

3) Dispersion equations:

$$qc_F = qc_R + \theta q_d \tag{3.98}$$

$$q_d = -D\frac{\partial c_R}{\partial x} - \beta\frac{\partial q_d}{\partial t} \tag{3.99}$$

The concentration c_s of the sorbing phase must be understood to be the ratio

of sorbed mass to pore volume, just like c_R is the ratio of solved mass to pore volume. The parameter ν, occurring in (3.96) and (3.97) is the decay constant of the contaminant. For instance, if κ_1 and κ_2 were zero, then the solution of (3.96) would be

$$c_s(t) = c_s(0)e^{-\nu t} \tag{3.100}$$

which describes first order decay. The parameters κ_1 and κ_2 in (3.96) govern the sorption rate and the equilibrium distribution of the contaminant between solute and sorbent. This formulation is sufficiently general to allow for various physical interpretations. In case of sorption to grains, for instance, the usual notation of (3.96) reads

$$\frac{\partial s}{\partial t} = \kappa(\kappa_d c - s) - \nu s \tag{3.101}$$

where s is the quantity of mass sorbed on the grains and κ_d is the distribution coefficient, or partition coefficient, of the Freundlich isotherm (Domenico and Schwartz [1990], p 441; Freeze and Cherry [1979], p 403). In this case, c_s would have to be defined by

$$c_s = \frac{\rho}{\theta} s \tag{3.102}$$

where ρ is the mass density of the grains and θ is the porosity of the porous medium. The parameter κ in (3.101) determines the exchange rate of contaminant between sorbent and solute. Consequently, we would get

$$\kappa_1 = \frac{\rho}{\theta} \kappa \kappa_d \tag{3.103}$$

$$\kappa_2 = \kappa \tag{3.104}$$

On a quite different scale, one might distinguish immobile zones within a heterogeneous porous medium, that are apt to penetration by contaminants through a diffusion-like process (Coates and Smith [1964], Herr et al. [1988]). In that case s will be the concentration (mass/porosity) in the immobile phase, and

$$c_s = \frac{\theta_{im}}{\theta_m} s \tag{3.105}$$

where θ_{im} and θ_m are the porosities of the immobile and mobile zones, respectively. Equation (3.96) would then read

$$\frac{\partial s}{\partial t} = \kappa(c - s) - \nu s \tag{3.106}$$

and thus,

$$\kappa_1 = \frac{\theta_{im}}{\theta_m} \kappa \tag{3.107}$$

$$\kappa_2 = \kappa \tag{3.108}$$

It is not difficult to think of more complicated models than (3.96), many of which would not obstruct the procedure to be outlined below, but we feel that the present formulation serves our purpose sufficiently well.

Equation (3.97) is a mere extension of (3.14), which we need not comment on. The dispersion equations (3.98) and (3.99), finally, are only reformulations of (3.62) and (3.63).

From (3.96) through (3.99) we obtain

$$
\alpha_L v \frac{\partial^2 c}{\partial x^2} - \beta v \frac{\partial^2 c}{\partial x \partial t} - \beta \frac{\partial^2 c}{\partial t^2} - v \frac{\partial c}{\partial x} - \frac{\partial c}{\partial t} =
$$
$$
-\kappa_2 \beta \frac{\partial c_s}{\partial t} + (\kappa_1 + \nu)\beta \frac{\partial c}{\partial t} - \kappa_2 c_s + (\kappa_1 + \nu)c \tag{3.109}
$$

and

$$
\frac{\partial c_s}{\partial t} = \kappa_1 c - (\kappa_2 + \nu)c_s \tag{3.110}
$$

Elimination of c_s gives a single differential equation in c:

$$
\alpha_L v \frac{\partial^3 c}{\partial x^2 \partial t} - \beta v \frac{\partial^3 c}{\partial x \partial t^2} - \beta \frac{\partial^3 c}{\partial t^3} + \kappa_2^* \alpha_L v \frac{\partial^2 c}{\partial x^2} - v(1 + \beta \kappa_2^*) \frac{\partial^2 c}{\partial x \partial t}
$$
$$
-\{1 + \beta(\nu + \kappa_1 + \kappa_2^*)\} \frac{\partial^2 c}{\partial t^2} - v \kappa_2^* \frac{\partial c}{\partial x} - \{(\kappa_1 + \kappa_2^*)(1 + \nu \beta) + \nu\} \frac{\partial c}{\partial t}
$$
$$
-\nu(\kappa_1 + \kappa_2^*)c = 0 \tag{3.111}
$$

where

$$
\kappa_2^* = \kappa_2 + \nu \tag{3.112}
$$

This equation holds for both the volume-averaged concentration ($c = c_R$) and the flux-averaged concentration ($c = c_F$). We have not attempted to solve (3.111) exactly, but it may be observed that a special case occurs if $\kappa_2^* = 1/\beta$. Equation (3.111) changes then into:

$$
\alpha_L v \frac{\partial^2 c}{\partial x^2} - \beta v \frac{\partial^2 c}{\partial x \partial t} - \beta \frac{\partial^2 c}{\partial t^2} - v \frac{\partial c}{\partial x} - \{\beta(\kappa_1 + \nu) + 1\} \frac{\partial c}{\partial t} - (\beta \kappa_1 + 1)\nu c = 0 \tag{3.113}
$$

(Check: $\frac{\partial}{\partial t}$ [3.113] $+\kappa_2^*$ [3.113] = [3.111] if $\kappa_2^* = 1/\beta$).

For a semi-infinite column which has originally zero concentration, while at $t = 0$ the concentration at $x = 0$ is suddenly raised to 1 and kept constant there ever after, we find the following solution:

$$
c_F(X, T) = e^{\frac{1}{2}X - ab} + ae^{\frac{1}{2}X} \int_a^c \frac{e^{-a\tau}}{\sqrt{\tau^2 - a^2}} I_1\{\sqrt{\tau^2 - a^2}\} d\tau \tag{3.114}
$$

where

$$a = \frac{\lambda + 2A}{\sqrt{(\lambda + 2A)^2 - \lambda(\lambda + 4)(4B + 1)}} \tag{3.115}$$

$$b = \tfrac{1}{2} \frac{X}{\sqrt{\lambda(\lambda + 4)}} \sqrt{(\lambda + 2A)^2 - \lambda(\lambda + 4)(4B + 1)} \tag{3.116}$$

$$c = \tfrac{1}{2} \frac{2T + \lambda X}{\lambda(\lambda + 4)} \sqrt{(\lambda + 2A)^2 - \lambda(\lambda + 4)(4B + 1)} \tag{3.117}$$

while

$$\lambda = \frac{\beta v}{\alpha_L} \tag{3.118}$$

$$A = \beta(\kappa_1 + \nu) + 1 \tag{3.119}$$

$$B = \frac{\alpha_L \nu}{v}(\beta \kappa_1 + 1) \tag{3.120}$$

X is dimensionless distance (x/α_L) and T is dimensionless time (vt/α_L). This solution applies when $a \le b$, the concentration $c(X, T)$ being zero if this condition is not met. There occurs a concentration jump at dimensionless time

$$T_f = \tfrac{1}{2} X \{ \sqrt{\lambda(\lambda + 4)} - \lambda \} \tag{3.121}$$

which propagates at dimensionless velocity

$$v_f = \tfrac{1}{2}\left(\sqrt{1 + \tfrac{4}{\lambda}} + 1 \right) \tag{3.122}$$

Notice that (3.114) is literally the same as (3.80): only the meanings of the parameters a, b, and c differ. (For this reason there is no documentation of (3.114) in the appendix). The propagation velocity of the front appears not at all to be affected by sorption or decay (compare [3.122] with [3.85]).

    We intend to use (3.114) to check an approximation by the Pearson III approach, but we will calculate the parameters of Pearson III for the more general case (3.111). As Pearson III has just three parameters we need only the first three central moments of $c(X, T)$, and we don't have to bother too much about recursion formulae. We avail ourselves of the opportunity to outline an alternative method to calculate central moments.

    For convenience we rewrite (3.111) as

$$A\frac{\partial^3 c}{\partial x^2 \partial t} + B\frac{\partial^3 c}{\partial x \partial t^2} + C\frac{\partial^3 c}{\partial t^3} + D\frac{\partial^2 c}{\partial x^2} + E\frac{\partial^2 c}{\partial x \partial t} + F\frac{\partial^2 c}{\partial t^2} + G\frac{\partial c}{\partial x} + H\frac{\partial c}{\partial t} + Ic = 0$$
$$\tag{3.123}$$

where

$$
\begin{array}{lll}
A = \alpha_L v & B = -\beta v & C = -\beta \\
D = \kappa_2^* \alpha_L v & E = -v(1 + \beta \kappa_2^*) & F = -\{1 + \beta(\nu + \kappa_1 + \kappa_2^*)\} \\
G = -v\kappa_2^* & H = -\{(\kappa_1 + \kappa_2^*)(1 + \nu\beta) + \nu\} & I = -\nu(\kappa_1 + \kappa_2^*) \\
\kappa_2^* = \kappa_2 + \nu
\end{array}
$$

We derive from the definition of moments that

$$\int_{-\infty}^{\infty} t^n c\, dt = M_0 M_n \tag{3.124}$$

$$\int_{-\infty}^{\infty} t^n \frac{\partial c}{\partial t}\, dt = \begin{array}{cc} -nM_0 M_{n-1} & (n > 1) \\ -M_0 & (n = 1) \\ 0 & (n < 1) \end{array} \tag{3.125}$$

$$\int_{-\infty}^{\infty} t^n \frac{\partial^2 c}{\partial t^2}\, dt = \begin{array}{cc} n(n-1)M_0 M_{n-2} & (n > 2) \\ -2M_0 & (n = 2) \\ 0 & (n < 2) \end{array} \tag{3.126}$$

$$\int_{-\infty}^{\infty} t^n \frac{\partial^3 c}{\partial t^3}\, dt = \begin{array}{cc} -n(n-1)(n-2)M_0 M_{n-3} & (n > 3) \\ -3.2M_0 & (n = 3) \\ 0 & (n < 3) \end{array} \tag{3.127}$$

where $c = c(t)$ is the impulse response according to (1.123). Integration of (3.123) with respect to t gives

$$D\frac{d^2 M_0}{dx^2} + G\frac{dM_0}{dx} + IM_0 = 0 \tag{3.128}$$

yielding

$$M_0 = e^{\gamma x} \tag{3.129}$$

where

$$\gamma = \frac{-G - \sqrt{G^2 - 4DI}}{2D} = \frac{1}{2\alpha_L}\left(1 - \sqrt{1 + \frac{4\alpha_L(\kappa_1 + \kappa_2^*)\nu}{\nu\kappa_2^*}}\right) \tag{3.130}$$

Notice that $M_0 = 1$ if $\nu = 0$ (no decay) as expected. Sorption enhances decay, if measured against x. This is also obvious, because sorption increases the mean travel time, as we will see next. The second step is to multiply all terms of (3.123) by t and integrate, to find

$$-A\frac{d^2 M_0}{dx^2} + D\frac{d^2 M_1 M_0}{dx^2} - E\frac{dM_0}{dx} + G\frac{dM_0 M_1}{dx} - HM_0 + IM_0 M_1 = 0 \tag{3.131}$$

We know from convolution theory (Chapter 2) that in homogeneous media $M_1 :: x$, so $d^2 M_1/dx^2 = 0$. Using this and equation (3.128) and (3.129), equation (3.131) simplifies to

$$(2\gamma D + G)\frac{dM_1}{dx} = A\gamma^2 + E\gamma + H \tag{3.132}$$

and thus

$$M_1 = \frac{A\gamma^2 + E\gamma + H}{2\gamma D + G}x \tag{3.133}$$

or

$$\mu = \frac{\alpha_L v \gamma^2 - v(1 + \beta\kappa_2^*)\gamma - \{(\kappa_1 + \kappa_2^*)(1 + \nu\beta) + \nu\}}{2\alpha_L v \kappa_2^* \gamma - v\kappa_2^*} x \tag{3.134}$$

This is a quite complicated expression, considering that the parameter γ is itself already intricate. If there were no decay, we would just obtain

$$\mu = \frac{\kappa_1 + \kappa_2}{\kappa_2} \frac{X}{v} \tag{3.135}$$

which shows that, indeed, sorption increases the mean travel time.

The third step, which involves multiplication of (3.123) by t^2 and integration, leads in a similar fashion to

$$\overset{c}{M}_2 = \frac{-2D(M_1')^2 + (4A\gamma + 2E)M_1' - 2B\gamma - 2F}{2\gamma D + G} x \tag{3.136}$$

where accents denote differentiation with respect to x. Use has been made of the relation

$$M_2 = \overset{c}{M}_2 + M_1^2 \tag{3.137}$$

(see [2.26]) and of the fact that $d^2 \overset{c}{M}_2 / dx^2 = 0$ in a homogeneous medium. It follows that

$$\sigma^2 =$$

$$\frac{-2\alpha_l v \kappa_2^* (M_1')^2 + \{4\alpha_L v \gamma - 2v(1 + \beta\kappa_2^*)\}M_1' - 2\beta v\gamma + 2\{1 + \beta(\nu + \kappa_1 + \kappa_2^*)\}}{2\alpha_L v \kappa_2^* \gamma - v\kappa_2^*}$$
$$\tag{3.138}$$

If there were no decay, then (3.138) would simplify to

$$\sigma^2 = \frac{2}{v^2} \left\{ \alpha_L \left(\frac{\kappa_1 + \kappa_2}{\kappa_2}\right)^2 + \frac{v\kappa_1}{\kappa_2^2} \right\} x \tag{3.139}$$

It is apparent that sorption increases the variance of the breakthrough curve. Sorption causes dispersion, even if $\alpha_L = 0$.

Proceeding to the third moment, we find in a completely analogous way that

$$\overset{c}{M}_3 = \frac{6A[\gamma \overset{c}{M}_2' + (M_1')^2] - 6BM_1' + 6C - 6D\overset{c}{M}_2' M_1' + 3E\overset{c}{M}_2'}{2\gamma D + G} x \tag{3.140}$$

or

$$\frac{1}{\gamma}\sigma^3 = \frac{6\alpha_L v[\gamma \overset{c}{M}_2' + (M_1')^2] + 6\beta v M_1' - 6\beta - 6\alpha_L v \kappa_2^* \overset{c}{M}_2' M_1' - 3v(1 + \beta\kappa_2^*)\overset{c}{M}_2'}{2\alpha_L v \kappa_2^* \gamma - v\kappa_2^*} x$$
$$\tag{3.141}$$

We made use of the fact that $d^2 \overset{c}{M}_3/dx^2 = 0$, and of relation (2.27):

$$M_3 = \overset{c}{M}_3 + 3\overset{c}{M}_2 M_1 + M_1^3 \qquad (3.142)$$

Without decay, (3.141) would just yield

$$\tfrac{1}{\gamma}\sigma^3 = \frac{6(1 + \beta\kappa_2)\{\alpha_L(\kappa_1 + \kappa_2)^2 + v\kappa_1\}}{v^2\kappa_2^3}x \qquad (3.143)$$

So sorption contributes also to the skewness of the breakthrough profile. We recall that the three parameters of the Pearson III distribution are

$$a = \frac{2}{\tfrac{1}{\gamma}\sigma} \qquad (3.144)$$

$$n = \frac{4}{\left(\tfrac{1}{\gamma}\right)^2} \qquad (3.145)$$

$$b = \mu - \frac{2\sigma}{\tfrac{1}{\gamma}} \qquad (3.146)$$

(see [2.74], [2.75] and [2.76]). They can now be evaluated since μ, σ, and $\tfrac{1}{\gamma}$ follow immediately from M_1, $\overset{c}{M}_2$ and $\overset{c}{M}_3$.

One may notice that the numerical evaluation of (3.130) becomes impossible if $D = 0$. In that case we find from (3.128) and (3.129) that

$$\gamma = -\frac{I}{G} \qquad (D = 0, \; G \neq 0) \qquad (3.147)$$

Likewise, evaluation of M_1, $\overset{c}{M}_2$ and $\overset{c}{M}_3$ becomes impossible if $2\gamma D + G = 0$. It follows from the physical nature of the constants involved that this would imply $D = 0$ and $G = 0$ (provided that the velocity v is non-zero). $G = 0$ implies also that $I = 0$, and equation (3.123) simplifies to

$$A\frac{\partial^2 c}{\partial x^2} + B\frac{\partial^2 c}{\partial x \partial t} + C\frac{\partial^2 c}{\partial t^2} + E\frac{\partial c}{\partial x} + F\frac{\partial c}{\partial t} + Hc = 0 \qquad (3.148)$$

which leads us ultimately to

$$\gamma = \frac{-E - \sqrt{E^2 - 4AH}}{2A} \qquad (D = 0, G = 0) \qquad (3.149)$$

$$M_1 = \frac{\gamma B + F}{2A\gamma + E}x \qquad (D = 0, G = 0) \qquad (3.150)$$

$$\overset{c}{M}_2 = \frac{-2A(M_1')^2 + 2BM_1' - 2C}{2A\gamma + E}x \qquad (D = 0, G = 0) \qquad (3.151)$$

$$\overset{c}{M}_3 = \frac{3B\overset{c}{M}_2' - 6A\overset{c}{M}_2' M_1'}{2A\gamma + E}x \qquad (D = 0, G = 0) \qquad (3.152)$$

Finally, evaluation of (3.149) would be obstructed by (A=0), in which case it can be shown that

$$\gamma = -\frac{H}{E} \qquad (D = 0, G = 0, A = 0) \tag{3.153}$$

E being greater than or equal to one, there are no further numerical obstacles, except for our finding that $\overset{c}{M}_2$ and $\overset{c}{M}_3$ may become minus zero under exceptional conditions, due to numerical round off. This hinders evaluation of the parameters of Pearson III. This pitfall is easily avoided, of course, by setting a lower bound to these quantities, equal to the smallest positive number.

We have tested this approach against (3.114) for many different combinations of v, α_L, β, κ_1, and ν, always finding good to excellent performance as long as $x > 5\alpha_L$. Figure 3.16 gives a typical example. Having no exact solution of (3.113) at hand, there is as yet no confirmation of the accuracy of this approach for the general case where $\kappa_2^* \neq 1/\beta$.
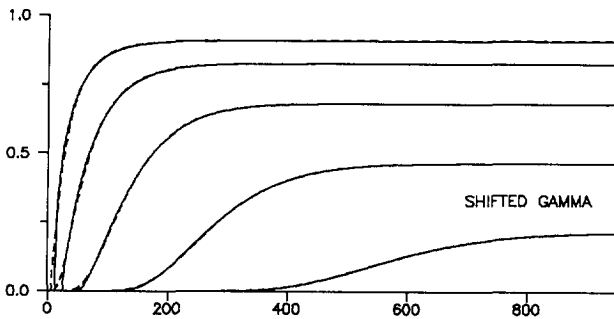
Figure 3.16 *Breakthrough curves by the Pearson III approach, check-ed against equation (3.114). Vertical axis: dimension-less concentration; Horizontal axis: time in days. Break-through distances shown are $x = 2, 4, 8, 16$ and 32 m. Other parameter values: $v = 0.1$ m/d, $\alpha_L = 1$ m, $\beta = 1$ d, $\kappa_1 = 1$ d^{-1}, $\nu = 0.0025$ d^{-1}, $\kappa_2 = 1$ d^{-1}.*

3.9 Non-uniform flow

It can be shown that equation (3.111) remains unaltered if x is chosen along a (presumably) curvilinear stream line in a non-uniform flow field. The method outlined in the preceding section remains basically unaltered, too, but the second derivatives of the various moments vanish no longer. The expressions found for the various moments are not accurate, if applied to non-uniform flow. We expect them not to be far off, however, because the second derivatives fluctuate about

zero (going along an alternately converging and diverging flow path) while the moments themselves increase more or less steadily. As an example we evaluated several breakthrough curves along the curvilinear stream line shown in Figure 3.17. This line almost hits a stagnation point, which is about the worst thing to happen to our method. Figure 3.18 displays approximative breakthrough curves against "exact" solutions, evaluated by the method of characteristics (Fairbrother, 1992). The curves are calculated at equidistant points along the stream line. The non-uniformity of the flow field shows clearly from the uneven spacing in time of the curves, as the point of stagnation is being passed.
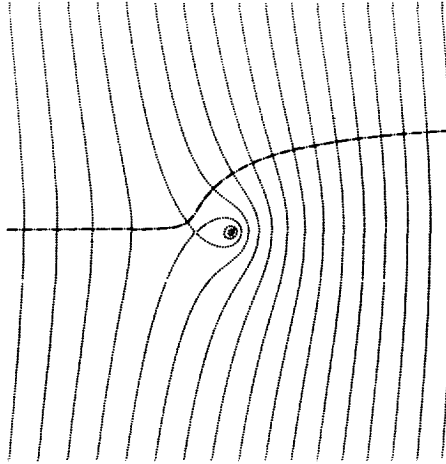
Figure 3.17   *Non-uniform flow field. (Courtesy M.D. Fairbrother, Univ. of Minn.)*

Exact solutions of M_0 through M_3 are still possible in the non-linear case, but the expressions become prohibitively involved and they contain integrals of the inverse of the velocity, which have to be evaluated numerically anyway. As the travel time of a particle is already computed numerically in most groundwater models, we recommend to do the same with the various moments. The equations to be integrated are

$$D\frac{d^2 M_0}{dx^2} + G\frac{dM_0}{dx} + IM_0 = 0 \tag{3.153}$$

$$D\frac{d^2 M_1}{dx^2} + (2M_0'D + G)\frac{dM_1}{dx} = AM_0'' + EM_0' + \overset{.}{H} \tag{3.154}$$

$$D\frac{d^2 \overset{c}{M}_2}{dx^2} + (2DM_0' + G)\frac{d\overset{c}{M}_2}{dx}$$
$$= (4AM_0' + 2E)M_1' - 2D(M_1')^2 - 2BM_0' - 2F \tag{3.155}$$
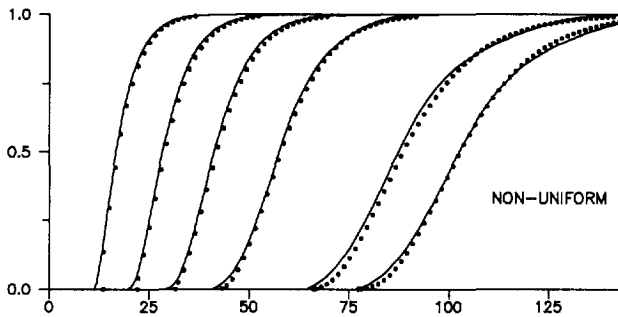
Figure 3.18   *Some breakthrough curves along a curvilinear stream line, approximated by (3.133), (3.136), and (3.140) (solid), versus exact curves (dotted). (Courtesy M.D. Fairbrother, Univ. of Minn.)*

$$D\frac{d^2 \overset{c}{M}_3}{dx^2} + (2M_0'D + G)\frac{d\overset{c}{M}_3}{dx}$$
$$= 6A[M_0'\overset{c}{M}_2' + (M_1')^2] - 6BM_1' + 6C - 6D\overset{c}{M}_2'M_1' + 3E\overset{c}{M}_2' \qquad (3.156)$$

Accents and double accents denote differentiation with respect to x. (We adopted this notation to distinguish moments, whose values are known from the previous equations, from the particular moment to be solved). The parameters A through I were given along with equation (3.123). Notice that A through I, C excepted, depend on v, which is a function of x when the flow field is non-uniform. All parameters, except E and F, may be absent, depending on the physical application.

There exist various numerical schemes to integrate second order ordinary differential equations. Most of them rewrite the equation as a system of two first order equations, which is solved by a Runge-Kutta method or any of its alternatives. The reader is referred to Press et al. (1992) for a concise overview and sample routines.

3.10 Appendix

3.10.1 *Derivation of (3.73) and (3.74)*

The differential equation to be solved is

$$\frac{\partial^2 c_R}{\partial X^2} - \frac{\partial c_R}{\partial X} = \frac{\partial c_R}{\partial T} + \lambda \left(\frac{\partial^2 c_R}{\partial X \partial T} + \frac{\partial^2 c_R}{\partial T^2} \right) \qquad (B.1)$$

under the boundary conditions

$$c_R(-\infty, T) = 1 \tag{B.2}$$

$$c_R(+\infty, T) = 0 \tag{B.3}$$

and the initial conditions

$$
\begin{aligned}
c_R(X,0) = 1 \quad & (X < 0) \\
\tfrac{1}{2} \quad & (X = 0) \\
0 \quad & (X > 0)
\end{aligned}
\tag{B.4}
$$

$$\frac{\partial c_R}{\partial T}(X,0) = 0$$

It is convenient to make the shift $(X, T) \to (u, T)$ where

$$u = X - T \tag{B.5}$$

which changes the differential equation into

$$\frac{\partial^2 c_R}{\partial u^2} = \frac{\partial c_R}{\partial T} + \lambda \left(-\frac{\partial^2 c_R}{\partial u \partial T} + \frac{\partial^2 c_R}{\partial T^2} \right) \tag{B.6}$$

The boundary and initial conditions stay formally unaltered, except for the fact that X has to be replaced by u in (B.4). Laplace transformation of the system gives

$$\frac{d^2 \bar{c}_R}{dX^2} + \lambda s \frac{d\bar{c}_R}{du} - s(1 + \lambda s)\bar{c}_R = 0 \tag{B.7}$$

$$\bar{c}_R(-\infty, s) = \frac{1}{s} \tag{B.8}$$

$$\bar{c}_R(+\infty, s) = 0 \tag{B.9}$$

which can be solved to give

$$\bar{c}_R(u, s) = A e^{-\frac{1}{2}u\{\lambda s + \sqrt{\lambda^2 s^2 + 4s(1+\lambda s)}\}} \qquad \text{if} \quad u > 0 \tag{B.10}$$

and

$$\bar{c}_R(u, s) = B e^{-\frac{1}{2}u\{\lambda s - \sqrt{\lambda^2 s^2 + 4s(1+\lambda s)}\}} + \frac{1}{s} \quad \text{if} \quad u < 0 \tag{B.11}$$

The concentrations and their gradients of both branches should match at $u = 0$, yielding

$$A = \tfrac{1}{2}\lambda \frac{1}{\sqrt{\lambda^2 s^2 + 4s(1 + \lambda s)}} + \frac{1}{2s} \tag{B.12}$$

$$B = \tfrac{1}{2}\lambda \frac{1}{\sqrt{\lambda^2 s^2 + 4s(1 + \lambda s)}} - \frac{1}{2s} \tag{B.13}$$

Set

$$a = \frac{4}{\lambda(\lambda + 4)} \tag{B.14}$$

$$b = 0 \tag{B.15}$$

$$c = \tfrac{1}{2} u \sqrt{\lambda(\lambda + 4)} \tag{B.16}$$

then

$$\bar{c}_R(u, s) = \left\{ \frac{\lambda}{2\sqrt{\lambda(\lambda + 4)}} \cdot \frac{1}{\sqrt{(s + a)(s + b)}} + \frac{1}{2s} \right\} e^{-\frac{1}{2} u \lambda s} \cdot e^{-c\sqrt{(s+a)(s+b)}}$$

$$u > 0 \tag{B.17}$$

and

$$\bar{c}_R(u, s) = \left\{ \frac{\lambda}{2\sqrt{\lambda(\lambda + 4)}} \cdot \frac{1}{\sqrt{(s + a)(s + b)}} - \frac{1}{2s} \right\} e^{-\frac{1}{2} u \lambda s} \cdot e^{c\sqrt{(s+a)(s+b)}}$$

$$u < 0 \tag{B.18}$$

of which expressions we are to find the inverse Laplace transforms. We note that

$$L^{-1} \left\{ e^{-\frac{1}{2} \lambda s u} \right\} = \delta(T - \tfrac{1}{2} \lambda u) \tag{B.19}$$

and

$$L^{-1} \left\{ \frac{1}{s} e^{-\frac{1}{2} \lambda s u} \right\} = H(T - \tfrac{1}{2} \lambda u) \tag{B.20}$$

where δ is Dirac's delta function and H is Heaviside's step function. It follows from tables (Oberhettinger and Badii, 1973, formula [5.138]) that

$$L^{-1} \left\{ \frac{1}{\sqrt{(s + a)(s + b)}} e^{-c\sqrt{(s+a)(s+b)}} \right\} =$$
$$e^{-\frac{1}{2}(a+b)T} \cdot I_0 \left\{ \tfrac{1}{2}(a - b)\sqrt{T^2 - c^2} \right\} \cdot H(T - c) \tag{B.21}$$

from which we find through differentiation with respect to $(-c)$ that

$$L^{-1} \left\{ e^{-c\sqrt{(s+a)(s+b)}} \right\} = e^{-\frac{1}{2}(a+b)c} \cdot \delta(T - c)$$
$$+ \frac{(a - b)c}{2\sqrt{T^2 - c^2}} \cdot e^{-\frac{1}{2}(a+b)T} \cdot I_1 \left\{ \tfrac{1}{2}(a - b)\sqrt{T^2 - c^2} \right\} \cdot H(T - c) \tag{B.22}$$

The inverse transforms of (B.17) and (B.18) can now be found by convolution:

if $u > 0$, then

$$c_R(u, T) = \frac{\lambda}{2\sqrt{\lambda(\lambda + 4)}} \int_0^T e^{-\frac{1}{2}(a+b)\tau} \cdot I_0 \left\{ \tfrac{1}{2}(a-b)\sqrt{\tau^2 - c^2} \right\} \cdot$$

$$\cdot H(\tau - c) \cdot \delta(T - \tau - \tfrac{1}{2}\lambda u)d\tau + \frac{1}{2} \int_0^T e^{-\frac{1}{2}(a+b)c} \cdot \delta(\tau - c) \cdot H(T - \tau - \tfrac{1}{2}\lambda u)d\tau$$

$$+ \frac{1}{2} \int_0^T \frac{(a-b)c}{2\sqrt{\tau^2 - c^2}} e^{-\frac{1}{2}(a+b)\tau} I_1 \left\{ \tfrac{1}{2}(a-b)\sqrt{\tau^2 - c^2} \right\} \cdot$$

$$\cdot H(\tau - c) \cdot H(T - \tau - \tfrac{1}{2}\lambda u)d\tau$$

$$(B.23)$$

and likewise if $u < 0$. Evaluation of these integrals gives:
if $u > 0$ then

$$c_R(u, T) = \frac{\lambda}{2\sqrt{\lambda(\lambda + 4)}} e^{-\frac{1}{2}(a+b)T} \cdot I_0 \left\{ \tfrac{1}{2}(a-b)\sqrt{T^2 - c^2} \right\}$$

$$+ \tfrac{1}{2}e^{-\frac{1}{2}(a+b)c} + \frac{1}{2} \int_c^{T - \frac{1}{2}\lambda} \frac{(a-b)c}{2\sqrt{\tau^2 - c^2}} e^{-\frac{1}{2}(a+b)\tau} \cdot I_1 \left\{ \tfrac{1}{2}(a-b)\sqrt{\tau^2 - c^2} \right\} d\tau$$

$$\text{if } T > c + \tfrac{1}{2}\lambda u, \text{ else } c_R(u, T) = 0 \qquad (B.24)$$

This can be rewritten as:
if $T < X$ then

$$c_R(X, T) = \frac{\lambda}{2\sqrt{\lambda(\lambda + 4)}} e^{-\alpha} \cdot I_0 \left\{ \sqrt{\alpha^2 - \beta^2} \right\}$$

$$+ \tfrac{1}{2}e^{-\beta} + \tfrac{1}{2}\beta \int_\beta^\gamma \frac{e^{-\tau}}{\sqrt{\tau^2 - \beta^2}} \cdot I_1 \left\{ \sqrt{\tau^2 - \beta^2} \right\} d\tau$$

$$\text{if } T \geq T_f, \text{ else } c_R(X, T) = 0 \qquad (B.25)$$

with

$$\alpha = \frac{2T}{\lambda(\lambda + 4)} \qquad (B.26)$$

$$\beta = \left| \frac{X - T}{\sqrt{\lambda(\lambda + 4)}} \right| \qquad (B.27)$$

$$\gamma = \frac{T(2 + \lambda) - \lambda X}{\lambda(\lambda + 4)} \qquad (B.28)$$

$$T_f = \tfrac{1}{2}X \left\{ \sqrt{\lambda(\lambda + 4)} - \lambda \right\} \qquad (B.29)$$

where T_f is the arrival time of the contaminant front at X. As T_f is positive or zero, it follows from (B.29) that the front can never occur to the left (i.e. to

the negative side) of the origin $X = 0$. Along similar lines we find for the other branch of the solution:
if $T > X$ then

$$c_R(X,T) = \frac{\lambda}{2\sqrt{\lambda(\lambda+4)}} e^{-\alpha} \cdot I_0 \left\{ \sqrt{|\alpha^2 - \beta^2|} \right\}$$

$$+1 - \tfrac{1}{2}e^{-\beta} - \tfrac{1}{2}\int_\beta^\gamma \frac{e^{-\tau}}{\sqrt{\tau^2 - \beta^2}} I_1 \left\{ \sqrt{\tau^2 - \beta^2} \right\} d\tau$$

$$\text{if } T \leq T_t, \text{ else } c_R(X,T) = 1 \tag{B.30}$$

with

$$T_t = -\tfrac{1}{2}X \left\{ \sqrt{\lambda(\lambda+4)} + \lambda \right\} \tag{B.31}$$

where T_t is the arrival time of the tail. It follows from (B.31) that the tail can only occur to the negative side of the origin $X = 0$, i.e. the tail moves always against the direction of flow.

3.10.2 *Derivation of (3.114)*

The differential equation to be solved is

$$\frac{\partial^2 c_F}{\partial X^2} - \frac{\partial c_F}{\partial x} = \frac{\partial c_F}{\partial T} + \lambda \left(\frac{\partial^2 c_F}{\partial X \partial T} + \frac{\partial^2 c_F}{\partial T^2} \right) \tag{B.32}$$

subject to the boundary conditions

$$c_F(0,T) = 1 \tag{B.33}$$
$$c_F(\infty,T) = 0 \tag{B.34}$$

and the initial conditions

$$\begin{aligned} c_F(X,0) &= 1 \quad (X = 0) \\ c_F(X,0) &= 0 \quad (X > 0) \\ \frac{\partial c_F}{\partial T}(X,0) &= 0 \end{aligned} \tag{B.35}$$

The solution proceeds along exactly the same lines, except for the fact that there is no need to make the substitution $u = X - T$. The result reads

$$c_F(X,T) = e^{\frac{1}{2}X - \alpha\beta} + \beta e^{\frac{1}{2}x} \int_\beta^\gamma \frac{e^{-\alpha\tau}}{\sqrt{\tau^2 - \beta^2}} \cdot I_1 \sqrt{\tau^2 - \beta^2} d\tau$$

$$\text{if } T \geq T_f, \text{ else } c_F(X,T) = 0 \tag{B.36}$$

where

$$\alpha = \tfrac{1}{2}(\lambda + 2) \tag{B.37}$$

$$\beta = \frac{X}{\sqrt{\lambda(\lambda + 4)}} \tag{B.38}$$

$$\gamma = \frac{2T + \lambda X}{\lambda(\lambda + 4)} \tag{B.39}$$

$$T_f = \tfrac{1}{2}X\{\sqrt{\lambda(\lambda + 4)} - \lambda\} \tag{B.40}$$

3.10.3   Cumulants of Strack's dispersion equation

The Fourier transform of (B.32) reads

$$\frac{d^2\bar{c}_F}{dX^2} - \frac{d\bar{c}_F}{dX} = i\omega\bar{c}_F + \lambda\left(i\omega\frac{d\bar{c}_F}{dX} - \omega^2\bar{c}_F\right) \tag{B.41}$$

Under the boundary conditions of Section 3.10.2 we find that

$$\bar{c}_F(X,\omega) = \exp\{\tfrac{1}{2}X(1 - i\omega\lambda)\} \cdot \exp\left[-\tfrac{1}{2}X\sqrt{(1 - \lambda i\omega)\{1 - (\lambda + 4)i\omega\}}\right] \tag{B.42}$$

and thus

$$\ln\bar{c}_F(X,\omega) = \tfrac{1}{2}X(1 - i\omega\lambda) - \tfrac{1}{2}X\sqrt{1 - \lambda i\omega} \cdot \sqrt{1 - (\lambda + 4)i\omega} \tag{B.43}$$

In order to determine the Taylor series of $\sqrt{1 - \lambda i\omega} \cdot \sqrt{1 - (\lambda + 4)i\omega}$, notice that

$$\ln\{\sqrt{1 - \lambda i\omega} \cdot \sqrt{1 - (\lambda + 4)i\omega}\} = \tfrac{1}{2}\ln(1 - \lambda i\omega) + \tfrac{1}{2}\ln\{1 - (\lambda + 4)i\omega\} \tag{B.45}$$

The logarithmic terms in the right-hand side of (B.45) are easily expanded:

$$\ln(1 - \lambda i\omega) = -\lambda i\omega - \tfrac{1}{2}\lambda^2(i\omega)^2 - \tfrac{1}{3}\lambda^3(i\omega)^3 - \cdots \tag{B.46}$$

and

$$\ln\{1 - (\lambda + 4)i\omega\} = -(\lambda + 4)i\omega - \tfrac{1}{2}(\lambda + 4)^2(i\omega)^2 - \tfrac{1}{3}(\lambda + 4)^3(i\omega)^3 - \cdots \tag{B.47}$$

from which we derive that

$$\begin{aligned}
\ln\{\sqrt{1 - \lambda i\omega} \cdot \sqrt{1 - (\lambda + 4)i\omega}\} &= -\tfrac{1}{2}\left[\{\lambda + (\lambda + 4)\}i\omega + \tfrac{1}{2}\{\lambda^2 + (\lambda + 4)^2\}(i\omega)^2 \right. \\
&\quad \left. + \tfrac{1}{3}\{\lambda^3 + (\lambda + 4)^3\}(i\omega)^3 + \cdots\right] \\
&= -\tfrac{1}{2}\sum_{n=1}^{\infty}\frac{1}{n}\{\lambda^n + (\lambda + 4)^n\}(i\omega)^n
\end{aligned} \tag{B.48}$$

or inversely,

$$-\tfrac{1}{2}X\sqrt{1 - \lambda i\omega} \cdot \sqrt{1 - (\lambda + 4)i\omega} = -\tfrac{1}{2}Xe^{-\frac{1}{2}\sum_{n=1}^{\infty}\frac{1}{n}\{\lambda^n + (\lambda + 4)^n\}(i\omega)^n} \tag{B.49}$$

and thus

$$\ln \bar{c}_F(X,\omega) = \tfrac{1}{2}X(1 - \lambda i\omega) - \tfrac{1}{2}Xe^{-\frac{1}{2}\sum_{n=1}^{\infty} \frac{1}{n}\{\lambda^n + (\lambda+4)^n\}(i\omega)^n} \tag{B.50}$$

Set

$$\exp\left[-\tfrac{1}{2}\sum_{n=1}^{\infty} \frac{1}{n}\{\lambda^n + (\lambda+4)^n\}(i\omega)^n\right] = \sum_{n=0}^{\infty} A_n \frac{(i\omega)^n}{n!} \tag{B.51}$$

or

$$\exp\left\{\sum_{n=1}^{\infty} \frac{B_n}{n!}(i\omega)^n\right\} = \sum_{n=0}^{\infty} A_n \frac{(i\omega)^n}{n!} \tag{B.52}$$

with

$$B_0 = 0 \tag{B.53}$$

$$\frac{B_n}{n!} = -\frac{1}{2n}\{\lambda^n + (\lambda+4)^n\} \qquad (n > 0) \tag{B.54}$$

then

$$\frac{A_n}{n!} = \sum_{i=1}^{n} \frac{i}{n}\frac{A_{n-i}}{(n-i)!}\cdot\frac{B_i}{i!} \qquad (n > 0) \tag{B.55}$$

$$A_0 = 1 \tag{B.56}$$

so that

$$\ln \bar{c}_F(X,\omega) = \tfrac{1}{2}X(1 - \lambda i\omega) - \tfrac{1}{2}X\{1 - (\lambda+2)i\omega\} - \tfrac{1}{2}X\sum_{n=2}^{\infty} \frac{A_n}{n!}(i\omega)^n \tag{B.57}$$

or

$$\ln \bar{c}_F(X,\omega) = X(i\omega) - \tfrac{1}{2}X\sum_{n=2}^{\infty} \frac{A_n}{n!}(i\omega)^n \tag{B.58}$$

The cumulants are, by definition, the coefficients of $(i\omega)^n/n!$, hence

$$K_1 = X \tag{B.59}$$

$$K_n = \tfrac{1}{2}X A_n \tag{B.60}$$

where

$$\frac{A_n}{n!} = \frac{1}{2n}\sum_{i=1}^{n} \frac{A_{n-i}}{(n-i)!}\frac{\{\lambda^i + (\lambda+4)^i\}}{i!} \tag{B.61}$$

$$A_0 = 1 \tag{B.62}$$

Note If only the first few cumulants are needed it is much easier to use a symbolic algebra program. The program DERIVE gives

$$-\tfrac{1}{2}X\sqrt{1 - \lambda i\omega}\cdot\sqrt{1 - (\lambda+4)i\omega} = 1 - (\lambda+2)i\omega - 2(i\omega)^2 - 2(\lambda+2)(i\omega)^3$$
$$-2(\lambda^2 + 4\lambda + 5)(i\omega)^4 - 2(\lambda^3 + 6\lambda^2 + 5\lambda + 14)(i\omega)^5 \tag{B.63}$$

and thus

$$\ln \bar{c}_F(X, \omega) = X i\omega + X(i\omega)^2 + X(\lambda + 2)(i\omega)^3 + X(\lambda^2 + 4\lambda + 5)(i\omega)^4$$
$$+ X(\lambda^3 + 6\lambda^2 + 5\lambda + 14)(i\omega)^5 \qquad (B.64)$$

from which we can immediately conclude that

$$K_1 = X \qquad (B.65)$$
$$K_2 = 2! X \qquad (B.66)$$
$$K_3 = 3!(\lambda + 2) X \qquad (B.67)$$
$$K_4 = 4!(\lambda^2 + 4\lambda + 5) X \qquad (B.68)$$
$$K_5 = 5!(\lambda^3 + 6\lambda^2 + 5\lambda + 14) X \qquad (B.69)$$

By definition we have

$$\overset{i}{\gamma} = \frac{K_{i+2}}{(K_2)^{\frac{1}{2}i+1}} \qquad (B.70)$$

so that we finally arrive at

$$\mu = X \qquad (B.71)$$
$$\sigma = \sqrt{2X} \qquad (B.72)$$
$$\overset{1}{\gamma} = \frac{3(\lambda + 2)}{\sqrt{2X}} \qquad (B.73)$$
$$\overset{2}{\gamma} = \frac{6(\lambda^2 + 4\lambda + 5)}{X} \qquad (B.74)$$

CHAPTER 4: SIMULATED COLUMN

EXPERIMENTS

4.1 Aim of the chapter

The heterogeneous structure of geological deposits displays itself at various scales, much like the layering we discussed in Section 3.6. It is common practice to distinguish between microscopic, macroscopic and megascopic features, although on this point the nomenclature may differ from one author to the other. For geohydrological purposes the micro scale is unanimously associated with the grain size, but there seem to exist no universal structural phenomena to fix the other scales. Various authors speak heuristically of regional or field (plot) scale and formation or (full) aquifer scale, the meaning of which has to be deducted from the context. Some authors seem to couple the concept of scales with the development of Fickian breakthrough curves (Güven and Molz, 1988). Instead of looking for physical features to associate the various scales with, we hold the opinion that it is fruitful to define scales with respect to the sizes of our models. After all, scaling has much to do with our perception of reality and little with reality itself. We propose to associate the mega scale with the size of a model area, no matter how big or how small it is chosen. Megascopic features, then, are all features distinguished individually within the model. To the groundwater modeler such features pose no special problems. At the other end of the scale it is only practical to take the grain size (or rather the pore size) as the measure of the micro scale, because features occurring on this scale are already accounted for by Darcy's law and the basic equations of groundwater flow and transport. They pose no modeling problems either. The term macro we reserve for all features in between micro and mega. Those are the features, larger than the pore scale, that are definitely there but just too small and too many to be modeled individually. Their actual sizes may range from pebbles to aquifers, depending on the size of the model area. An established technique to cope with such features is to regard their averaged action over a certain area, thereby replacing their heterogeneous characters by imaginary continuous ones. They then reappear as constituent constants in the differential equations to be solved by our models. Although it

is natural to attempt an upscaling of familiar equations that proved to work on the micro scale, it is realistic to expect new terms to emerge, that may change the mathematical statement of the problem. For instance, lumping the action of a drainage network in a two-dimensional steady groundwater model changes the governing differential equation from Laplacian to Poissonian.

It is generally agreed that the classical convection-dispersion equation, introduced to the field of groundwater flow by Scheidegger [1954], gives a fair description of dispersive groundwater transport on the micro scale. Its one-dimensional version, applied to homogeneous media, reads

$$\alpha_L v \frac{\partial^2 c}{\partial x^2} - v \frac{\partial c}{\partial x} = \frac{\partial c}{\partial t} \tag{4.1}$$

where α_L [L] is the longitudinal dispersivity, v is velocity and c is concentration. x is measured along a straight stream line (Section 3.15). The convection-dispersion equation is based on Fick's law of diffusion. As we discussed in Section 3.2, equation (4.1) appears to perform less satisfactory on the macro-scale. This phenomenon was recognized first about 1970 and it has received considerable attention ever since. Already heterogeneous laboratory columns are less well modeled by the convection-dispersion equation. The interpretation of field tracer tests by means of (4.1) required the magnitude of α_L to be raised several to many orders with respect to laboratory values (Fried, 1975, Anderson, 1979). This observation induced the term "macro-dispersion". Besides, early breakthrough curves did not correspond to solutions of (4.1). Various investigators (e.g. Sposito et al., 1986), though not all (e.g. Gillham et al., 1984), hold the believe that (4.1) would still apply eventually. The transition period, when breakthrough has not yet converged to a solution of (4.1), is referred to as the pre-Fickian or pre-asymptotic stage. On the basis of what has been demonstrated in Chapter 2 we tend to share this believe, although we have not shown the Gaussian (or Fickian) limit to exist for composite systems that are unbounded in the direction transverse to the main flow. We also expect certain media to be able to equip the Gaussian with a long tail of low conductivity, withholding a part of the contaminating material. Gupta and Bhattacharya [1986] assert that the velocity field must exhibit a somewhat repetitive structure in space for the Gaussian approximation to be possible. We do not see the necessity of a repetition in the direction of the main flow, but the requirement may be strict in the transverse direction (Matheron and De Marsily, 1980). There seems to be a quite general perception that an asymptotic Fickian approximation may take such a long time to achieve that it would be of little interest in making predictions (e.g. Smith and Schwartz, 1980). Güven et al. [1984] worked out some examples which suggest that the transition time may correspond to travel distances on the order of 5-100 km. Nevertheless, Gupta and Bhattacharya [1986], referring to the Borden test site (Devary and Simmons, 1984), think there is no empirical evidence against the applicability of Fickian approximations over time scales or distances of practical interest. Several investigators reported a dependence of the magnitude of α_L on the scale of the test (e.g. Domenico

and Robins, 1984, Güven et al., 1984, Sposito et al., 1986), which phenomenon prompted the introduction of the term "plume scale". Although it has puzzled many a hydrologist it is probably not so surprising after all. The riddle is closely related to Mandelbrot's classical question "How long is the coastline of Great Britain?" (Mandelbrot, 1967) and has been explained elegantly by Wheatcraft and Tyler [1988] in terms of fractal geometry. Their view seems to be supported by the outcomes of a study by Neuman [1990], who indicates that α_L, obtained by numerical model calibration, is typically two orders of magnitude smaller than the model area. (We must emphasize at this point that Neuman takes a somewhat different view). On the other hand, there is a recent paper by Gelhar et al. (1992), who scrutinized 59 different field tests reported earlier in the literature. They found that the trend of systematic increase is much less clear when the reliability of the data is considered. They also found that improved interpretations most often lead to smaller coefficients of longitudinal dispersion.

In the present chapter we are interested in the transition zone, where (4.1) does not (yet?) apply. Strack proposed to replace the intricate dispersive transport process generated by macroscopic heterogeneities by

$$\alpha_L v \frac{d^2 c}{dx^2} - v \frac{dc}{dx} = \frac{\partial c}{\partial t} + \beta v \frac{\partial^2 c}{\partial x \partial t} + \beta \frac{\partial^2 c}{\partial t^2} \qquad (4.2)$$

where x is the distance travelled along a straight stream line in a hypothetical homogeneous medium that replaces the heterogeneous one (Section 3.7). The parameter $\alpha_L[L]$ is a coefficient of longitudinal dispersion, v is velocity and c is concentration. $\beta[T]$ is a new parameter whose order of magnitude was unknown when we started the experiments to be reported in this chapter. β controls the velocity of the quickest fluid particles. The derivation of (4.2), although being an integral part of the LCMR-project, has been reported elsewhere (Strack, 1992). Solutions of Strack's equation differ from solutions of the convection-dispersion equation only in the transition zone, when the Fickian limit has not been reached yet (Section 3.7). Strack's equation can therefore be seen as an attempt to better model the pre-Fickian stage.

Remark: the formulation of (4.2) differs from that in Strack [1992] with respect to the parameter β. Rather than β, Strack [1992] regards βv as a parameter, which will be shown to be recommendable in this chapter. However, (4.2) was the working version at the onset of our investigations.

4.2 Experimental apparatus

The experimental apparatus we used is a computer simulation of the familiar laboratory column. The advantages over a physical column are: easy manipulation, the absence of scaling problems, and the possibility to carry out many tests, as a run with a simulated column is incomparably quicker than a physical column

run. The simulated flow pattern is two-dimensional. This drawback is believed to be acceptable, as field evidence has recently shown up that dispersion may be negligible in the vertical direction. Molz and Widdowson [1988], Garabedian et al. [1991], Rajaram and Gelhar [1991], and Jensen et al. (1993) all reported vertical dispersion to have the order of molecular diffusion (Section 3.2). As a result contaminant plumes are usually very thin and show considerable dispersion in the horizontal directions only. From a theoretical point of view one might also conjecture that a simulated medium reflects only our conception of the physical medium. The results that will be obtained may show artifacts that we are not aware of. Given the time schedule set for this project the disadvantages were taken for granted.

In choosing a computational technique for the simulation model it is of special importance to make sure that no numerical dispersion is introduced, as this phenomenon is hard to distinguish from the dispersive action of the medium proper. The analytical element method developed by Strack [1989] meets this condition. Added to the fact that expertise on this method was readily available, there was sufficient reason to opt for this technique. Only one type of analytical element was used, namely the circular inhomogeneity, whose action we will briefly explain.

Let a circle in the complex z-plane ($z = x + iy$) be given by

$$|z - z_0| = R \qquad (4.3)$$

This circle has its center at $z = z_0$ and its radius is R. For sake of generality a dimensionless complex variable $Z = X + iY$ is defined by

$$Z = \frac{z - z_0}{R} \qquad (4.4)$$

The circle now has its center in the origin, and its radius is unity.

A complex potential function $\Omega(Z)$ is introduced:

$$\Omega = \sum_{j=1}^{n} \bar{a}_j Z^{-j} \qquad (|Z| \geq 1) \qquad (4.5)$$

and

$$\Omega = \sum_{j=1}^{n} a_j Z^j + A \qquad (|Z| < 1) \qquad (4.6)$$

where A is a real constant and the a_j are complex constants, while $\bar{a}_j$ is the complex conjugate of a_j. This function is able to create a jump across the circle: Let $Z = e^{i\theta}$ be an arbitrary point on the circle, then it follows from (4.5) and (4.6) that the magnitude of the jump is

$$\lambda = -\sum_{j=1}^{n} \left[a_j e^{ij\theta} + \bar{a}_j e^{-ij\theta} \right] - A \qquad (4.7)$$

or

$$\lambda = -2\sum_{j=1}^{n} \left[\Re(a_j)\cos(j\theta) - \Im(a_j)\sin(j\theta)\right] - A \tag{4.8}$$

which is a real expression. A jump in the real part of Ω can be associated with a jump in hydraulic conductivity across the circle. As (4.8) contains $2n + 1$ parameters it is possible to meet jump conditions in $2n + 1$ points along the circle. (We refer to Strack [1987] and [1989] for details).

The simulated column existed of a large number of such circular inhomogeneities with different radii and conductivities, superimposed on an infinite plane with uniform flow. A rectangular part thereof with its large axis in the direction of the uniform flow component, was considered to be the experimental apparatus (Figure 4.1).
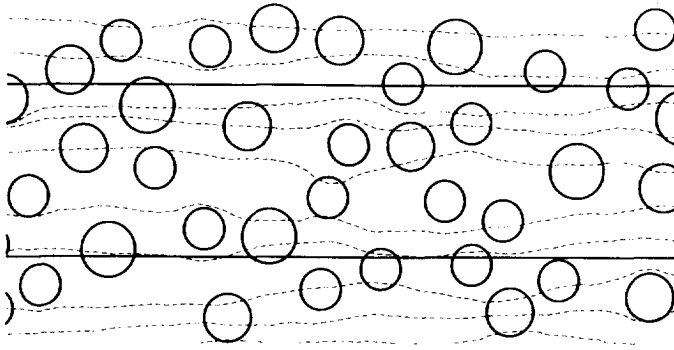
Figure 4.1 *Part of the simulated column*

Circular heterogeneities are arranged in such a way that a prescribed packing density was obtained. The following packing procedure was used:
- a circle was chosen at random from a set of three circles with different radii,
- the center of the circle was positioned randomly within the bounds of the column,
- its distance to neighboring circles was checked: the sum of the two radii, times a tolerance factor (greater than 1) had to be smaller than the distance between the two centers. If not, the circle is dismissed and a new guess made.
- the procedure continued until the area covered by circles approximated a prescribed part of the total area of the column (the ratio is called "packing density").

The conductivities of the circles were chosen randomly out of a log normal distribution with mean equal to the "background material" and variable standard deviation. The choice of a log normal distribution is supported by investigations of Freeze [1975], Hoeksema and Kitanides [1985], and Dagan [1986]. Recently, log normality was also demonstrated by Bronders and De Smedt [1991] for eleven Belgian formations, of which they analyzed 654 pump and piezometer tests. From a modeling point of view the log normal distribution has the advantage

of producing strictly positive conductivity values. Theoretically, the effective conductivity of a heterogeneous medium is expected to lie somewhere between the arithmetic mean and the harmonic mean of the conductivity values. Gut-jahr et al. [1978] showed that the effective conductivity of a two-dimensional heterogeneous medium with a log normal conductivity distribution equals the geometric mean of that distribution. For our model this phenomenon offers an additional advantage: the band containing the circles might otherwise attract stream lines from the surrounding homogeneous medium, or diverge them. As opposed to physical laboratory columns the simulated column has no imperme-able walls. Flow patterns were traced by an improved Euler method (Strack, 1989) and a random step was added in order to account for transverse micro dispersion (Kinzelbach, 1988):

$$x(t + dt) = x(t) + v_x dt - N\sqrt{2\alpha_T v dt}\frac{v_y}{v} \tag{4.9}$$

$$y(t + dt) = y(t) + v_y dt + N\sqrt{2\alpha_T v dt}\frac{v_x}{v} \tag{4.10}$$

where

$$v = \sqrt{v_x^2 + v_y^2} \tag{4.11}$$

Here α_T is the coefficient of transverse micro dispersion and N is a random num-ber with mean zero and standard deviation one. Longitudinal micro dispersion was not taken into account, as its effect is negligible as compared to the disper-sive effect of the circles. We also did not account for terms deriving from the spatial variation of the micro dispersion tensor. (These two measures were only taken after a comparison of runs made with and without these terms).

The number of "control points" on the circular boundaries, where the jump conditions are set, was three per circle unless the conductivity was less than one third of the background material. In that case we used seven control points. In terms of (4.5) and (4.6) this means that the circles were usually modeled by a first order function ($j = 1$) and occasionally by a third order one ($j = 3$). A typical realization of a heterogeneous column included some 260 circles and the number of equations to be solved amounted to circa 1000. The solution method used is LDU decomposition with column pivoting. For each run 1000 particles were released at the upstream end of the column, randomly distributed over the column width. Their detention times were registered at ten equidistant cross sections, including the downstream end of the column. A typical run on a 486 PC with 33 MHz clock speed took 8 hours.

4.3 Experiments conducted

The two main topics to be studied by means of simulated column experiments were
  1) the performance of the dispersion equation proposed by Strack, especially in the pre-Fickian stage,

2) the usefulness of Pearson III (or rather its integral, the incomplete gamma function shifted along the time-axis) to describe breakthrough curves.

It was only natural, in the process, that we also made observations on how the parameters of the equations are affected by the heterogeneous structure of the medium. This issue was not addressed in-depth, however.

The experimental column had a number of characteristics that could be varied in magnitude:
- the conductivity of the "background material",
- magnitude and direction of the component of uniform flow,
- the sizes of the circles and their packing density,
- the log normal distribution from which the conductivities of the circles are picked,
- the magnitude of the transverse micro dispersion,
- the dimensions of the column.

Moreover, as the heterogeneous structure of the column was generated by a chance process, different realizations might yield columns with different dispersive properties.

We varied various parameters with respect to a reference set, as shown in Table 4.1. The table displays all parameter values chosen for the reference set. For the other runs it is only indicated which parameters deviated from the reference values.

The reference set was selected with a regional groundwater model in mind. The conductivity chosen (25 m/d, Darcyan velocity $\approx$ 0.6 m/d) corresponds to a T-value of 1000 m^2/d for an aquifer of 40 m thickness. The component of uniform flow (.2 m/d) then corresponds to a mean gradient of head of 2.4:1000, which is in the range of common values for regional groundwater flow. The results to be obtained are amenable to scaling, of course. We do not have much field evidence available as to the sizes of the heterogeneities and their packing density, but in order to test the theories they should not be small on one hand, and they should be many on the other hand. The geometric mean of the log normal distribution from which their conductivities were picked equals the conductivity of the background material and its standard deviation is 28.75 m/d, again without reference to field data. The transverse micro-dispersivity reported from laboratory column tests with homogeneous porous media is in the order of the grain size. More general, one might expect this coefficient to have the order of some representative heterogeneity. As it is not likely that heterogeneities with the dimensions of the circles are themselves completely homogeneous we chose a value of .1 m for the transverse dispersivity. The column length was chosen to be 15 km, partly because this corresponds to the order of lengths one may be interested in in regional groundwater problems, and partly to keep calculation time within reasonable bounds.

Test run# 1 is merely a repetition of the reference run. This run was decided to be necessary because the random walk involves a random step, so the results itself are essentially random. Test run # 1 was to point out if 1000 particles gave a good impression of the mean results.

	reference set	1	2	3	4	5	6	7	8	9	10	11	12	13	14	15	16	17	18
background conductivity	25m/d																		
uniform flow component	.2m/d		.05	.1	.4	.8	1.6			-.2									
diameters of circles	60,70,80m																		
packing density	.75																		
mean conductivity of the circles	25m/d																		
standard deviation of conductivities	28.5m/d														57	57	57	57	57
transverse micro dispersion	.1m								.001										
column length	15km							30											
column width	500m																		
plain repetition		x																	
different realization											x	x	x	x	x	x	x	x	x

Table 4.1 *Specification of runs made with the simulated column*

Test runs # 2 through # 6 were conducted because it was seen in Chapter 3 that various differential equations lead to the skew Gaussian limit. At the same time it was found that different equations yield different expressions for the standard deviation and the skewness of the impulse response functions. Especially the velocity enters in different ways in the expressions derived. In testing the equation proposed by Strack it was paramount that runs be made for various velocities.

Test run # 7 had twice the column length of the reference run, in order to study the development of the Gaussian limit in more detail.

Test run # 8 was included to get a feeling for the influence of transverse micro dispersion on the coefficient of longitudinal macro dispersion.

In test run # 9 we reversed the direction of flow, because the theory in Section 2.8 predicts that the macro dispersive properties of a heterogeneous medium may be dependent on the direction of flow. For instance in numerical example (A.44) reversing the direction of flow corresponds to reversing the order of the matrix multiplication. One still gets a product matrix with linearly dependent columns and ditto rows, but the ratios between the columns and between the rows are different.

Test runs # 10 through # 13 are all runs with columns that have the same characteristics as the reference column. They are just different realizations of the randomly constructed heterogeneous medium. On the basis of the theory in Section 2.5 we expected them to yield breakthrough curves with different standard deviations and skewnesses.

Test runs # 14 through # 18 are repetitions of # 10 through # 13, with an augmented standard deviation of the log normal distribution from which the conductivities of the circles were picked.

4.4 Results: breakthrough curves

Figure 4.2a presents the breakthrough curves obtained by the reference run, at $x = 3, 6, 9, 12$ and 15 kilometers, respectively. Only 26 particles are depicted, out of the 1000 particles that were released, in order to prevent the plot from getting cluttered. The first and the last particles to arrive at a given cross-section are always included in the plotted curves. The vertical axis can be interpreted as relative concentration. The horizontal axis shows detention times, scaled by

$$t := \frac{vt}{1000} \tag{4.12}$$

where v is the magnitude of the uniform flow component (in m/d) and t is time (in days). This way of scaling causes the means of the breakthrough curves to arrive (theoretically) at a scaled time equal to the distance traveled, expressed in kilometers. It helps us to identify the curves and makes the results of all runs readily comparable.
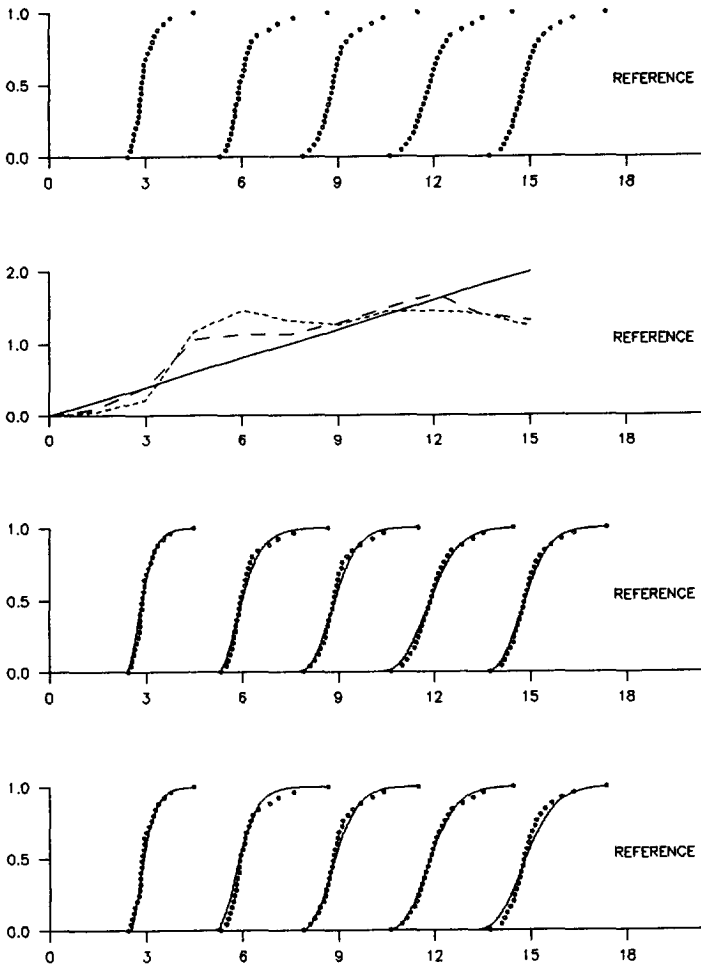
Figure 4.2   *Results of the reference run. a: Observed breakthrough curves (horizontal scale shows time [days] $*v$ [m/d] $*10^{-3}$); b: Behavior of M_1 (drawn), $\overset{c}{M}_2$ (dashed) and $\overset{c}{M}_3$ (dotted) as functions of distance (horizontal scale shows distance [km]; vertical scaling is arbitrary); c: Breakthrough curves matched by the shifted incomplete gamma function, using individual values of parameters a, n, and b; d: Same as c), using mean values of a, n, and b.*

Means were calculated at ten equidistant cross-sections, according to

$$M_1 = \frac{1}{n} \sum t_i \tag{4.13}$$

where the t_i are the travel times of the individual particles, and $n = 1000$. The drawn line in Figure 4.2b shows that the mean travel time is a linear function of x indeed. The horizontal axis in this plot represents the distance traveled in kilometers. The vertical axis has been scaled such as to obtain a theoretical mean value of 1 in the middle of the simulated column, (only reason for this choice being graphical convenience). The second central moment, or variance, of each breakthrough curve should also be proportional to x. This turns out to be true only in a very rough sense, witness the dashed line in Figure 4.2b. $\overset{c}{M}_2$ was calculated by

$$\overset{c}{M}_2 = \frac{1}{n-1} \sum (t_i - M_1)^2 \tag{4.14}$$

Likewise, the third central moment (being a measure of skewness) is expected to be a linear function of x. The dotted line in Figure 4.2b shows that the skewness takes the theory even less serious than the variance does. $\overset{c}{M}_3$ was calculated using

$$\overset{c}{M}_3 = \frac{n}{(n-1)(n-2)} \sum (t_1 - M_1)^3 \tag{4.15}$$

Figure 4.2c shows the breakthrough curves, matched by the shifted incomplete gamma function, which is the integral with respect to time of the Pearson-III distribution (Section 2.6). The three parameters a, n, and b of this function, given by (2.74) through (2.76), can be recast in the form

$$a = 2\frac{\overset{c}{M}_2}{\overset{c}{M}_3} \tag{4.16}$$

$$n = 4\frac{(\overset{c}{M}_2)^3}{(\overset{c}{M}_3)^2} \tag{4.17}$$

$$b = M_1 - 2\frac{(\overset{c}{M}_2)^2}{\overset{c}{M}_3} \tag{4.18}$$

Each breakthrough curve of Figure 4.2c was matched individually, that is: individual values of M_1, $\overset{c}{M}_2$ and $\overset{c}{M}_3$, derived from a single curve were used to evaluate the incomplete gamma function. The results turn out to be quite satisfactory, from a curve-matching point of view. Physically speaking, however, we would prefer the values of M_1/x, $\overset{c}{M}_2/x$, and $\overset{c}{M}_3/x$ to be invariant from curve to curve. (In other words, we would like to find that parameters like v, α_L, and β in [4.2] are constants, not depending on x). Figure 4.2d shows, therefore, calculated breakthrough curves based on mean values of M_1/x, $\overset{c}{M}_2/x$, and $\overset{c}{M}_3/x$. The result is less convincing, though not at all disappointing, considering the wild behavior of $\overset{c}{M}_2/x$ and $\overset{c}{M}_3/x$, shown in Figure 4.2b.

We had the intention to depict also exact breakthrough curves according to Strack's dispersion equation (4.2), given by (3.80) but they appeared to be optically indistinguishable from the shifted incomplete gamma-function.

A complete overview of the results of all runs specified in Table 4.1 is included in Appendix 4.7.

4.5 Discussion of results

Run #1 was a mere repetition of the reference run. Differences in outcome can only be attributed to the two random steps involved in the simulations. They should tend to zero if the number of traced particles would increase indefinitely. It is not statistically justified to draw a conclusion with some reliability from only two samples. However, the results of run # 1 (Appendix 4.7) resemble those of the reference run close enough as to feel confident that 1000 particles sufficed.

Tests # 2 to 6 were run to investigate how the coefficient of longitudinal dispersion α_L and Strack's β-coefficient behave as a function of velocity. Our method of scaling allows us to compare the results already on the face. As it appears, the outcomes of the various runs are basically identical. The slight differences are likely to stem from the random processes discussed above. The coefficient of longitudinal dispersion α_L relates to the second central moment $\overset{c}{M}_2$ by

$$\overset{c}{M}_2 = \frac{2\alpha_L x}{v^2} \qquad (4.19)$$

for both classical and Strackian dispersion. (This follows from [3.20], [3.21], [3.45], and [3.90]). Strack's β-coefficient relates to $\overset{c}{M}_3$ according to

$$\overset{c}{M}_3 = 12\frac{\alpha_L^2 x}{v^3} + 6\frac{\alpha_L \beta x}{v^2} \qquad (4.20)$$

(which follows from [3.20], [3.21], [3.69], and [3.91]). Figure 4.3 shows the mean values of α_L, obtained from runs # 1 to 6, plotted versus velocity. They appear to be essentially constant, their numerical values for this particular medium being circa 20 m.

Figure 4.4a shows the mean values of β, obtained from the same six runs. The graph suggests that β might be inversely proportional to v, hence βv would be constant. Figure 4.4b proves this to be the case indeed. *We conclude that βv is to be regarded as a medium property, rather than β itself.* Like α_L, the product βv has dimension $[L]$. Its numerical value for this medium amounts to circa 200 m.

It can be inferred from the behavior of $\overset{c}{M}_2$ versus x, Figure 4.2b, that α_L fluctuates as the plume progresses. The reason for this behavior is easily
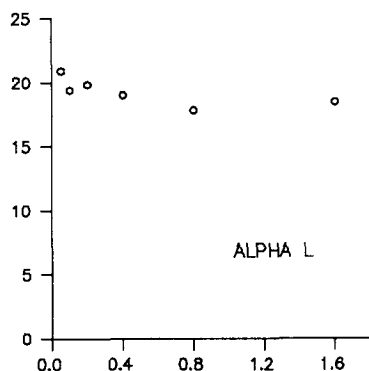
Figure 4.3 α_L *versus velocity.   Horizontal axis: velocity (m/d).*
Vertical axis: α_L (m).
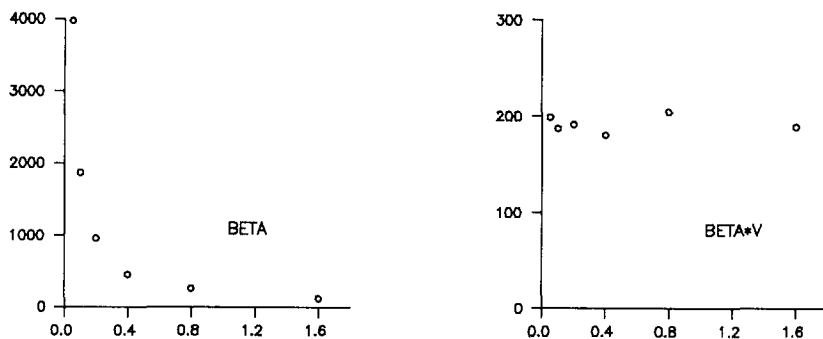
Figure 4.4   *a: β_L versus velocity. Horizontal axis: velocity (m/d).*
Vertical axis: β (d).   b: $\beta*v$ versus velocity.   Horizontal
axis: velocity (m/d). Vertical axis: $\beta * v$ (m).

detected: the originally sharp front is broken up in fingers, moving at different speeds, (Figure 2.14). Their growth is governed by the random nature of the heterogeneities and one may expect fluctuations of $\overset{c}{M}_2$ as long as there is no complete mixing. Mixing was far from complete in all tests conducted, even at the ends of the columns. Figure 4.5 shows a cross-profile of the concentration at the end of the reference column. Similar profiles were recorded for all sections sampled during the tests.

It is generally assumed that the fluctuations of α_L would disappear if the distance travelled becomes large, as compared to the sizes of the heterogeneities.

Run # 7 was conducted to confirm this expectation. The column-length during this run was 30 km (instead of 15). The behavior of α_L is shown in Figure 4.6a; Figure 4.6b shows that of βv. There appears to be a tendency of α_L to settle down to a constant value. The same cannot be said of β, which even
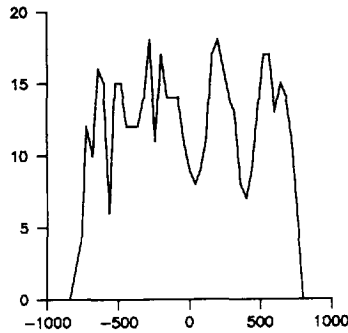
Figure 4.5 *Cross-sectional profile at the end of the reference col-*
umn. Horizontal axis: width (m). Vertical axis: num-
ber of particles counted within intervals of 20 m.
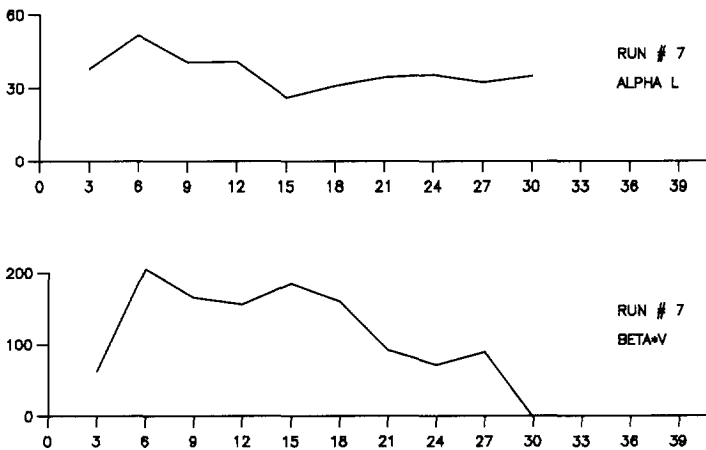
Figure 4.6 *Behavior of α_L and βv as functions of distance. Hor-*
izontal axis: distance (km). Vertical axis: α_L, respec-
tively βv (m).

assumes a slightly negative value at $x = 30$ km.

The cross-sectional profile taken at the end of the column (not shown) was still very irregular. We conclude that the Fickian stage had not been reached, even after 30 km.

Run # 8 was carried out with a smaller coefficient α_T of transverse disper-
sion (.001 m instead of .1 m). This caused the breakthrough curves to become considerably less smooth than those of the reference run (Figure 4.7). The fluc-
tuations of the second and third moments did not increase, however. On the

other hand, the mean value of α_L was found to be amply 10% bigger than those of the previous runs, which difference is probably significant. This shows us at the same time that the medium at hand differs fundamentally from layered media, for which α_L is inversely proportional to α_T (Marle et al., 1967).
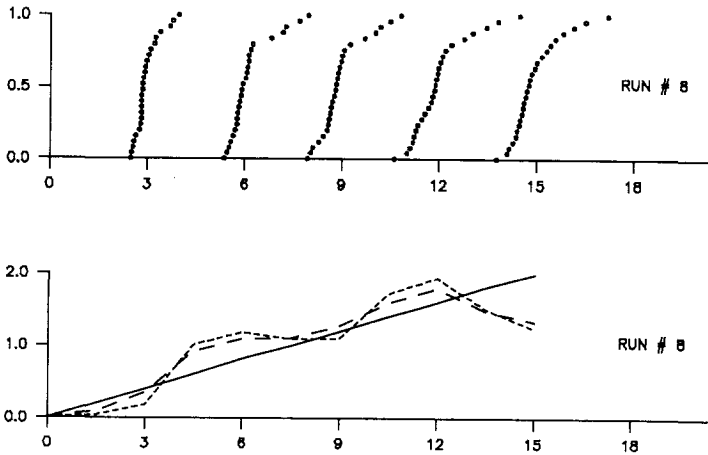
Figure 4.7   *Breakthrough curves and moments of Run # 8 ($\alpha_T = 0.001$ m instead of 0.1 m).*

Run #9 was the reference run with reversal of the direction of flow. Not unlike our expectation we found the results to be quite different from the reference run (Figure 4.8). The mean value of βv was 30 m (against 200 m).

This run can, in fact, be considered as another statistical realization of the reference column, with the same set of circles and conductivities. More such realizations are runs # 10 through 13. We refer to Appendix 4.7 for a complete overview of the results. Figure 4.9 combines the breakthrough curves of these runs, including run #9 and the reference run. It must be concluded that the parameter set mentioned in Table 4.1 does not yield a unique breakthrough curve and, for that matter, no unique values of α_L and β can be derived from them. The graph of Figure 4.9 suggests that the variations in breakthrough, although being significant, are restricted to certain bounds. Such bounds (if they exist) must be related to the statistics of the medium. They could probably have been derived in advance, but that subject has been no part of our research.

Runs # 14 through 18 are five different realizations of a medium constructed from the same set of circles as used for the previous runs, but with an increased contrast in conductivities. The results of run # 14 are presented in Figure 4.10. We refer once more to Appendix 4.7 for an impression of the remaining outcomes. The most remarkable feature of these runs is a pronounced tailing effect. Although the tails carry only a small portion of the particles, they obstruct our method of curve-matching by moments. It was found empirically that a
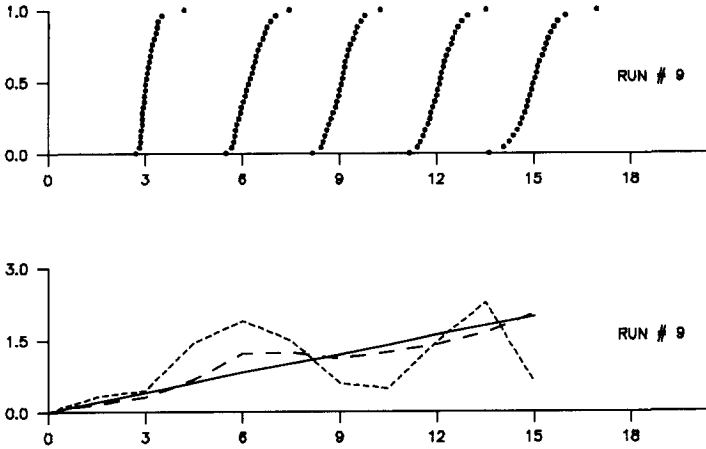
Figure 4.8   *Breakthrough curves and moments of run # 9 (reversal of flow).*
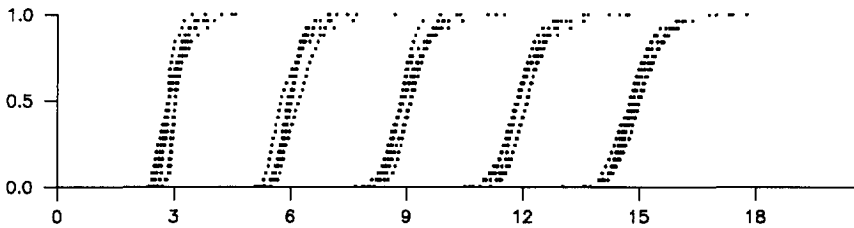
Figure 4.9   *Effect of rearranging the heterogeneities. (The figure shows the breakthrough curves of the reference run and runs # 9 through 13).*

satisfactory match could still be obtained if the number of points, from which the moments are calculated, was reduced. The results shown were obtained by using only three points per breakthrough curve, which is the absolute minimum.

Figure 4.11 displays the breakthrough curves of all five runs (i.e. # 14 through 18). The tailing effect is sometimes explained by postulating the presence of stagnant zones (Herr et al. [1989], Van Genuchten and Wierenga [1976]). As there are no stagnant zones in our simulated columns, the parallel systems model presented in Appendix 2.8 (Figure 2.15) might be more realistic. This model leads to a separation of the plume into a number of distinct sub-plumes, each of them behaving as if it traveled through a single layer. The dominant eigenvalue of the system generates the main body of the composite breakthrough curve. This part has the highest velocity of propagation and shows the least dispersion. As compared to this main component, the other components disperse rapidly, although the amount of mass contained by them is constant. The result
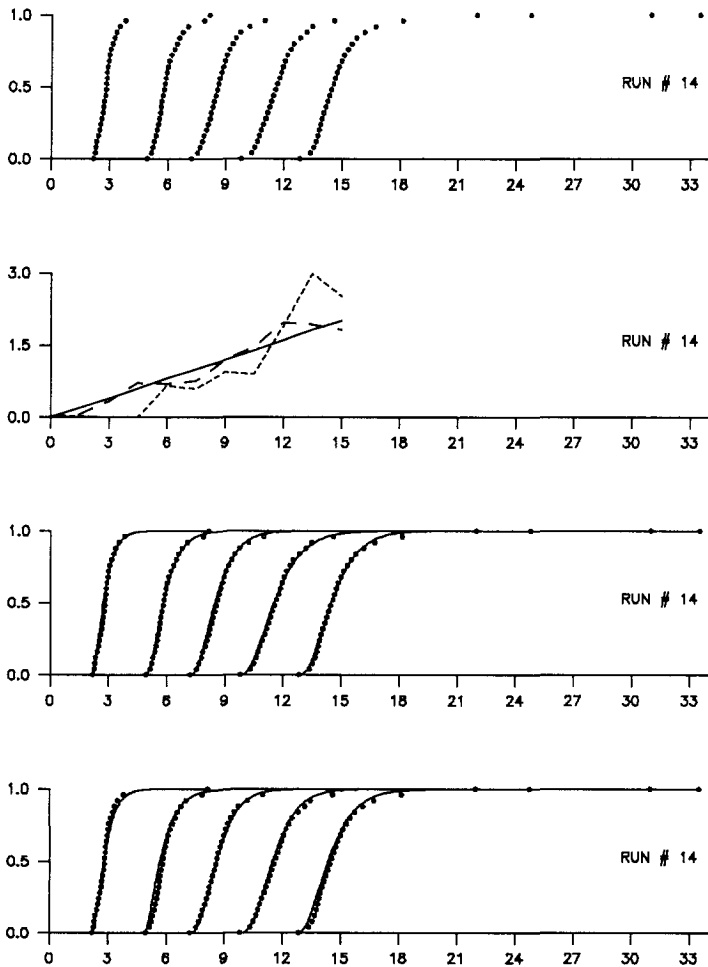
Figure 4.10 *Results of run #14, which is a variation on the refer-*
ence run (Figure 4.2) with increased contrast of con-
ductivities.

is a pronounced smearing of the tail of the composite breakthrough curve.

We now turn to the arrival time of the first particle of a front of contami-
nation. Strack's dispersion equation yields the following prediction:

$$t_f = \tfrac{1}{2}\frac{x}{v}\left\{\sqrt{\lambda(\lambda+4)} - \lambda\right\} \tag{4.21}$$

where

$$\lambda = \frac{\beta v}{\alpha_L} \tag{4.22}$$
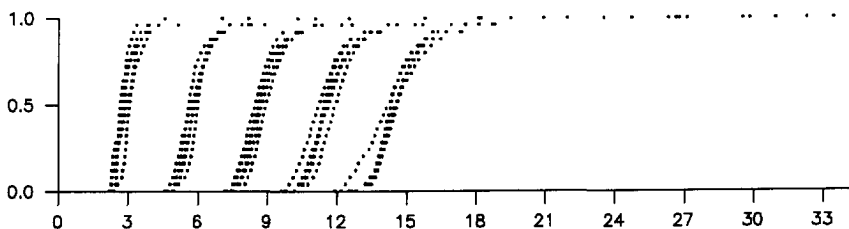
Figure 4.11 *Same as Figure 4.9, with increased contrast of conductivities.*

(This follows from [3.20], [3.21], [3.69] and [3.78]). Put in terms of moments:

$$t_f = \tfrac{1}{2} M_1 \left\{ \sqrt{\lambda(\lambda+4)} - \lambda \right\} \tag{4.23}$$

where

$$\lambda = \tfrac{2}{3} \frac{M_1 \overset{c}{M}_3}{\left(\overset{c}{M}_2\right)^2} - 2 \tag{4.24}$$

The shifted incomplete gamma function gives also an estimate of the arrival time of the first particle, which is simply the parameter b (4.18). Figure 4.12 is a plot of calculated arrival times versus measured arrival times, evaluated for the reference run. This example is typical: we found good to excellent agreement for all 18 runs. It is to be noted that the values of M_1, $\overset{c}{M}_2$ and $\overset{c}{M}_3$ chosen to evaluate t_f and b were the overall values, used to produce Figure 4.2d. Moments derived from individual breakthrough curves gave also fair results, but there were exceptions where t_f could not be evaluated because λ assumed a negative value. The parameter b could still be evaluated, in these exceptional cases, but the results were poor. The reason, of course, is the wild behavior of the third central moment $\overset{c}{M}_3$. The arrival time of the first particle, on the other hand, behaves very consistent. We propose, therefore, to drop $\overset{c}{M}_3$ as an observable and to replace it by t_f. Setting b in (4.18) equal to t_f and eliminating $\overset{c}{M}_3$ from (4.16) and (4.18) we find

$$a = \frac{M_1 - t_f}{\overset{c}{M}_2} \tag{4.25}$$

$$n = \frac{(M_1 - t_f)^2}{\overset{c}{M}_2} \tag{4.26}$$

$$b = t_f \tag{4.27}$$

These estimates are far less prone to idiosyncrasies of the medium than the set (4.16) to (4.18). We reinterpreted many of the runs by means of (4.25) to (4.27).
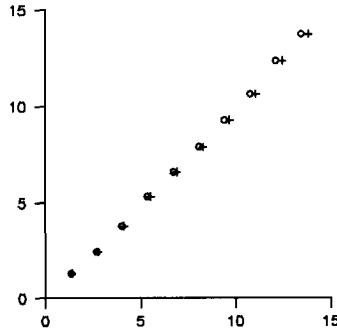
Figure 4.12   *Measured versus calculated arrival times of the front at 3, 6, 9, 12, and 15 km (reference run). + = Strack, 0= incomplete gamma function. Horizontal axis: measured. Vertical axis: calculated.*

The results were always almost identical to the former outcomes. The present method is to be preferred, because of its absolute robustness.

   Since we saw that the medium properties α_L and β are far from stable (Figure 4.6) the question arose as to what extent it would still be possible to predict the future development of a plume from observations of early breakthrough curves. Equations (4.25) to (4.27) give a partial clue. The first moment M_1 and the first arrival time t_f behave very regular. The main uncertainty stems, therefore, from variations of $\overset{c}{M}_2$ as a function of x. The deviations from the ideally straight line show no clear tendency to dampen, as can be seen from the b-graphs of all test runs (Appendix 4.7). They show no tendency to grow either, hence their amplitude of fluctuation is probably characteristic of a medium. Useful extrapolation of breakthrough curves seems to become only possible when the fluctuations of $\overset{c}{M}_2$ have become small as compared with its proper value. (This is another way of stating that α_L should have stabilized to a constant value). The criterion does not seem to have been met by anyone of the test runs. Our conclusion seems to be supported by our finding that the reference run and runs # 9 to 13 (whose columns were all constructed from the same set of heterogeneities) produced quite different mean values of α_L: 25, 26, 53, 48, and 26 m, respectively. There may be a way of deriving the fluctuations of $\overset{c}{M}_2$ in advance from the statistics of the medium. Again, this subject has been no part of the research project.

   We finally addressed the issue of how the classical dispersion equation (CDE) would have performed. As Strack's equation and the CDE are known to behave asymptotically identical, we concentrated on the first half (0 - 7.5 km) of the test columns. Figure 4.13a displays the breakthrough curves of the reference run at .1L, .2L, .3L, .4L, and .5L, respectively, matched by the CDE. Each theoretical

curve was evaluated using the individual value of α_L obtained from the observed breakthrough curve. Figure 4.13b shows the same for Strack's equation. It is apparent that Strack's equation is better suited to accommodate the shape of the observed breakthrough curves. A comparable difference between the two is observed if the mean value of α_L is used, instead of individual values (Figure 4.13c and d). (Strack's curves were matched by means of [4.25] to [4.27] rather than [4.16] to [4.18]).

4.6 Conclusion and final remarks

Eighteen simulated column experiments were conducted, to investigate the performance of Strack's dispersion equation, with special reference to the pre-Fickian stage, and to test the usefulness of the shifted incomplete gamma function (= integral with respect to time of Pearson's type III distribution) in describing breakthrough curves in heterogeneous porous media. As a by-product we also did a number of observations on the behavior of breakthrough curves under various changes of the porous medium.

The Fickian stage, where breakthrough profiles are completely defined by the velocity v and a constant coefficient of longitudinal dispersivity α_L, was reached in none of the tests. The variances $\overset{c}{M}_2$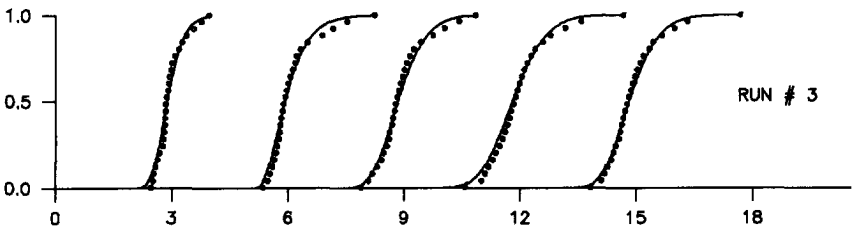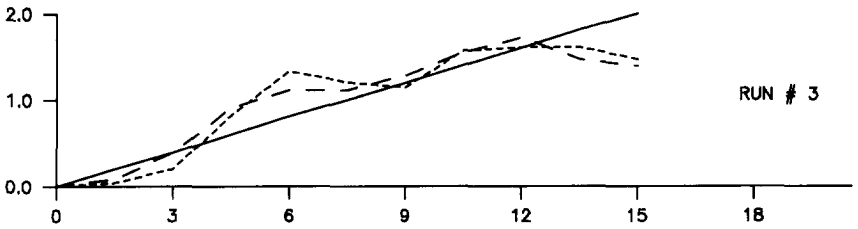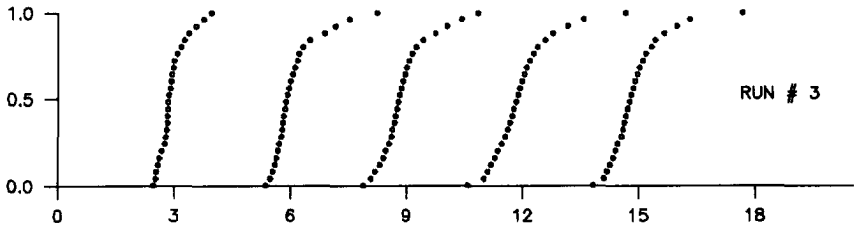 of the breakthrough curves, when pictured as functions of distance traveled by the plume, appeared to fluctuate about a possibly straight line through the origin. (A straight line would correspond to a constant value of α_L). The amplitudes of fluctuation did seem neither to increase nor decrease with the distance traveled. They are probably characteristic of a medium. The only reason for α_L to settle down to a constant value is that the magnitude of the fluctuations of $\overset{c}{M}_2$ becomes eventually small with respect to the magnitude of $\overset{c}{M}_2$ itself. Knowledge of the amplitude would improve our description of breakthrough curves in the pre-Fickian stage. There may be a relation with the statistics of the medium (which has been no subject of this research). Cross-sectional profiles of the concentration, taken at the end of the columns, showed large fluctuations (Figure 4.5), giving another indication that the Fickian stage was not reached.

The phenomenon of varying α_L corresponds to field observations. It was found earlier by similar model experiments (Smith and Schwartz, 1980, Tompson and Gelhar, 1990) and predicted theoretically by Dagan [1989], p 319), using stochastic methods. Unlike Dagan's prediction we found that α_L approached its limiting value in a non-monotonical manner. This seems to be explainable: as long as no complete mixing is achieved on the micro-scale there is an ongoing reformation of the fingering front. One could even imagine an apparent demixing, when quicker fingers slow down to be surpassed by others.

Rearrangement of the heterogeneities in our columns had a distinct effect on the shape of the breakthrough curves. This phenomenon was also observed
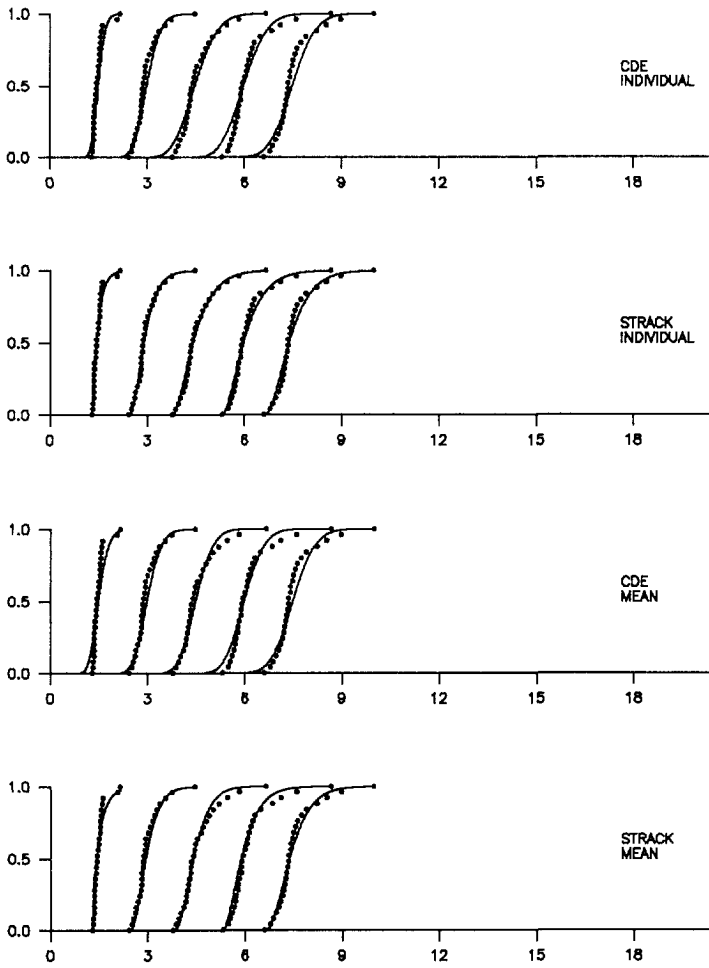
Figure 4.13   *Performance of Strack's equation as compared with the CDE. a: Breakthrough curves matched individually by the CDE; b: As a, using Strack's equation; c: Breakthrough curves matched by the CDE, using the mean value of α_L; d: As c, using Strack's equation.*

by Smith and Schwartz (1980). Our first impression was that characteristics like α_L and β depend on the direction of flow (because the particular arrangement of the heterogeneities, encountered by a plume, will depend on the direction of its path). However, the breakthrough curves of different columns, constructed from the same set of heterogeneities, appeared to form bundles of limited width (Figures 4.9 and 4.11). Their widths did not seem to increase or decrease with

the distance from the origin, suggesting that they are related to the fluctuations of $\overset{c}{M}_2$. It is to be expected, therefore, that our presumed dependence of α_L and β on the direction of flow will play a role only in the pre-Fickian zone, when the variations of $\overset{c}{M}_2$ are still large with respect to $\overset{c}{M}_2$ itself. We take this as a warning that it is precarious to extrapolate breakthrough curves before the Fickian stage has been reached. It is probable that the observed bandwidths of the breakthrough bundles would have been smaller, had we imposed a spatial autocorrelation structure on the conductivities of the heterogeneities. (A strong autocorrelation structure is not likely to occur in practice, though, on a scale of several kilometers. Bronders and De Smet [1991] investigated eleven geological formations in the central part of Belgium. Seven of them showed no spatial correlation at all, while the remaining four showed only a regional trend).

An increase in contrast of the conductivities of the heterogeneities appeared to cause a distinct tailing of the breakthrough curves. Tailing, to the extent observed, is not incorporated in the Classical Dispersion Equation, nor in Strack's model. The model depicted by Figure 2.15 may be helpful in explaining this effect (as well as the other phenomena mentioned above). Tailing may also be responsible for the fact that it was impossible, in the well-controlled field-scale dispersion tests mentioned in Section 3.2, to trace all of the injected mass.

Decreasing the coefficient of transverse dispersion appeared to affect the smoothness of the breakthrough profiles (Figure 4.7). A decrease of α_T of two orders of magnitude increased α_L with only 20%. This shows that our medium is essentially different from perfectly layered media, where α_L is expected to be inversely proportional to α_T.

Strack's equation accommodates the measured breakthrough curves in the pre-Fickian zone better than the CDE does. The differences are especially observable at the beginning of breakthrough (Figure 4.13). Strack's model was found to predict the breakthrough time t_f of the front with high accuracy in most cases (Figure 4.12). The breakthrough time (as calculated by Strack's model) is governed by the β-coefficient in Strack's equation. This coefficient appeared to be inversely proportional to the velocity v (Figure 4.4). The product βv is independent of the velocity and is, therefore, to be preferred as a medium characteristic. (This recommendation has already been followed in Strack [1992]). Calculation of β from an observed breakthrough curve requires evaluation of the third moment of that curve (equation [4.20]). The third moment was found to fluctuate strongly with the distance traveled, however. Alternatively, β can be evaluated from the arrival time of the front (equation [4.21] and [4.22]), which is a very consistent observable. We strongly recommend the latter method.

Breakthrough curves evaluated by the incomplete gamma function, shifted in time, were found to be optically indistinguishable from Strack's breakthrough

curves. Differences might have shown closer to the source, where we had no observations. The incomplete gamma function is believed to be of good use in modeling contaminant transport by groundwater. (The reader may wish to consult Chapter 3 for more information on this subject). Formulas were given that relate the three parameters a, b, and n of the incomplete gamma function to the first moment M_1, the second central moment $\overset{c}{M}_2$, and the arrival time of the front of the breakthrough curve (equations [4.25], [4.26], and [4.27]).

The technique of curve-matching by means of moments proved to be useful. However, long tails were found to obstruct the method. Good matches were still found in such cases if the tails were ignored. (An alternative fitting procedure employed by us, but not reported, was the Marquardt-Levenberg method of non-linear least squares. The results were good whenever convergence was reached, which was only in a minority of cases).

4.7 Appendix

This appendix presents the main results of the simulated column tests. All tests were conducted and interpreted by Jogesh C. Panda, graduate student at the Department of Civil and Mineral Engineering of the University of Minnesota, who also did most of the programming for the experimental apparatus described in Section 4.2. The specifications of all runs are given in Table 4.1. Each page of this appendix gives the results of one test. The layout of the pages is identical:

The *first graph* shows observed breakthrough curves at .2, .4, .6, .8, and 1. L, where L is the column length. The horizontal (time-) axis gives time (days)∗velocity $(m/d) * 10^{-3}$. The resulting figures along this axis are in kilometers. They correspond roughly to the distances from the origin where the breakthrough curves are observed. The vertical axis can be interpreted as dimensionless concentration.

The *second graph* shows the evaluation of the fist moment or mean (drawn), the second central moment or variance (dashed), and the third central moment (dotted) of the breakthrough curves. The horizontal axis is in kilometers. The vertical axis is arbitrary. The three characteristics shown would be linear functions of distance if the medium were homogeneous. They are also expected to become linear in heterogeneous media, once the Fickian stage has been reached.

The *third graph* shows how the shifted incomplete gamma function (= integral with respect to time of Pearson's type III distribution) fits the measuring data. The theoretical curves are matched to the measured breakthrough curves by equating their individual first three moments, given by the second graph. Breakthrough curves according to Strack's dispersion equation appeared to be optically indistinguishable from the incomplete gamma function.

The *fourth graph* shows how the theory would match the measuring data if the first moment and the second and third central moments are supposed to be linear functions of distance. (In other words: if the coefficient of longitudinal dispersion α_L and Strack's β-coefficient are supposed to be constants). The values of α_L and β, used to produce these breakthrough curves, were the means of the values obtained from the observed breakthrough curves.

RUN # 1

RUN # 1

RUN # 1

RUN # 1

RUN # 2

RUN # 2

RUN # 2

RUN # 2

RUN # 3

RUN # 3

RUN # 3

RUN # 3

RUN # 4

RUN # 4

RUN # 4

RUN # 4

RUN # 5

RUN # 5

RUN # 5

RUN # 5

RUN # 6

RUN # 6

RUN # 6

RUN # 6

RUN # 8

RUN # 8

RUN # 8

RUN # 8

RUN # 9

RUN # 9

RUN # 9

RUN # 9

RUN # 11

RUN # 11

RUN # 11

RUN # 11

RUN # 13

RUN # 13

RUN # 13

RUN # 13

RUN # 14

RUN # 14

RUN # 14

RUN # 14

RUN # 15

RUN # 15

RUN # 15

RUN # 15

RUN # 16

RUN # 16

RUN # 16

RUN # 16

RUN # 17

RUN # 17

RUN # 17

RUN # 17
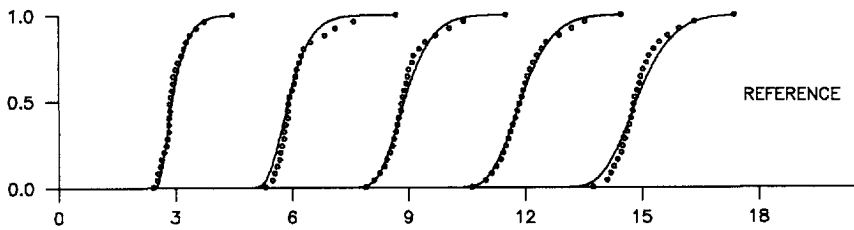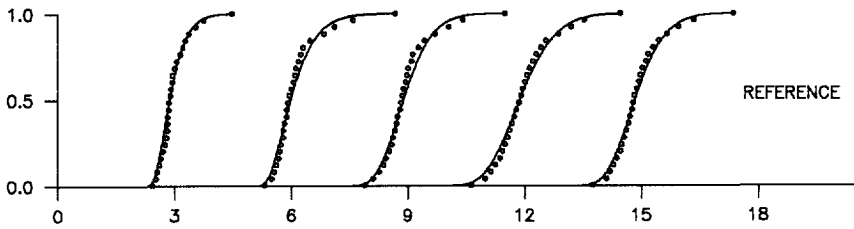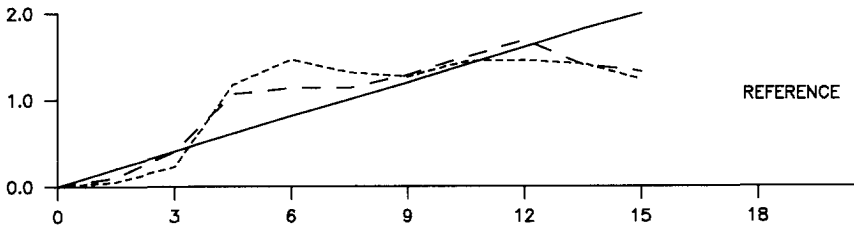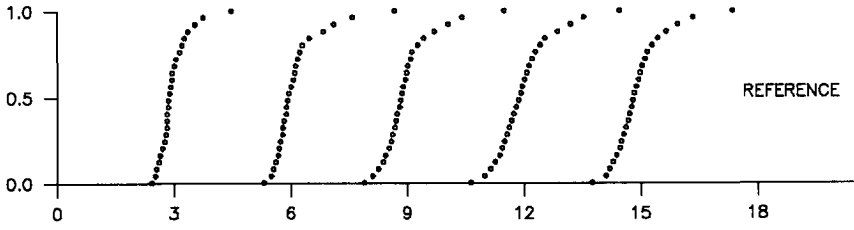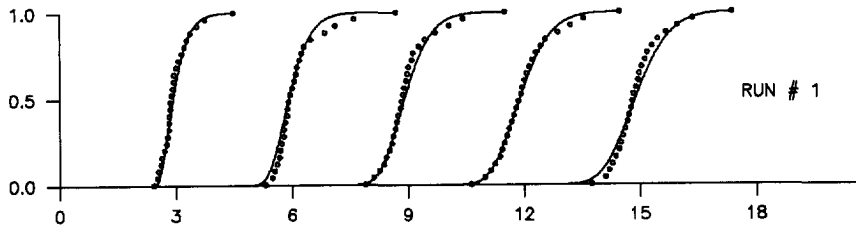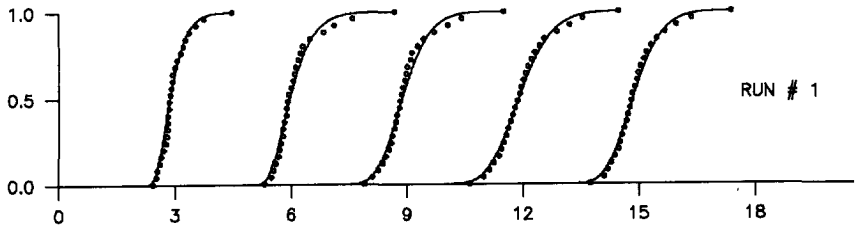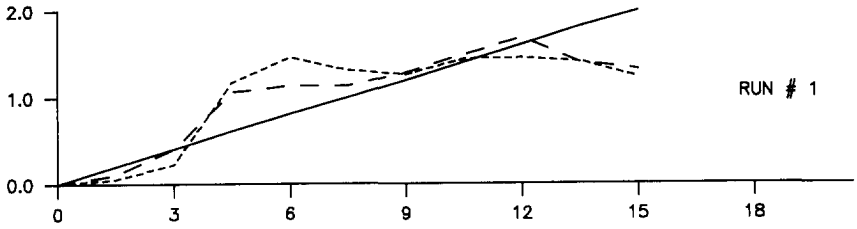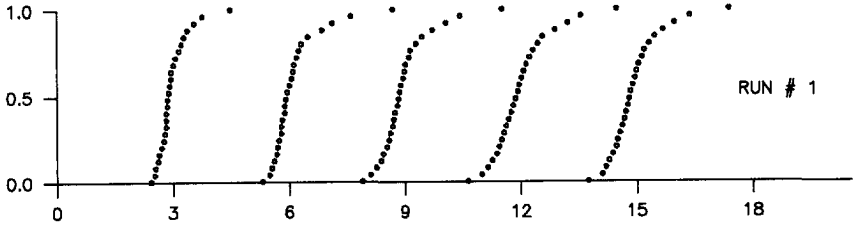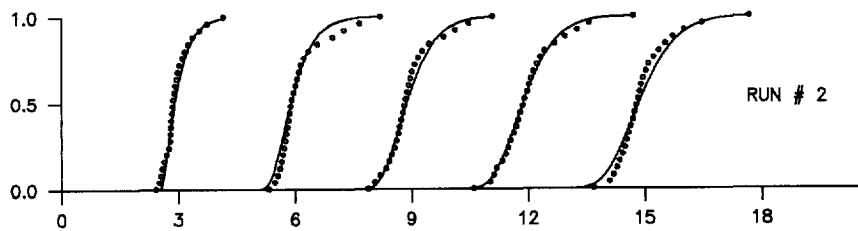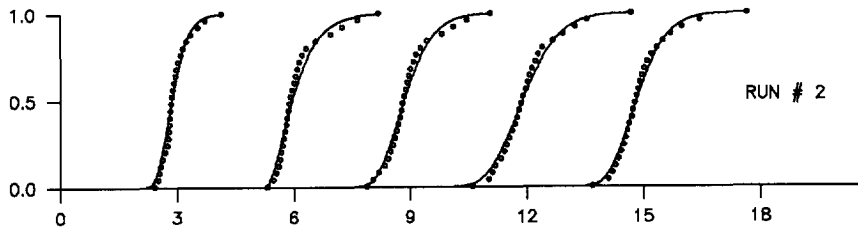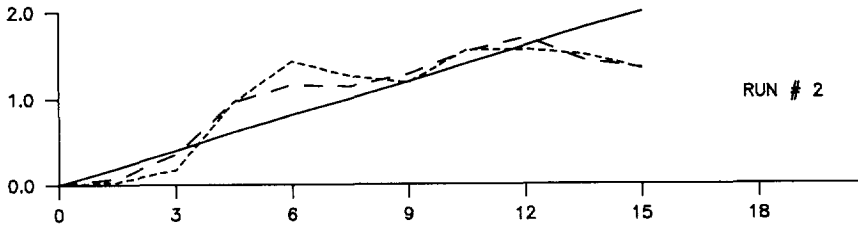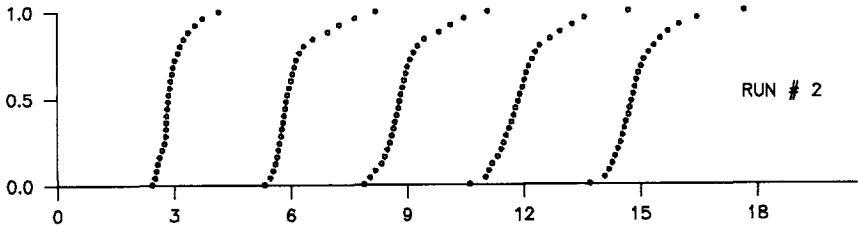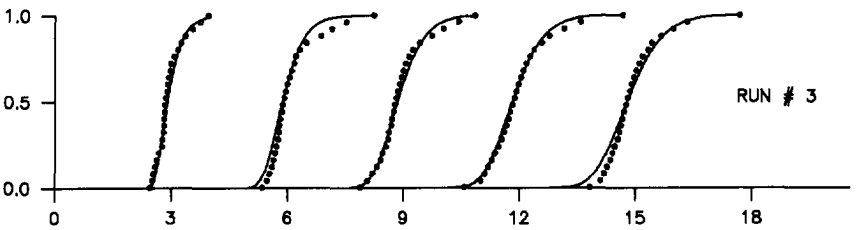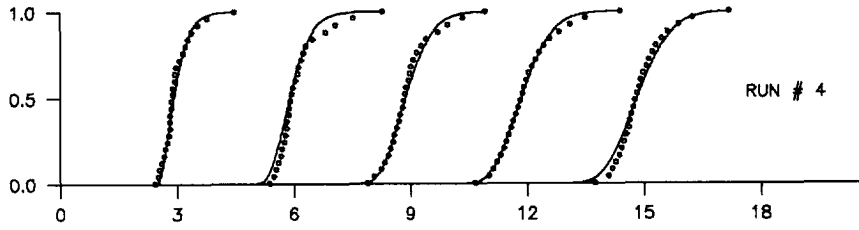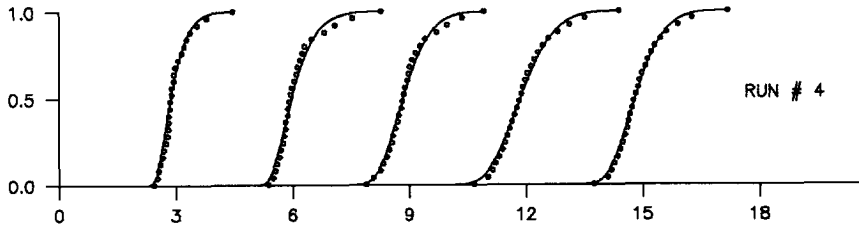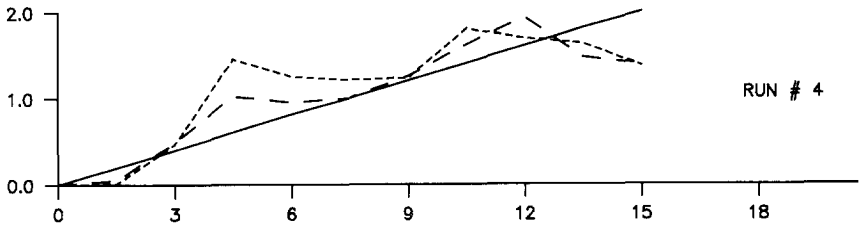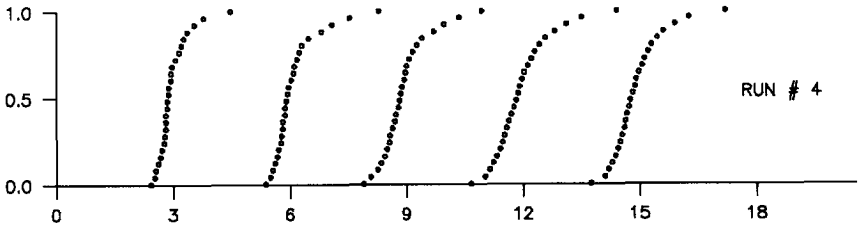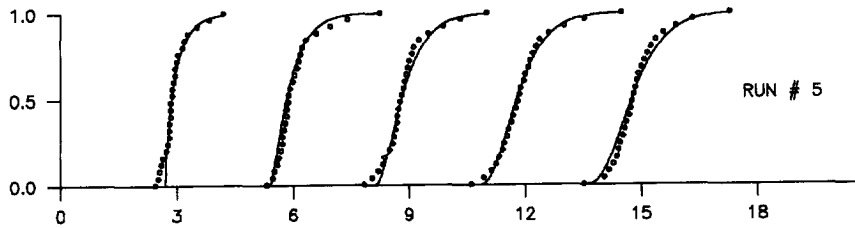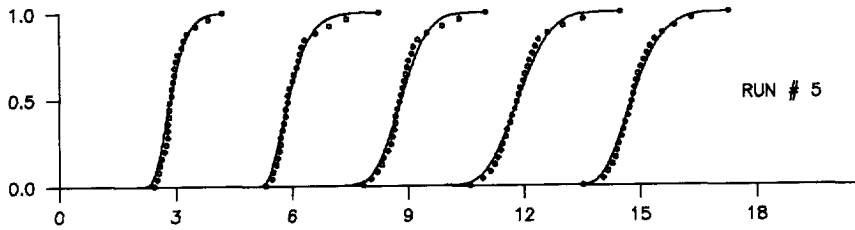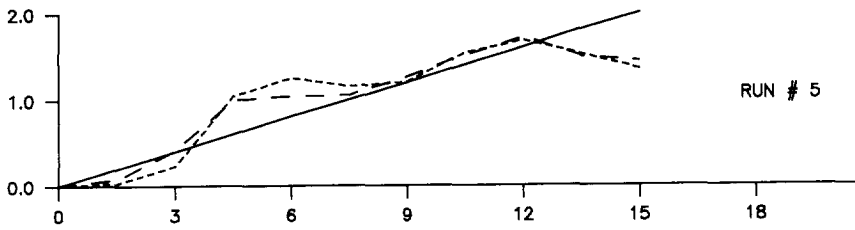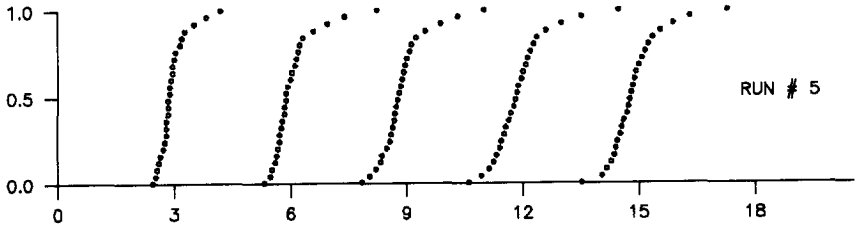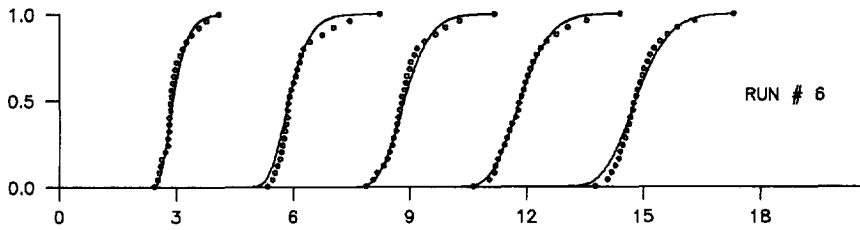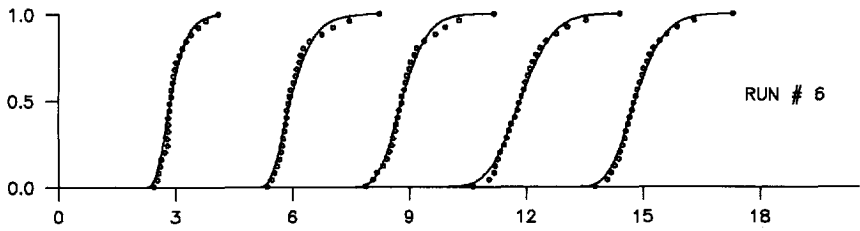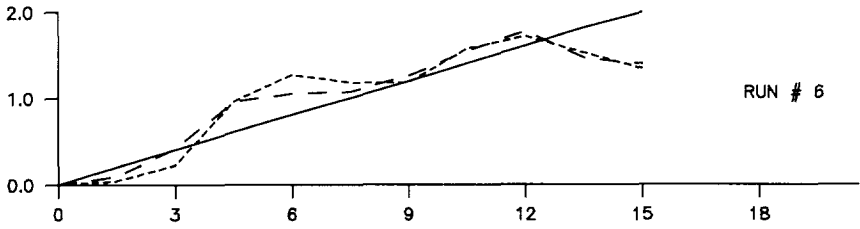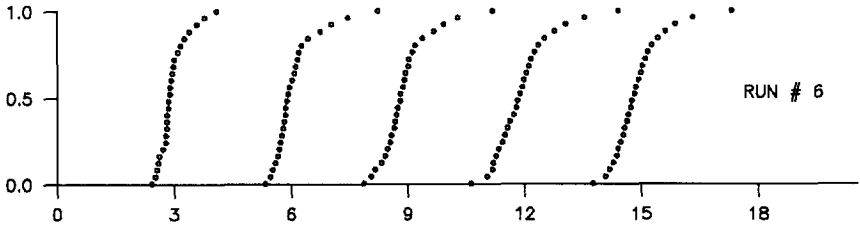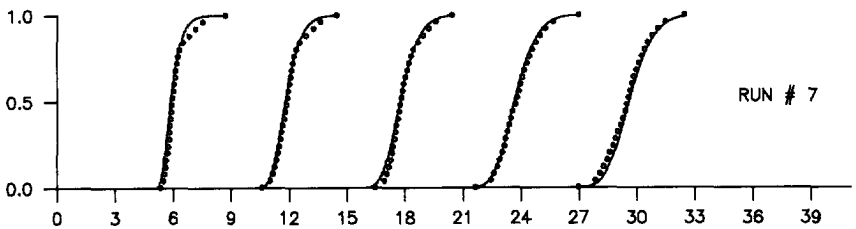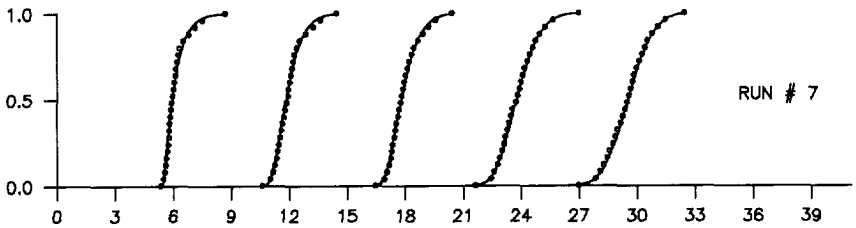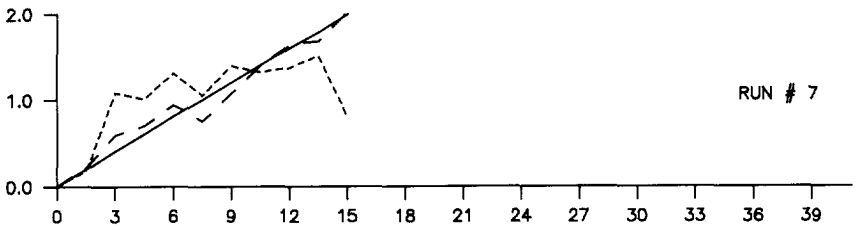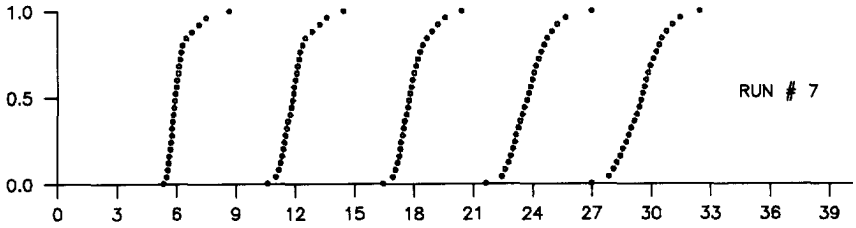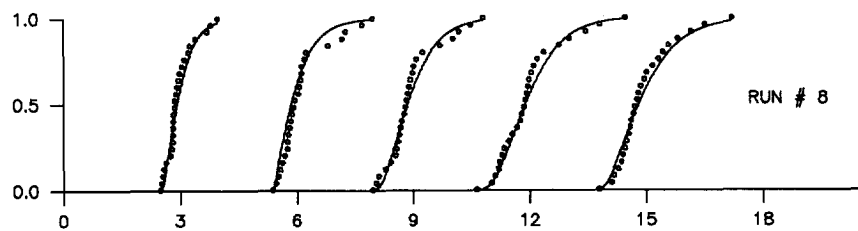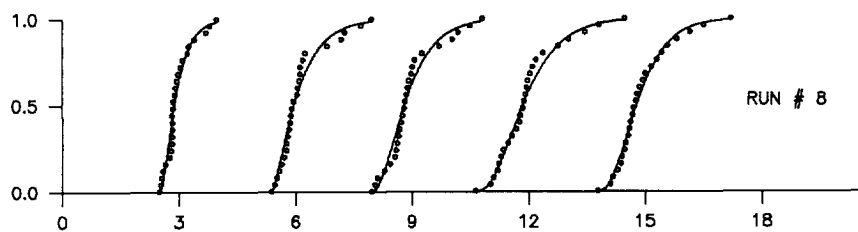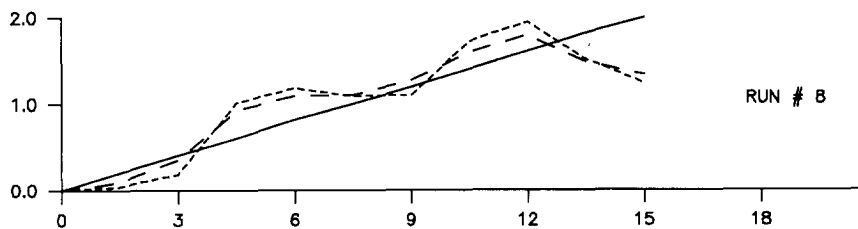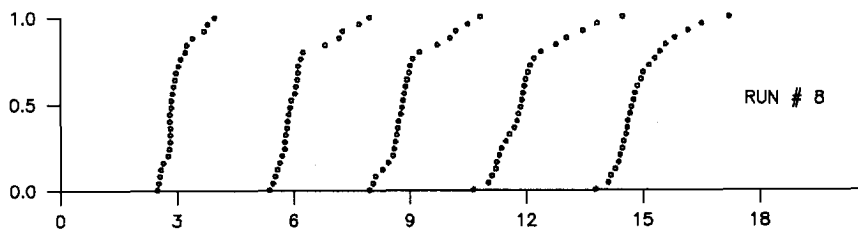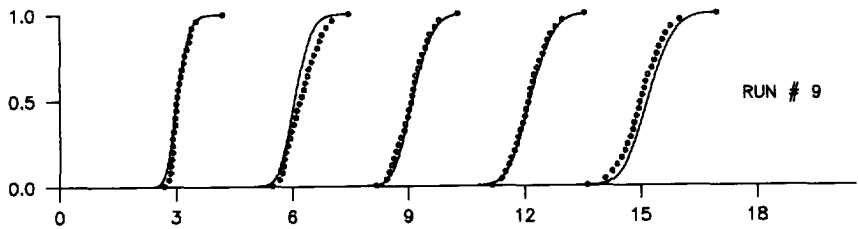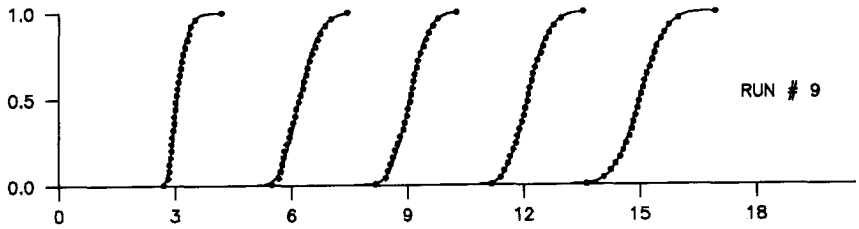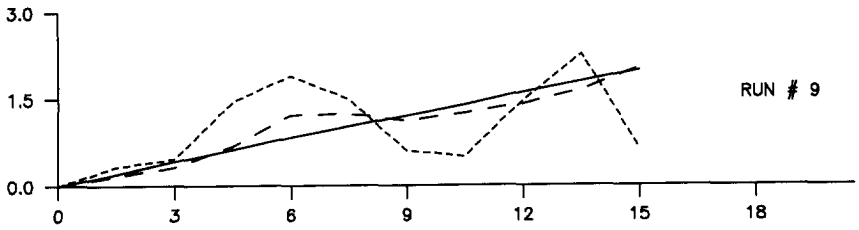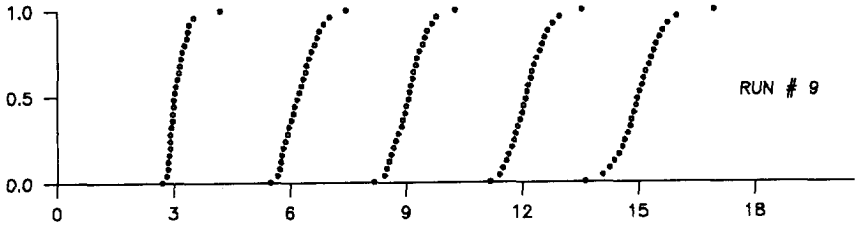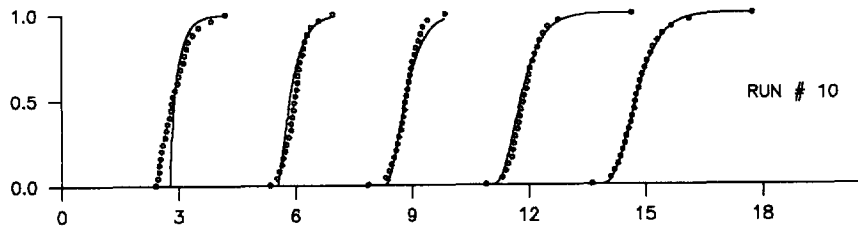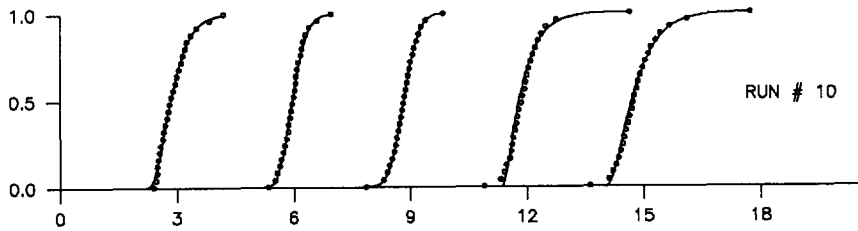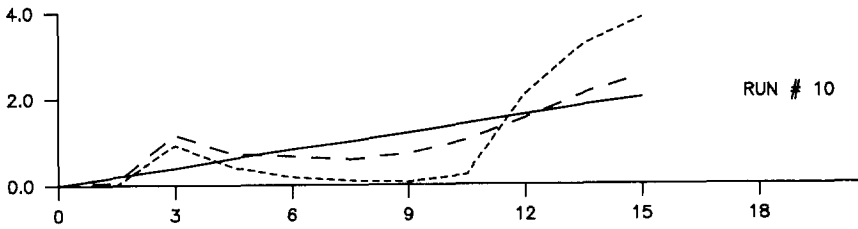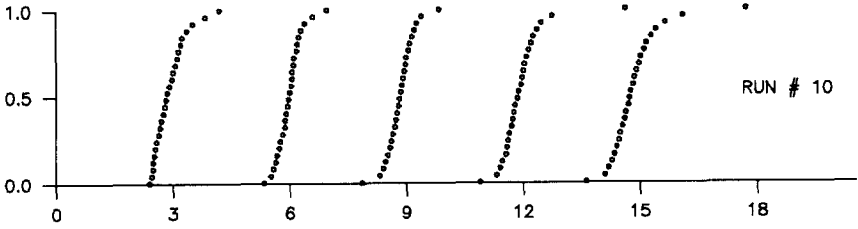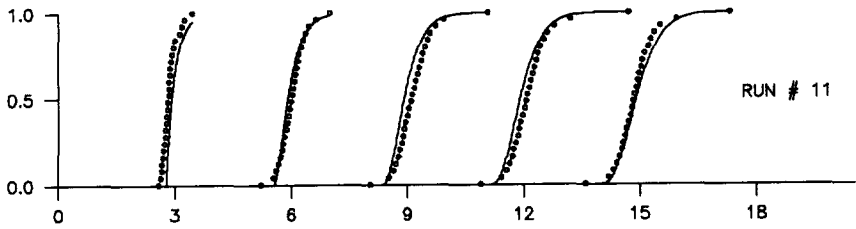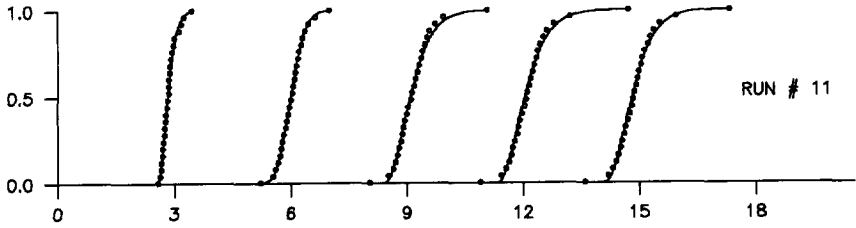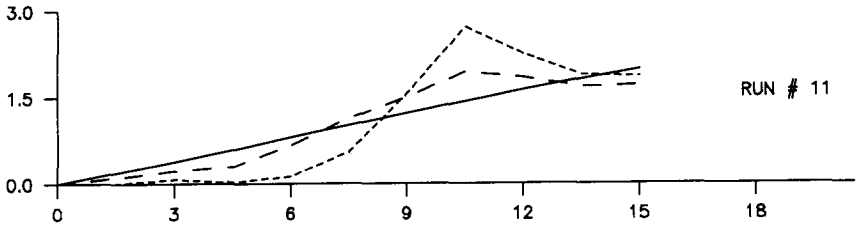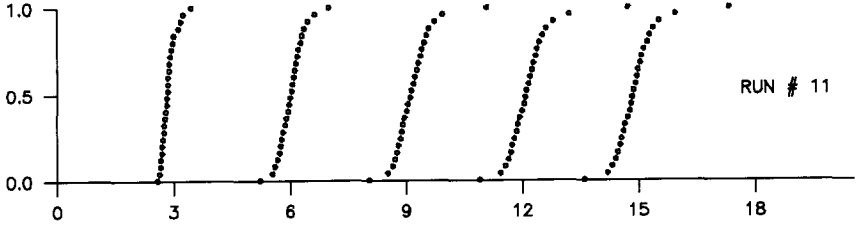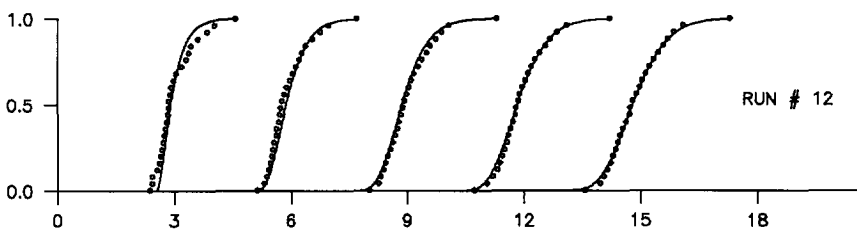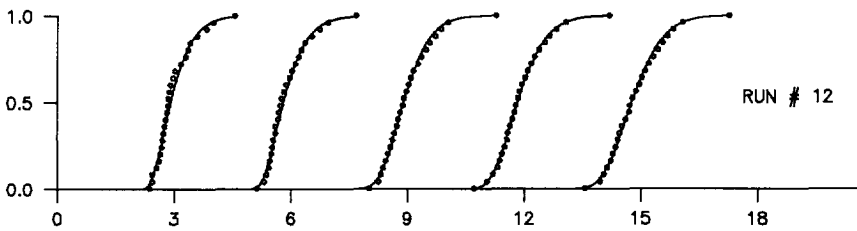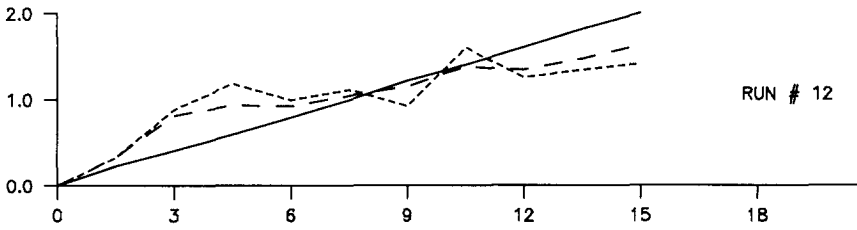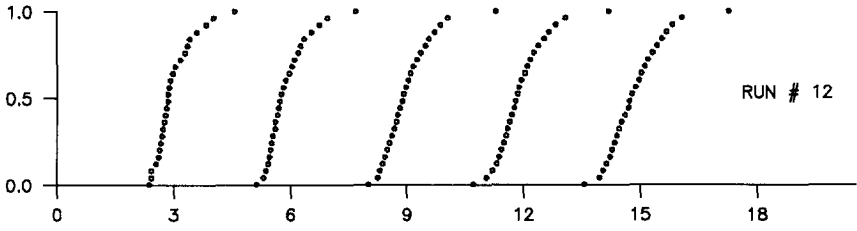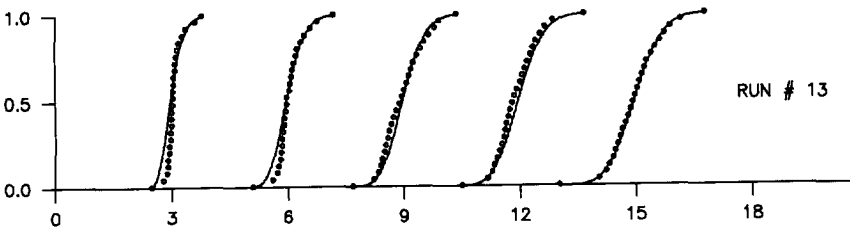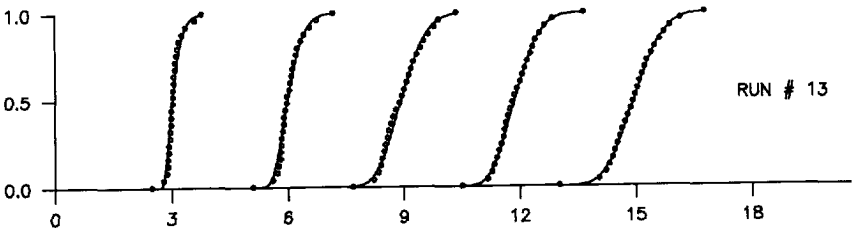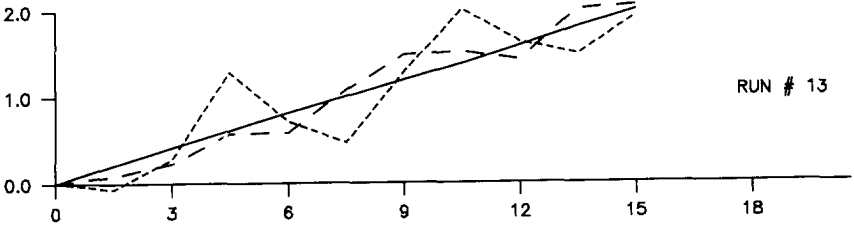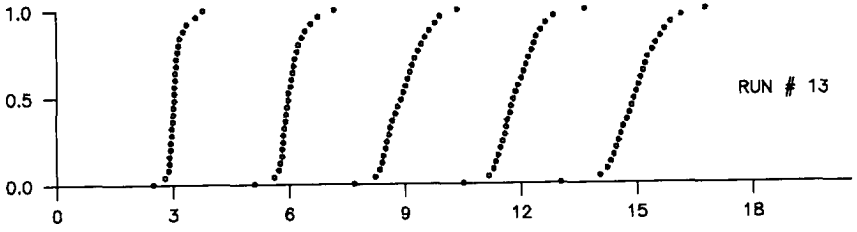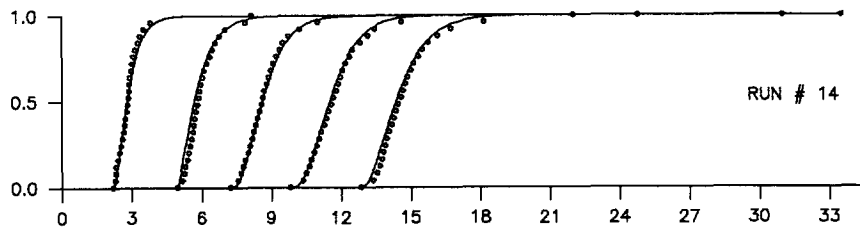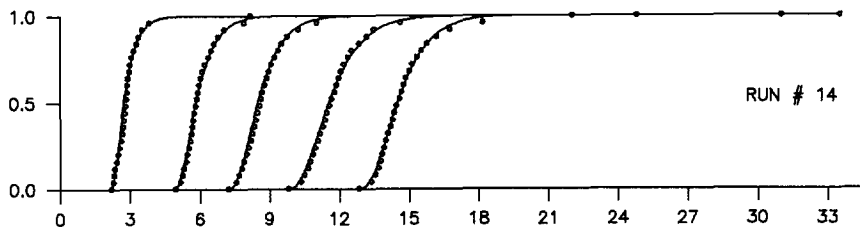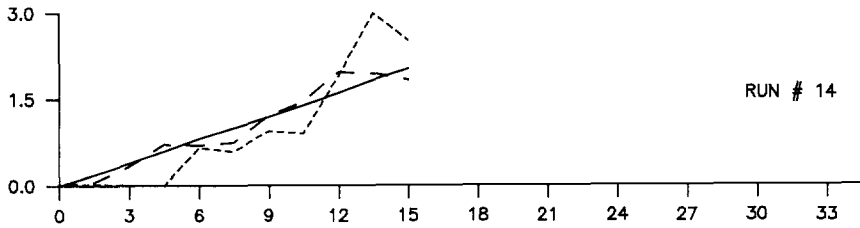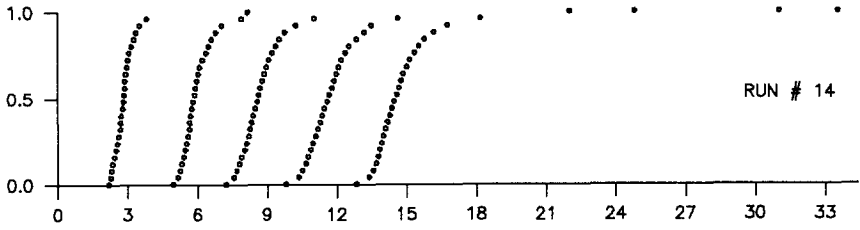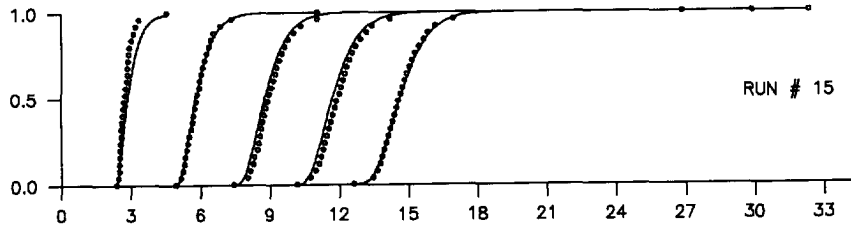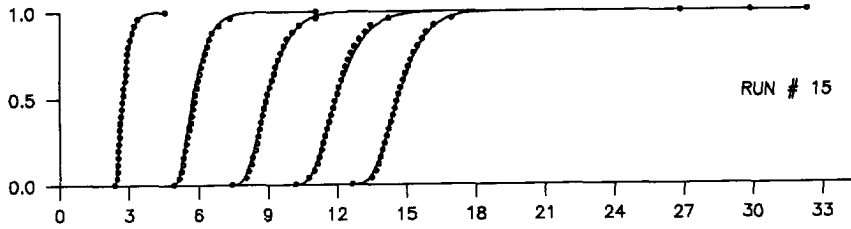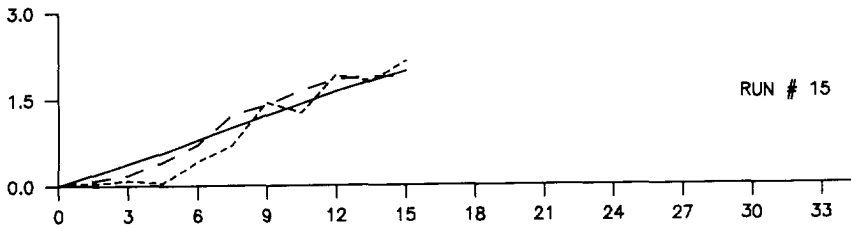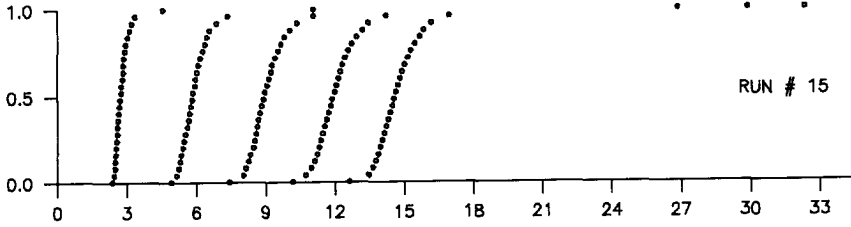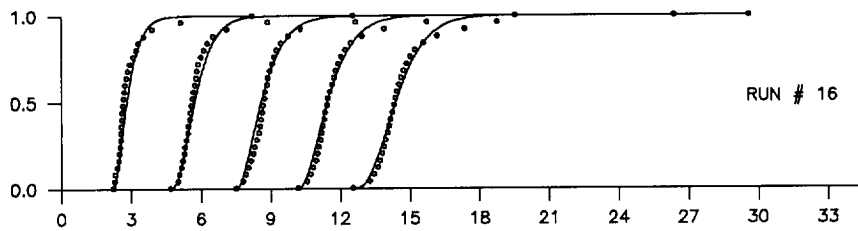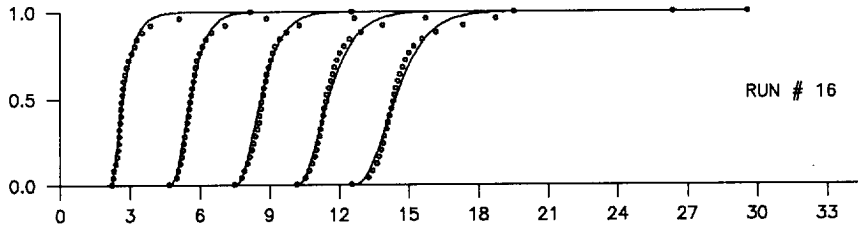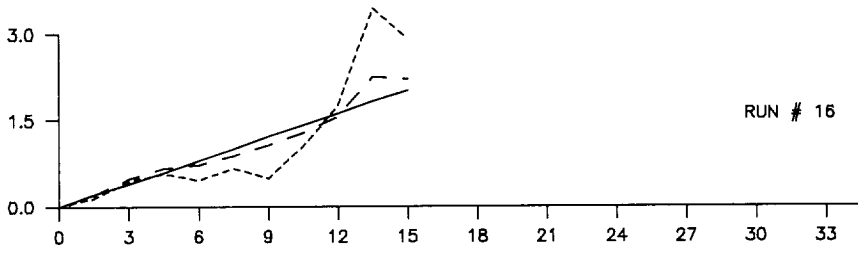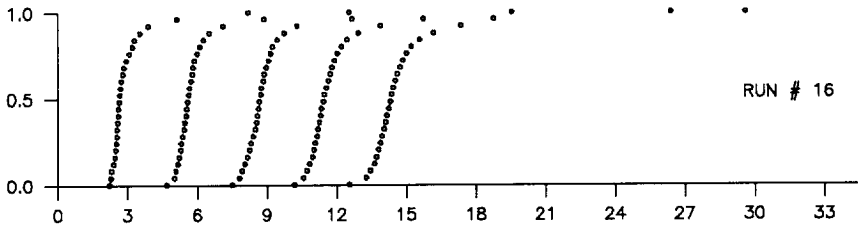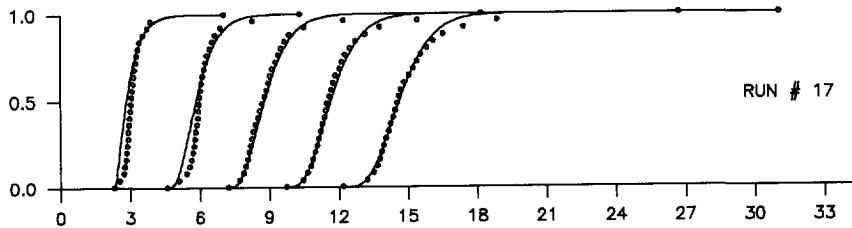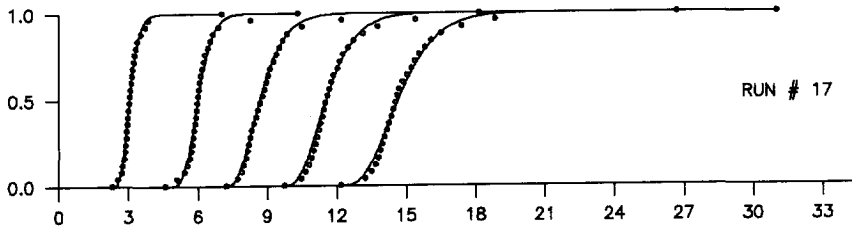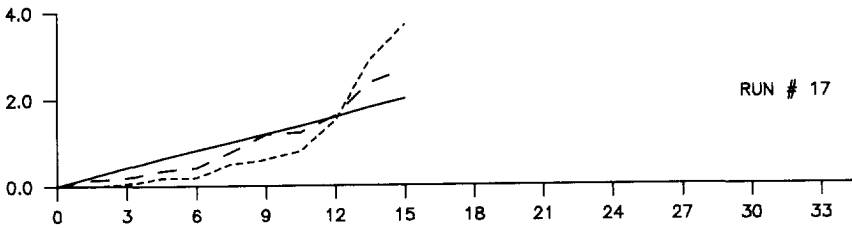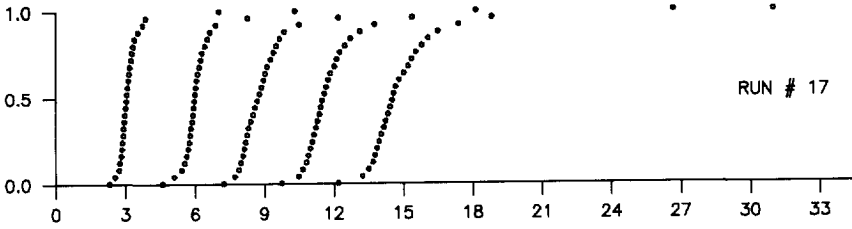
SUMMARY

While designing a bank groundwater recovery plant it was found that a temporary contamination of the river water would appear in the bank groundwater recovered as a Gaussian-like function of time, no matter how the well field was arranged. An analysis of the flow pattern showed that the contaminated water had to pass through a series of distinct flow systems. The relation between the in-going and the out-going signal of a single system could be given in the form of a convolution integral. It was conjectured that the convolutional process was to be held responsible for the Gaussian-like shape of the output. In Chapter 2 of this thesis this was found to be true under fairly general conditions: whenever a signal of finite duration has to pass through a long series of linear systems, whose impulse responses fulfill certain conditions, then that signal will ultimately be transformed into the skew-Gaussian shape given by equation (2.45). The convolutional process turned out to be mathematically analogous to addition of random variables, and our result could be linked to the Central Limit Theorem of mathematical statistics. Equation (2.45) is known, in that field of science, as Edgeworth's asymptotic expansion of a random variable. The skew-Gaussian shape of the output signal is characterized by a limited number of parameters, only two of whom (its mean or first moment and its variance or second central moment) appear to increase in magnitude during the transpo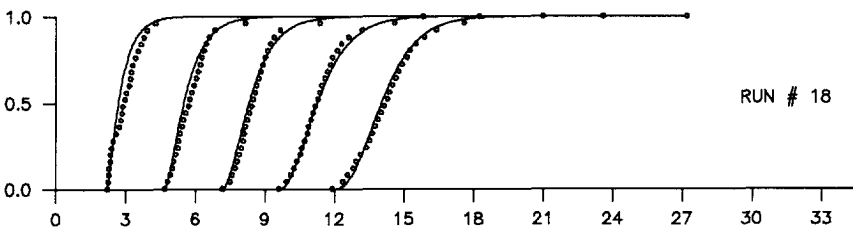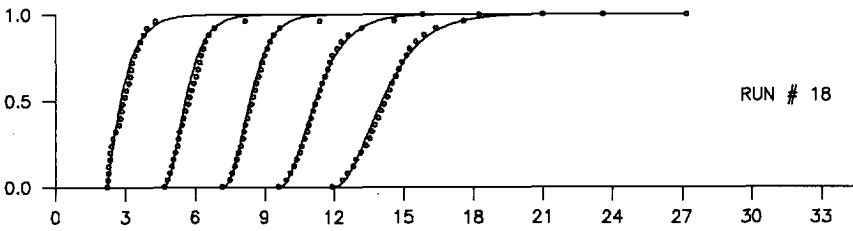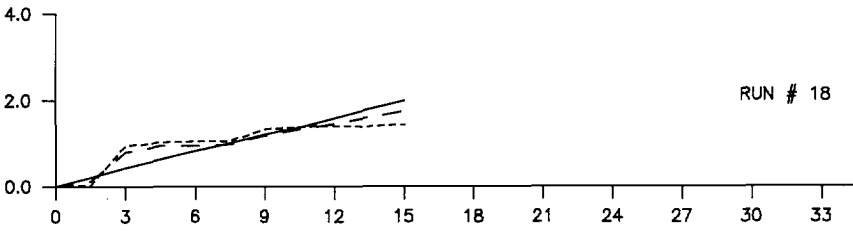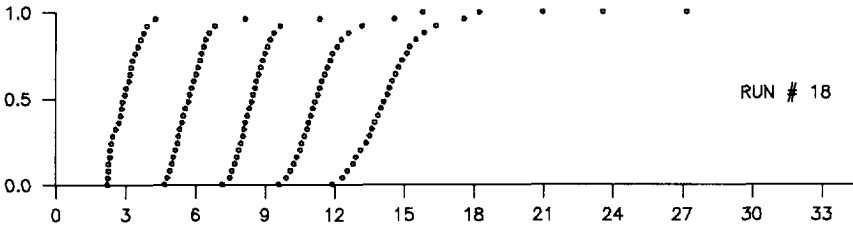rt process. The other ones disappear gradually, as the signal moves along. The one to persist longest is the skewness, which is related to the third central moment of the signal. These three moments suffice in many cases to describe an out-going signal mathematically. It will often be possible to estimate their orders of magnitude without having to model the flow processes in all of the sub-systems in great detail.

This finding is likely to have various applications in the drinking water industry, for example to predict water quality at a consumer's tap, when a source of water gets contaminated. It might also assist in the design of artificial infiltration plants. The only application elaborated in this thesis is contaminant transport by groundwater. The leading idea is that a heterogeneous porous medium (the subsoil) can be regarded as a series of systems transmitting a signal. Such a series is likely to produce a skew-Gaussian output signal, after a certain transition length (the 'Pre-Fickian' stage). In view of our application we also analyzed a system of parallel series with transverse interaction, which turned out to produce

Gaussian-like signals with very long tails.

The mathematical description (2.45) of the output signal turned out to become unstable if a signal is to be described at short distances from its source. Two alternative ways to describe a convolutional signal were selected, one presumably being due to Von Mises and the other one deriving from the theory of ideal mixing reservoirs, the latter leading us to Pearson's type III distribution.

It was demonstrated in Chapter 3 how the theory applies to solve various equations of dispersive groundwater flow approximately. We confined ourselves to longitudinal transport. This choice was justified by the outcomes of recent field experiments on dispersive groundwater flow. Only step responses (or breakthrough curves) had to be studied, as the response to any other input signal can be derived from them by superposition. Our method consisted in matching the first moments of our approximate output signal to the first moments of the exact solution. It was shown how such moments could be derived from a given linear differential equation, even if no exact solution were available. Edgeworth's expansion (truncated after three terms) was found to become useful as an approximate solution only at a certain distance from the source. Von Mises' method gave good results at any distance, but his approximation is valid at discrete points and requires the evaluation of many moments. Pearson's type III distribution, or rather its integral with respect to time (being the incomplete gamma function shifted along the time axis), was found to be superior. In all cases considered was this function able to describe the output signal well at distances greater than at most five times the length of the longitudinal dispersion coefficient α_L. The most complete transport equation investigated accounted for Strackian dispersion, first order decay and non-instantaneous sorption. Expressions for the first three moments were presented. They are simple functions of the distance traveled by a plume of contaminant and can immediately be incorporated in Analytical Element models. Simpler cases can be derived from them by setting appropriate parameters equal to zero.

Chapter 4 reports experiments conducted with a heterogeneous soil column, simulated by the Analytical Element Method. Our aim was to test the performance of the dispersion equation proposed by Strack (1992) and to investigate if the shifted incomplete gamma function would be adequate to describe actual breakthrough profiles. We were especially interested in the pre-Fickian zone, where the classical dispersion equation does not yet apply. The experimental apparatus was a rectangular cutout of a simulated porous medium, consisting of circular heterogeneities imbedded in a homogeneous background. A uniform flow component was imposed in the longitudinal direction of the cutout. The circles were chosen at random from a predefined set of three different radii. Their conductivities were assigned at random from a predescribed lognormal distribution and they were placed randomly in the homogeneous background material, until a prescribed packing density had been reached. One thousand particles were released instantaneously at the upstream boundary of the cutout. Their travel

times were observed at ten equidistant cross sections. Eighteen test runs were conducted, involving various velocities and various stochastic realizations of the heterogeneous medium.

It was confirmed that the Fickian stage was reached in none of the experiments. Breakthrough curves according to Strack's dispersion equation turned out to match the observed breakthrough curves well to excellent in the vast majority of cases. They appeared to perform better than breakthrough curves following from the classical dispersion equation. However, the values of the coefficient of longitudinal dispersion α_L associated with them fluctuated strongly from one curve to the other. It seems to be impossible, therefore, to predict future breakthrough curves by extrapolation of observed curves that are still in the pre-Fickian stage.

Besides α_L there is a second parameter involved in the Strackian model of dispersion, tentatively termed Strack's β-coefficient. This coefficient is closely connected to the arrival time of the first contaminated particle. First arrival times following from Strack's theory were found to match measured first arrival times with high accuracy in most cases. Strack's model is far superior, in this respect, to the classical dispersion equation, which is not able to predict first arrival times at all. The β-coefficient turned out to be inversely proportional to the velocity associated with the component of uniform flow. It was suggested that βv, rather than β, is to be regarded as a medium constant, v being velocity. (This suggestion has been taken up by Strack [1992]. Consequently his β differs from ours). The β-coefficient can be calculated from the first three moments of an observed breakthrough curve. It was recommended, however, not to use the third moment for this purpose, but rather the arrival time of the first particle, which is a more consistent observable.

The incomplete gamma function, shifted in time, was found to yield breakthrough curves that were optically indistinguishable from Strack's breakthrough curves. The shift in time appeared to match the arrival time of the first particle in most cases with high accuracy. Our tests supported our previous conclusion that this function will be of use in Analytical Element models of contaminant transport.

SAMENVATTING
Convolutieprocessen en dispersief transport van grondwater

Tijdens het ontwerpen van een winplaats voor oevergrondwater bleek dat een tijdelijke verontreiniging in het rivierwater steeds als een soort Gauss-kromme in het gewonnen water tot uiting kwam, hoe het puttenveld ook gearrangeerd werd. Een analyse van het stromingspatroon toonde aan dat het verontreinigde rivierwater een reeks afzonderlijk te onderscheiden stromingssystemen moest passeren. De relatie tussen het "ingangssignaal" en het "uitgangssignaal" van een enkel systeem is in de vorm van een convolutie-integraal te schrijven. We veronderstelden dat het convolutieproces verantwoordelijk was voor de Gauss-achtige vorm van het uiteindelijke uitgangssignaal. In hoofdstuk 2 van dit proefschrift is aangetoond dat dit inderdaad waar is, onder tamelijk algemene omstandigheden: als een eindig signaal een lange reeks lineaire systemen moet passeren, waarvan de "impulsresponsies" aan zekere voorwaarden voldoen, dan zal het uiteindelijk de vorm van een scheve Gausskromme (vergelijking [2.45]) aannemen. Het bleek ons dat het convolutieproces wiskundig analoog is aan het optellen van kansvariabelen, en ons resultaat kon in verband gebracht worden met de Centrale Limietstelling uit de wiskundige statistiek. Vergelijking (2.45) is in die tak van wetenschap bekend als Edgeworth's asymptotische ontwikkeling van een kansvariabele. De Gauss-achtige vorm van het uitgangssignaal wordt gekarakteriseerd door een beperkt aantal parameters, waarvan er slechts twee (het gemiddelde of eerste moment en de variantie of tweede centrale moment van het signaal) in grootte blijken toe te nemen tijdens het transport proces. De anderen verdwijnen geleidelijk, terwijl het signaal zich verplaatst. De parameter die het langst blijft bestaan is de scheefheid (skewness), die gerelateerd is aan het derde centrale moment van het signaal. Deze drie momenten zijn in veel gevallen toereikend om een uitgangssignaal wiskundig te beschrijven. Het zal vaak mogelijk zijn om hun orde van grootte te schatten, zonder dat alle deelsystemen in detail gemodelleerd hoeven te worden.

We verwachten dat deze bevinding verschillende toepassingen kan hebben in de drinkwaterindustrie, bijvoorbeeld om de waterkwaliteit aan de kraan te voorspellen, als een drinkwaterbron verontreinigd raakt. Hij kan ook behulpzaam zijn bij het ontwerpen van kunstmatige infiltratiesystemen. De enige toepassing die in dit proefschrift nader is uitgewerkt is het transport van verontreinigingen

via het grondwater. De leidende gedachte daarbij is dat een poreus medium (de ondergrond) beschouwd kan worden als een reeks systemen die een signaal doorgeven. Na een zekere instellingsafstand (de "pre-Fickiaanse" zone) zal zo'n reeks waarschijnlijk een Gaussvormig uitgangssignaal produceren. Met het oog op onze toepassing hebben we ook parallelle reeksen van systemen met onderlinge uitwisseling geanalyseerd, hetgeen Gauss-achtige signalen met zeer lange staarten bleek op te leveren.

De wiskundige beschrijving (2.45) van het uitgangssignaal bleek onstabiel te worden als hij te dicht bij de bron van verontreiniging wordt toegepast. We hebben twee alternatieve methoden geselecteerd om "convolutiesignalen" te beschrijven; één ervan is waarschijnlijk toe te schrijven aan Von Mises, terwijl de ander afgeleid is uit de theorie van de ideale mengreservoirs. Het laatste leidde tot de verdeling van Pearson, type III.

In hoofdstuk 3 is getoond hoe de theorie benut kan worden om verschillende vergelijkingen voor dispersief grondwatertransport benaderend op te lossen. We hebben ons daarbij beperkt tot longitudinaal transport. Deze keuze is te recht-vaardigen door de uitkomsten van recente veldonderzoekingen van dispersieve grondwaterstroming. We behoefden alleen stapresponsies (of doorbraakkrom-men) te bestuderen, omdat de respons op elk ander ingangssignaal hieruit door superpostie afgeleid kan worden. Onze methode bestond uit het met elkaar in overeenstemming brengen van de eerste momenten van de exacte oplossing en die van de benaderende beschrijving van het uitgangssignaal ("matching of mo-ments"). Er is gedemonstreerd hoe die momenten altijd uit een gegeven (lineaire) differentiaalvergelijking afgeleid kunnen worden, zelfs als er geen exacte oploss-ing beschikbaar is. De ontwikkeling van Edgeworth (afgebroken na drie termen) bleek pas bruikbaar te worden op enige afstand van de bron van verontreiniging. De methode van Von Mises gaf goede resultaten op elke afstand, maar de be-nadering levert slechts een aantal discrete punten van de doorbraakkromme op en vereist het berekenen van een groot aantal momenten. De verdeling van Pearson, type III, of liever de integraal daarvan met betrekking tot de tijd (hetgeen de onvolledige gammafunctie oplevert, verschoven langs de tijd-as) bleek superieur te zijn. In alle beschouwde gevallen beschreef deze functie het uitgangssignaal goed op afstanden groter dan hoogstens vijf keer de coëfficiënt van longitudinale dispersie α_L. De meest volledige transportvergelijking die we onderzochten hield rekening met dispersie volgens Strack, afbraak van de eerste orde en geleidelijke sorptie. Er werden uitdrukkingen afgeleid voor de eerste drie momenten van deze vergelijking. Het zijn eenvoudige functies van de afgelegde weg, die direct in een analytisch elementenmodel zijn in te bouwen. Eenvoudiger gevallen kunnen uit deze uitdrukkingen afgeleid worden door parameters die daarvoor in aanmerking komen nul te stellen.

In hoofdstuk 4 wordt verslag gedaan van experimenten met heterogene grondkolommen, die met de analytische elementenmethode gesimuleerd wer-den. We hadden als doel de prestaties te toetsen van de dispersievergelijking

van Strack (1992), en te onderzoeken of de verschoven onvolledige gammafunctie geschikt is om echte doorbraakkrommen te beschrijven. We waren in het bijzonder geïnteresseerd in de pre-Fickiaanse zone, waarin de klassieke dispersievergelijking nog niet opgaat. Het proefapparaat was een rechthoekige uitsnede uit een gesimuleerd poreus medium, dat cirkelvormige heterogeniteiten bevatte die ingebed lagen in een homogene achtergrond. In de lengterichting van de uitsnede werd een uniforme stromingscomponent opgelegd. De cirkels werden in een willekeurige volgorde gekozen uit een voorgeschreven verzameling van cirkels met drie verschillende stralen. Ze kregen doorlatendheden toegewezen die willekeurig gekozen werden uit een voorgeschreven lognormale verdeling, waarna ze willekeurig geplaatst werden in het homogene achtergrondmateriaal, totdat een voorgeschreven pakkingsdichtheid bereikt was. Duizend deeltjes werden plotseling losgelaten aan de bovenstroomse grens van de uitsnede. Hun doorkomsttijden werden waargenomen in tien dwarsdoorsneden op gelijke onderlinge afstanden. Er werden achtien tests uitgevoerd met verschillende stroomsnelheden en verschillende stochastische realisaties van het heterogene medium.

We konden bevestigen dat de Fickiaanse fase in geen van de experimenten bereikt werd. Het bleek dat doorbraakkrommen volgens de dispersievergelijking van Strack in de overgrote meerderheid van de gevallen goed tot zeer goed met de waargenomen krommen overeenstemden. Strack's krommen bleken beter te voldoen dan krommen die met de klassieke dispersievergelijking berekend werden. De waarden van de longitudinale dispersiecoëfficiënt α_L bleek echter van kromme tot kromme sterk te fluctueren. Het lijkt daardoor onmogelijk om toekomstige doorbraakkrommen te voorspellen uit waargenomen krommen die zich nog in de pre-Fickiaanse fase bevinden.

Behalve α_L bevat Strack's model een tweede parameter, die we zolang Strack's β-coëfficiënt noemen. Deze coëfficiënt houdt nauw verband met de aankomsttijd van het eerste verontreinigde deeltje. De eerste aankomsttijden volgens de theorie van Strack bleken in de meeste gevallen met grote nauwkeurigheid overeen te stemmen met de gemeten eerste aankomsttijden. In dit opzicht is het model van Strack verre superieur aan het klassieke dispersiemodel, dat immers in het geheel geen eerste aankomsttijden oplevert. De β-coëfficiënt bleek omgekeerd evenredig te zijn met de snelheid die met de uniforme stromingscomponent geassocieerd is. We doen daarom de suggestie om niet β maar βv als mediumconstante op te vatten, waarin v de stroomsnelheid is. (Deze suggestie is al overgenomen in Strack [1992]. Bijgevolg verschilt zijn β van de onze). De β-coëfficiënt kan berekend worden uit de eerste drie momenten van een gemeten doorbraakkromme. We bevelen echter aan om voor dat doel niet het derde moment te gebruiken, maar de aankomsttijd van het eerste deeltje, wat een veel beter waarneembare variabele is.

De onvolledige gammafunctie, verschoven langs de tijd-as, bleek doorbraakkrommen op te leveren die met het oog niet te onderscheiden waren van de doorbraakkrommen volgens Strack. De verschuiving langs de tijd-as bleek in de meeste gevallen met hoge nauwkeurigheid overeen te stemmen met de aankomst-

tijd van het eerste deeltje. De experimenten ondersteunen onze eerdere verwachting dat deze functie bruikbaar zal zijn in analytische elementenmodellen van de verspreiding van verontreinigingen door het grondwater.

REFERENCES

Abramowitz, M., and I. A. Stegun, 1964: *Handbook of Mathematical Functions*, Dover Publications Inc., New York.

Anderson, M. P., 1979: Using models to simulate the movement of contaminants through groundwater flow systems, *Crit. Rev. Environ. Control*, 9, 97-156.

Barton, D. E., and K. E. Dennis, 1952: The conditions under which the Gram-Charlier and Edgeworth curves are positive definite and unimodal, *Biometrika*, 39, 425-427.

Bear, J., 1969: Hydrodynamic dispersion. In: *Flow through Porous Media*, R.J.M. De Wiest, ed., Academic Press, New York.

Bronders, J., and F. De Smedt, 1991: Geostatische analyse van de hydraulische geleidbaarheid van watervoerende lagen in Midden-België, *Water*, 59, 127-132.

Chatwin, P. C., 1980: Presentation of longitudinal dispersion data, *ASCE Journ. of Hydr. Div.*, 71-83.

Coates, K. H., and B. D. Smith, 1964: Dead-end pore volume and dispersion in porous media, *Pet. Trans. AIME*, 231 (SPEJ 73), 73-84.

Cramér, H., 1970: *Random Variables and Probability Distributions*, Cambridge University Press.

Crank, J., 1957: *The Mathematics of Diffusion*, Clarendon Press, Oxford.

Dagan, G., 1986: Statistical theory of groundwater flow and transport: pore to laboratory, laboratory to formation, and formation to regional scale, *Water Resour. Res.*, 20 (9), 120-134.

Dagan, G., 1989: *Flow and Transport in Porous Media*, Springer Verlag, Berlin.

Dagan, G., and E. Bresler, 1985: Comment on "Flux-averaged and volume-averaged concentrations in continuum approaches to solute transport" by J. C. Parker and M. Th. van Genuchten, *Water Res. Res.*, 21 (8), 1299-1300.

Danckwerts, P. V., 1953: Continuous flow systems: distribution of residence times, *Chem. Eng. Sci.*, 2, 1-13.

Devary, J. L., and C. S. Simmons, 1984: Groundwater model parameter estimation using a stochastic-convective approach, *Top. Rep. EPRI-C5-3629*, Battelle Pac. Northwest Lab., Richland, Wash.

Domenico, D. A., and G. A. Robbins, 1984: A dispersion scale effect in model calibrations and field tracer experiments, *J. Hydrol.*, 70, 123-132.

Domenico, P. A., and F. W. Schwartz, 1990: *Physical and Chemical Hydrogeology*, Wiley & Sons, New York.

Fairbrother, M. D., 1992: *Numerical Solution to the Hyperbolic Differential Equation for Moving Front Dispersion with Rate Limited Sorption and Decay: A Method of Characteristic Approach*, Msc. Thesis, University of Minnesota, Graduate School.

Freeze, R. A., 1975: A stochastic-conceptual analysis of one-dimensional groundwater flow in nonuniform homogeneous media, *Water Resour. Res.*, 11 (5), 725-741.

Freeze, R. A., and J. A. Cherry, 1979: *Groundwater*, Prentice-Hall, New Jersey.

Fried, J. J., 1975: *Groundwater Pollution*, Elsevier, New York.

Freyberg, D. L., 1986: A natural gradient experiment on solute transport in a sand aquifer, 2: Spatial moments and the advection and dispersion of non-reactive tracers, *Water Res. Res.*, 22 (13), 2031-2046.

Garabedian, S. P., D. R. LeBlanc, L. W. Gelhar, and M. A. Celia, 1991: Large scale natural tracer test in sand and gravel, Cape Cod, Massachusetts, 2. Analysis of spatial moments for a nonreactive tracer , *Water Resour. Res.*, 27 (5), 911-924.

Gelhar, L. W., A. Mantaglou, C. Welty, and K. R. Rehfeldt, 1985: A review of field-scale physical solute transport processes in saturated and unsaturated porous media, *EPRI Rep. EA-4190, Elec. Power Res. Inst.*, Palo Alto, California.

Gelhar, L. W., C. Welty, and K. R. Rehfeldt, 1992: A critical review of data on field-scale dispersion in aquifers, *Water Res. Res.*, 28 (7), 1955-1974.

Gillham, R. W., E. A. Sudicky, J. A. Cherry, and E. O. Frind, 1984: An advection-diffusion concept for solute transport in heterogeneous unconsolidated geological deposits, *Water Resour. Res.*, 20 (3), 369-378.

Gupta, V. K., and R. N. Bhattacharya, 1986: Solute dispersion in multidimensional periodic saturated porous media, *Water Resour. Res.*, 22 (2), 156-164.

Gutjahr, A. L., L. W. Gelhar, A. A. Bakr, and J. R. MacMillan, 1978: Stochastic analysis of spatial variability in subsurface flows 2. Evaluation and applications. *Water Resour. Res.*, 14 (5), 953-959.

Güven, O., and F. J. Molz, 1988: Comment on "A field study of scale-dependent dispersion in a sandy aquifer", *J. Hydrol.*, 101, 359-365.

Güven, O., F. J. Molz, and J. G. Melville, 1984: An analysis of dispersion in a stratified aquifer, *Water Resour. Res.*, 20 (10), 1337-1354.

Haan, T. H., 1986: *Statistical Methods in Hydrology*, The Iowa State University Press/Ames.

Herr, M., G. Schäfer, and K. Spitz, 1989: Experimental studies of mass transport in porous media with local heterogeneities, *Journ. of Cont. Hydr.*, 4, 127-137.

Hoeksema, R. J., and P. K. Kitanides, 1985: Analysis of spatial structure properties of selected aquifers, Water Resour. Res., 21 (4), 563-572.

Jensen, K. H., K. Bitsch, and P. L. Bjerg, 1993: Large-scale dispersion experiments in a sandy aquifer in Denmark: observed tracer movements and numerical analyses, *Water Resour. Res.*, 29 (3), 673-696.

Jury, A., and K. Roth, 1990: *Transfer Functions and Solute Movement through Soil, Theory and Applications*, Birkhäuser Verlag, Basel.

Kreft, A., and A. Zuber, 1978: On the physical meaning of the dispersion equation and its solutions for different initial and boundary conditions, Chem. Eng. Sci., 33, 1471-1480.

Kreft, A., and A. Zuber, 1986: Comments on "Flux-averaged concentrations in continuum approaches to solute transport" by J. C. Parker and M. Th. van Genuchten, *Water Resour. Res.*, 22 (7), 1157-1158.

Lapidus, L., and N. R. Amundson, 1952: Mathematics of adsorption in beds, 6. The effect of longitudinal diffusion in ion exchange and chromatographic columns, *J. Phys. Chem.*, 56, 984-988.

LeBlanc, D. R., S. P. Garabedian, K. M. Hess, L. W. Gelhar, R. D. Quadi, K. G. Stollenwerk, and W. W. Wood, 1991: Large-scale natural gradient tracer test in sand and gravel, Cape Cod, Massachusetts, 1. Experimental design and observed tracer movement.

Maas, C. 1988: Effectenonderzoek ten behoeve van de stichting van een oever-grondwaterwinplaats nabij Opperduit, deelrapport 3: Hydrologisch ontwerp van het puttenveld. *KIWA-report SWO* 88.333, Nieuwegein, The Netherlands.

Mackay, D. M., D. L. Freyberg, P. V. Roberts, and J. A. Cherry, 1986: A natural gradient experiment on solute transport in a sand aquifer, 1: Approach and overview of plume movement, *Water Resour. Res.*, 22 (13), 2017-2029.

Mandelbrot, B. B., 1967: How long is the coastline of Great Britain? Statistical self-similarity and fractal dimensions, *Science*, 155, 636-638.

Marle, C., P. Simandoux, J. Pacsirsky, and C. Gaulier, 1967: Etude du déplacement de fluides miscibles en milieu poreux stratifié, *Rev. Inst. François Pétrol.*, 22 (2), 272-294.

Matheron, G., and G. de Marsily, 1980: Is transport in porous media always diffusive? A counter example, *Water Resour. Res.*, 16 (5), 901-917.

MFRC, 1989: Workprogram 1989, Implementation of spatial and seasonal variability of chemical transport in Minnesota groundwater; 2/16/89.

Molz, F. J., and M. A. Widdowson, 1988: Internal inconsistencies in dispersion-dominated models that incorporate chemical and microbial kinetics, *Water Resour. Res.*, 24 (4), 615-619.

Neuman, S. P., 1990: Universal scaling of hydraulic conductivities and dispersivities in geological media, *Water Resour. Res.*, 26 (8), 1749-1758.

Oberhettinger, F., and L. Badii, 1973: *Tables of Laplace Transforms*, Springer Verlag, Berlin.

Parker, J. C., and M. Th. van Genuchten, 1984: Flux-averaged and volume-averaged concentrations in continuum approaches to solute transport, *Water Resour. Res.*, 22 (7), 866-872.

Parker, J. C., and M. Th. van Genuchten, 1985: Reply, *Water Resour. Res.*, 21 (8), 1301-1302.

Parker, J. C., and M. Th. van Genuchten, 1986: Reply, *Water Resour. Res.*, 22 (7), 1159-1160.

Press, W. H., B. P. Flannery, S. A. Teukolsky, and W. T. Vetterling, 1992: *Numerical Recipes, The Art of Scientific Computing (Fortran version)*, Cambridge University Press, New York.

Rajaram, H., and L. W. Gelhar, 1991: Three-dimensional spatial moments analysis of the Borden tracer test, *Water Resour. Res.*, 27 (6), 1239-1251.

Rifai, M. N. E., W. J. Kaufman, and D. K. Todd, 1956: *Dispersion Phenomena in Laminar Porous Media*, University of California, Berkeley.

Scheidegger, A. E., 1954: Statistical hydrodynamics in porous media, *J. Appl. Phys.*, 25, 994-1001.

Shohat, J. A., and J. D. Tamarkin, 1943: The Problem of Moments, *Mathematical Surveys*, 1, American Mathematical Society, New York City.

Smith, L., and F. W. Schwartz, 1980: Mass transport 1. A stochastic analysis of macroscopic dispersion, *Water Resour. Res.*, 16 (2), 303-313.

Sposito, G., W. A. Jury, and V. K. Gupta, 1986: Fundamental problems in the stochastic convection-dispersion model of solute transport in aquifers and field soils, *Water Resour. Res.*, 22 (1), 77-88.

Springer, M. D., 1979: *The Algebra of Random Variables*, Wiley and Sons, New York.

Strack, O. D. L. 1987. The analytic element method for regional groundwater modeling. *Proceedings of the Solving Ground Water Problems with Models Conference and Exposition*, Vol. 2, Febr. 10-12, 1987, Colorado.

Strack, O. D. L., 1989: *Groundwater Mechanics*, Prentice Hall, Englewood Cliffs, N. J.

Strack, O. D. L., 1992: A mathematical model for dispersion with a moving front in groundwater, *Water Resour. Res.*, 28 (11), 2973-2980.

Strack, O. D. L., 1994: Moving front dispersion with rate limited sorption, to be published.

Strack, O. D. L., and M. Fairbrother, 1994: Numerical solution to the differential equation for moving front dispersion, to be published.

Stuart, A., and J.K. Ord, 1987: *Kendall's Advanced Theory of Statistics*, fifth edition of Volume 1, Distribution Theory. Griffin, London.

Sudicky, E. A., 1986: A natural gradient experiment on solute transport in a sand aquifer: Spatial variability of hydraulic conductivity and its role in the dispersion process, *Water Resour. Res.*, 22 (13), 2069-2082.

Tompson, F. B., and L. W. Gelhar, 1990: Numerical simulation of solute transport in three-dimensional randomly heterogeneous porous media, *Water Resour. Res.*, 26 (10), 2541-2562.

Van Genuchten, M. T., and P. J. Wierenga, 1976: Mass transfer studies in sorbing porous media, Division S-1, Soil Physics, *Soil Sci. Soc. Am. J.*, 40 (3), 473-480.

Van Mazijk, A., R. Noppeney, T. van Ellen, and P. Verwoerdt, 1989: Gevoeligheidsonderzoek Alarmmodel Rijn, *Mededeling van de Vakgroep Gezondheidstechniek & Waterbeheersing*, Dept. of Civil Engineering, Techn. University, Delft.

Von Mises, R., 1931: *Vorlesungen aus dem Gebiete der Angewante Mathematik, Vol. 1, Wahrscheinlichkeitsrechnung und ihre Anwendung in der Statistik und Theoretischen Physik*, Franz Deuticke, Leipzig, Wien.

Von Mises, R., 1964: *Mathematical Theory of Probability and Statistics*, Academic Press, New York.

Wheatcraft, S. W., and S. W. Tyler, 1988: An explanation of scale-dependent dispersivity in heterogeneous aquifers using concepts of fractal geometry, *Water Resour. Res.*, 24 (4), 566-578.
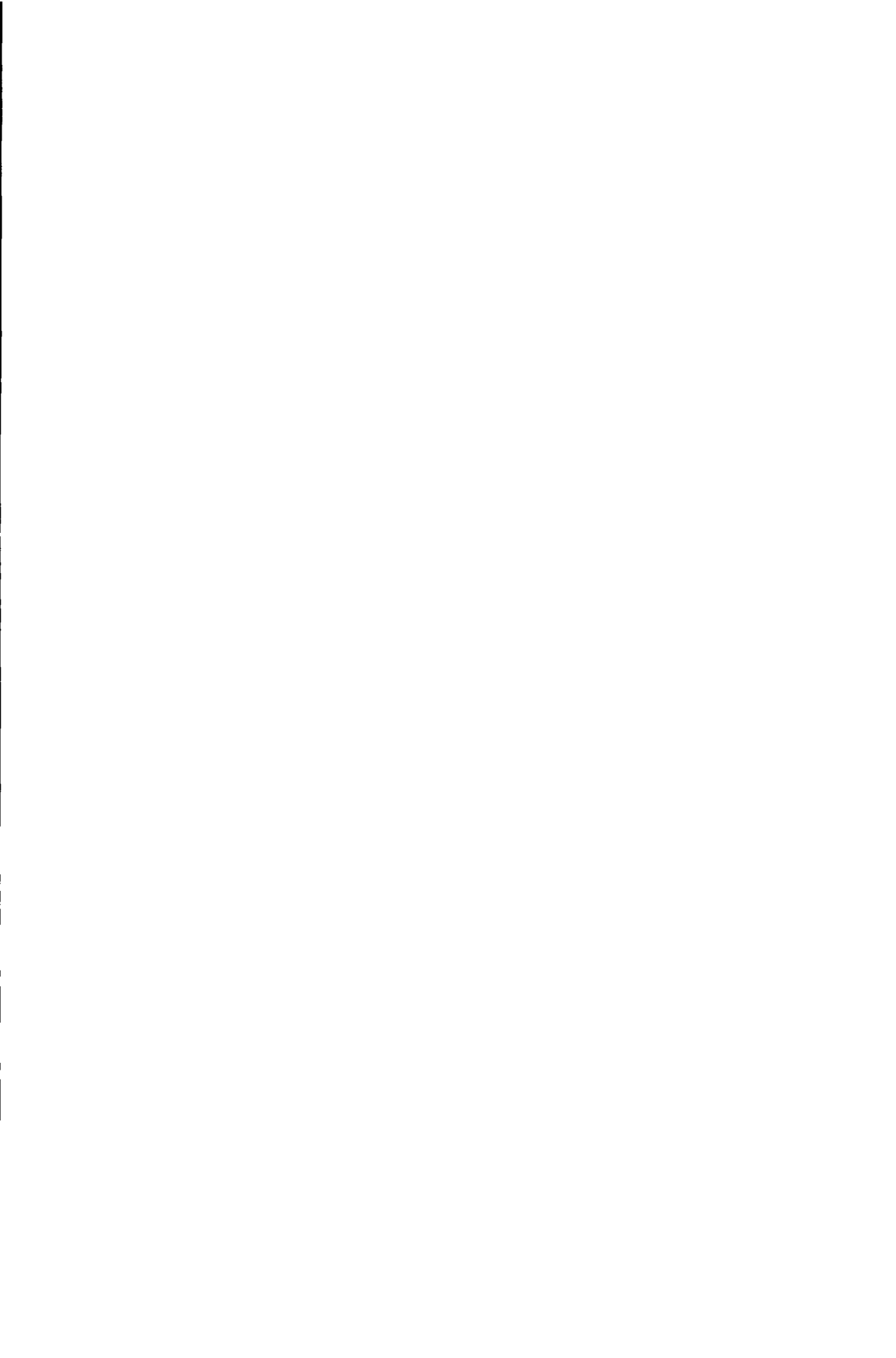
Curriculum vitae

Kees Maas werd op 8 februari 1947 in Den Haag geboren. Van 1959 tot 1965 volgde hij in Hollandia en in Leiden middelbaar onderwijs, dat hij afsloot met het examen HBS-B. Van 1965 tot 1972 studeerde hij weg- en waterbouwkunde aan de Technische Hogeschool Delft. Hij behaalde daar het diploma civiel-ingenieur, waarna hij als geohydroloog in dienst was van resp. het Rijksinstituut voor Drinkwatervoorziening, de Provincie Zeeland en (momenteel) het Keuringsinstituut van Waterleidingartikelen. Een eerdere aanzet tot een proefschrift brak hij af wegens verhuisperikelen. Voor een reeks artikelen over stroming van water in gelaagde poreuze media, die hij in dat kader publiceerde, ontving hij in 1991 de Vreedenburgh-prijs. Het huidige proefschrift vond zijn oorsprong in een samenwerkingsproject met de Universiteit van Minnesota, waarvoor hij in 1991 een half jaar in Minneapolis verbleef.

Stellingen

I   Het getij van grondwater nabij ondiepe kusten en getijderivieren kan voor-ijlen op het getij in het open water. *C. Maas en W.J. de Lange, J. Hydrol., 92(1987) 43-67.*

II   De stijghoogte van grondwater in diepe waarnemingsbuizen reageert meestal sneller op neerslag dan de stijghoogte in ondiepe buizen.

IIa   Bestaande modellen voor regionale grondwaterstroming (zoals MODFLOW) negeren ten onrechte het mechanisme dat dit verschijnsel veroorzaakt. Niet-temin is het eenvoudig in rekening te brengen.

III   De hoeveelheid doorspoelwater, die nodig is om de verzilting te bestrijden van aanvoerstelsels van zoet water op de Zeeuwse en Zuid-Hollandse eilan-den, kan sterk beperkt worden door langs de kust een rij artesische bronnen te slaan. *C. Maas, Proc. 9th Salt Water Intrusion Meeting, Delft 1986, 43-60.*

IV   Van het grondwater dat opgepompt wordt uit een homogeen freatisch pakket is de helft jonger (in jaren) dan 1 à 3 keer de pakketdikte (in meters). De factor 1 geldt als er geen sloten aanwezig zijn; de factor 3 geldt als er veel sloten aanwezig zijn.

V   Bij het formuleren en oplossen van stromingsproblemen in gelaagde me-dia kan het gebruik van matrixfuncties heel economisch zijn. *C. Maas, J. Hydrol., 88 (1986) 43-67.*

VI   Regionale stijghoogteproblemen waarbij het zoutgehalte van het grondwater van plaats tot plaats verschilt kunnen opgelost worden met modellen die voor zoet grondwater ontwikkeld zijn. *C. Maas, Natuurwet. Tijdschr. 70 (1988) 143-154.*

VII   Het is voor berekeningen in kustaquifers vaak zinvol om een overgang van zoet naar zout grondwater als een scherp grensvlak op te vatten. Het staps-gewijs benaderen van zo'n overgang door meerdere scherpe grensvlakken lijkt daarop een verbetering te zijn, maar leidt tot verrassingen.

VIII De grens tussen inzijgings- en kwelgebied op de flank van een heuvelrug van homogeen zand, geprojecteerd op een horizontaal vlak, vormt wiskundig gezien een vrije rand, waarvan de positie in principe te vinden is met de hodograafmethode. *C. Maas, Water Resour. Res., [28] 2, 1992, 365-371.*

IX Verschillende grondwaterbeheerders hanteren ten onrechte het begrip diepe kwel om de ecohydrologische waarde van vochtige natuurgebieden in te schatten. Een maatstaf die daarvoor wél bruikbaar is, is het oppervlak aan kwelhellingen, waar grondwater aan het maaiveld uittreedt. *A.J.M. Jansen en C. Maas, Proc. Symp. Eng. Hydrol., ASCE, 1993, 150-155.*

X   De ecologische interpretatie van grondwaterstandsduurlijnen is nodeloos ondoorzichtig, doordat er geen scheiding gemaakt wordt tussen gebiedseigenschappen en meteorologie.

XI Doorgaans wordt men van het schrijven van een proefschrift niet veel wijzer. *NRC-Handelsblad 21-10-1993.*